

Graphene-Hematite-Tungsten Trioxide

composite for efficient PhotoElectro-

Chemical water splitting.

by

Rida Shahzadi Haider

Reg#200-FBAS/MSPHY/F13



Supervisor

Dr Shamaila Sajjad

(Assistant Professor IIII)

Co Supervisor

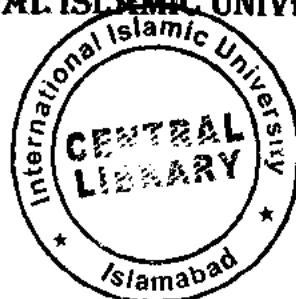
Dr Yaqoob Khan

(SSD NCP)

DEPARTMENT OF PHYSICS

FACULTY OF BASIC AND APPLIED SCIENCES

INTERNATIONAL ISLAMIC UNIVERSITY ISLAMABAD



Accession No TH-14946 (P)g

MS
530.537
HAG

- Electricity
- Physics.
- PhotoElectro-Chemical water
- Power Generation

Faculty of Basic and Applied Sciences
(Department of Physics)
(2015)

Graphene-Hematite-Tungsten Trioxide Composite for efficient
PhotoElectro-Chemical water splitting.

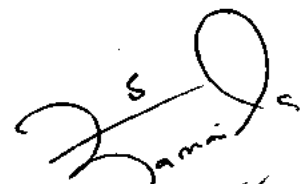
by
Rida Shahzadi Haider

(Reg#200-FBAS/MSPHY/F13)

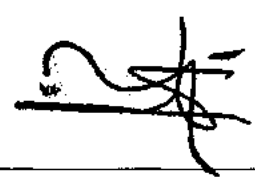
Thesis submission to the Department of Physics (Faculty of Basic and Applied Sciences), International Islamic University Islamabad (IIUI) for Masters of Science
(MS) in Physics

Chairman Department of Physics
International Islamic University,
Islamabad

Dean FBAS
International Islamic University,
Islamabad



Dr. Shahzadi Haider
Chairman Department of Physics
International Islamic University
Islamabad



Dr. Shahzadi Haider
Chairman Department of Physics
International Islamic University
Islamabad

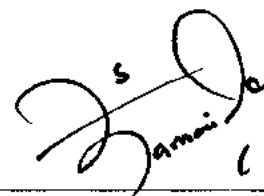
Faculty of basic and applied sciences
International Islamic university
(Department of physics)
(2015)

Final Approval

It is certified that work presented in this thesis entitled "Graphene-Hematite-Tungsten trioxide Composite For Efficient PhotoElectro-Chemical Water Splitting" by Rida Shahzadi Haider bearing Registration No. 200-FBAS/MSPHY/F13 and herviva held at 30 July 2015 is of sufficient standard in scope and quality for award of degree of MS Physics from international Islamic university , Islamabad.

Supervisor :

Dr Shamaila Sajjad
(Assistant Professor Physics ,IIUI)
(HOD Physics Department)



Dr. Shamaila Sajjad
Chairperson
Department of Physics (FC, FBAS)
International Islamic University
Islamabad

Co-Supervisor:

Dr Yaqoob Khan
(Senior Scientific Officer , NCP)



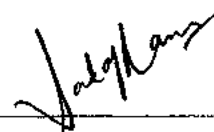
External Examiner:

Dr. Nazar Abbas
(Associate Professor Of *Physics* Principal Investigator)
CIIT



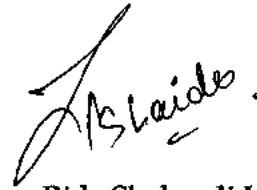
Internal Examiner :

Dr Sadaf (Assistant Professor IIUI)



Declaration

I hereby declare that this thesis work has not been copied from any other source. Further, work presented in this thesis has not been supported in any application or any other degree or qualification to any other University or Institute and considerable under the plagiarism rule of Higher Education Commission (HEC), Pakistan.



Rida Shahzadi Haider
(200-FBAS/MSPHY/F13)
(Department of Physics, IIUI)

بِسْمِ اللَّهِ الرَّحْمَنِ الرَّحِيمِ

In the Name of Allāh, the Most Gracious, the Most Merciful

Thesis Dedication

To

My family

*'Who supports me in every step, and give me courage in this span of
research work...specially my mother, thank you ami, I am here
because of you '*

Acknowledgement

Behind every successful step of mine is the divine force of my GREAT ALLAH MIGHTY, Who encourages me to accept newness in life. Marching towards perfection was my dream which seems possible now. After that I would like to acknowledge the nurturance and never ending prayers of my parents; Mr & Mrs Haider, without whom I could never be what I am. It will be un-justice if great support of my sisters would be unnoticed, who remain always therefore for me to support.

A special thanks to my supervisor Dr Shamaila Sajjad (Assistant Professor, HOD physics Department IIUI), she encouraged me and helped me in overcoming problems came while doing my research work.

A very special thanks to my co-supervisor Dr Yaqoob Khan (Senior Scientific Officer, NCP), for being so influential, inspirational and a purist who never let you fall down, he supports me by giving a free hand during research and encouraged me on every step.

Lastly, thanks to all lab fellows, for their support, their company, their collaboration.

Rida Shahzadi Haider

TABLE OF CONTENTS

CHAPTER 1

INTRODUCTION

1.0 Hydrogen as A Fuel Source.....	15
1.2 Why is hydrogen so important?	15
1.3 Hydrogen applications.....	16
1.4 Hydrogen demand up to 2050.....	17
1.5 Artificial Photosynthesis	18
1.6 PEC water splitting approach.....	18-19
1.7 Efficiency definitions of PEC	20-22
1.8 Production of H ₂ from water using solar light.....	23
1.9 Materials for PEC water splitting.....	24-26
1.10 Interface of semiconductor and electrolyte.....	27-28
1.11 $STH(\eta_{STH}) = \eta_{sep} * \eta_{cat} * \eta_{abs}$	29-30
1.12 Mechanism followed for PEC water splitting.....	30
1.13 Graphene as a transporter.....	31
1.14 Scope and Aim of the Thesis.....	32

CHAPTER 2

EXPERIMENTAL METHODS AND MATERIALS

2.1 Synthesis of Graphene from Graphite by modified Hummers method	34-37
2.2 Hydrothermal Synthesis of Hematite (α -Fe ₂ O ₃) Nano particles with different precursors.....	37-38
2.3 Hydrothermal Synthesis of tungsten trioxide (WO ₃) Nano particles	39-40
2.4 Thin film deposition on Fluorine doped Tin Oxide (FTO) substrates.....	40
2.4.1 Substrates Cleaning.....	40
2.4.2 Spray deposition.....	41
2.4.2.1 Iron oxide (α -Fe ₂ O ₃) Nano particles deposition on FTO (prepared from method 1 and method 3)	41
2.4.2.2 Tungsten trioxide (WO ₃) Nano particles deposition on FTO (prepared from method 1 and method2).....	42
2.4.3 Deposition of Nano-composites.....	43
2.4.3.1 Iron oxide-Tungsten Trioxide (α -Fe ₂ O ₃) - (WO ₃) Nano-composite deposition on FTO	43
2.4.3.2 Tungsten Trioxide -Graphene (WO ₃ -RGO) Nano- composite deposition on FTO.....	44
2.4.3.3 Iron oxide -Graphene (α -Fe ₂ O ₃ -RGO) Nano- composite deposition on FTO	44
2.4.3.4 Iron oxide -Tungsten Trioxide-Graphene (α -Fe ₂ O ₃ -WO ₃ -RGO) Nano -composite deposition on FTO.....	45

2.4.3.5 Iron oxide -Tungsten Trioxide-Graphene (α -Fe ₂ O ₃ -WO ₃ -RGO) Nano -composite deposition on FTO with different concentration	46
2.5 Hydrothermal deposition.....	46
2.5.1 Hydrothermal deposition of Tungsten trioxide (WO ₃) Nano particles on FTO.....	46
2.5.2 Hydrothermal deposition of Tungsten Trioxide-Graphene (WO ₃ -GO) on FTO	47
2.6 Characterization techniques.....	48
2.6.1 Scanning Electron Microscope (SEM).....	48
2.6.2 X- ray diffraction (XRD).....	48-49
2.6.3 Ultraviolet visible spectroscopy.....	49-50
2.6.4 Photo electro chemical measurements.....	50

CHAPTER 3

RESULTS AND DISCUSSIONS

3.1 X-Ray diffraction analysis.....	52
3.1.1 X-RD analysis of oxidized and reduced graphene (GO-RGO).....	52-53
3.1.2 XRD- analysis of tungsten trioxide (WO ₃).....	54
3.1.3 XRD-analysis of hematite (α -Fe ₂ O ₃).....	55
3.1.4 XRD analysis of tungsten trioxide-Graphene nano composite (WO ₃ -GO).....	56
3.1.5 XRD- Analysis of Hematite- Graphene nano composite (α -Fe ₂ O ₃ -RGO).....	57

3.1.6 XRD- Analysis of WO_3 - α - Fe_2O_3 -RGO nano composite.....	58
3.1.7 XRD- Analysis of WO_3 - α - Fe_2O_3 -RGO nano composite with different ratios.....	59
3.1.8 XRD-analysis of WO_3 - α - Fe_2O_3 nano composite.....	60
3.1.9 XRD-analysis of WO_3 - α - Fe_2O_3 (dark) nano composite.....	61
3.2 Scanning Electron Microscopy (SEM).....	62
3.2.1 SEM analysis of α - Fe_2O_3 nano particles prepared from method 1 and 3.....	62
3.2.2 SEM analysis of WO_3 nano particles prepared from method 1.....	63
3.2.3 SEM analysis of GO and RGO.....	64
3.2.4 SEM analysis of α - Fe_2O_3 -RGO nano composite thin film	65
3.2.5 SEM analysis of WO_3 - α - Fe_2O_3 (lite) nano composite thin film	66
3.2.6 SEM analysis of WO_3 - α - Fe_2O_3 (dark) nano composite thin film	67
3.2.7 SEM analysis of WO_3 -RGO nano composite thin film.....	68
3.2.8 SEM analysis of WO_3 - α - Fe_2O_3 -RGO nano composite thin film prepared with same ratio (1:1:1)	69
3.2.9 SEM analysis of WO_3 - α - Fe_2O_3 -RGO nano composite thin film prepared with different ratio (2:1:2).....	70
3.3 EDX Analysis.....	71
3.3.1 EDX Analysis of WO_3 - α - Fe_2O_3 nanocomposite thin film	71

3.3.2 EDX Analysis of $W\text{O}_3$ - α - Fe_2O_3 -RGO nanocomposite thin film prepared with (1:1:1) ratio.....	72
3.3.3 EDX analysis of $W\text{O}_3$ - α - Fe_2O_3 -RGO nanocomposite thin film prepared with (2:1:2) ratio.....	73
3.3.4 EDX analysis of α - Fe_2O_3 -RGO nano composite thin film	74
3.3 UV-Vis spectroscopy analysis	75
3.3.1 UV-Vis analysis of graphene oxide (GO).....	75
3.3.2 UV-Vis analysis of Reduced graphene oxide (RGO).....	76
3.3.3 UV-Visible Analysis of α - Fe_2O_3 (<i>lit</i>).....	77
3.3.4 UV-Visible analysis of α - Fe_2O_3 (<i>dark</i>).....	78
3.3.5 UV-Visible analysis of $W\text{O}_3$	79
3.3.6 UV-Visible analysis of $W\text{O}_3$ (prepared with different methods).....	80
3.3.7 UV-Visible Analysis of α - Fe_2O_3 -GO nano composite.....	81
3.3.8 UV-Visible analysis of α - Fe_2O_3 (<i>dark</i>) - $W\text{O}_3$ nano composite	82
3.3.9 UV-Visible analysis of α - Fe_2O_3 (<i>lit</i>) - $W\text{O}_3$ nano composite.....	83
3.3.10 UV-Visible analysis of α - Fe_2O_3 (<i>dark</i>) - $W\text{O}_3$ - RGO nano composite.....	84
3.3.11 UV-Visible analysis of α - Fe_2O_3 (<i>dark</i>) - $W\text{O}_3$ - RGO nano composite.....	85
3.4 Electrochemical analysis	86

3.4.1 Linear sweep voltammetry of WO ₃	86-87
3.4.2 Linear sweep voltammetry of hematite (α -Fe ₂ O ₃).....	88
3.4.3 Linear sweep voltammetry of WO ₃ -RGO.....	89
3.4.4 Linear sweep voltammetry of WO ₃ - α -Fe ₂ O ₃ (lite) nano composite	90
3.4.5 Linear sweep voltammetry of WO ₃ - α -Fe ₂ O ₃ (dark) nano composite	91
3.4.6 Linear sweep voltammetry of α -Fe ₂ O ₃ (dark) -RGO nano composite.....	92
3.4.7 Linear sweep voltammetry of WO ₃ - α -Fe ₂ O ₃ (lite) -RGO nano composite	93
3.4.8 Linear sweep voltammetry of WO ₃ - α -Fe ₂ O ₃ (dark) -RGO nano composite	94
3.5 Conclusions.....	95-96
3.6 References.....	97-110

CHAPTER 1

INTRODUCTION

1.0 Hydrogen as a fuel source:

Hydrogen is a renewable energy source and global energy demand is increasing rapidly. Primary source of energy for global economy is fossil fuels. Fossil fuel are non-renewable energy source and is replaced by hydrogen as a new future fuel. Hydrogen is an only carrier for future fuel [1-4]. Hydrogen has a potential to meet the energy demands in future and as a clean non fossil fuel in the future .There is a lot of space still between our required global energy demand which is just 2% (13 Tera watt) and potential of the sun which is still untapped is (120,000 Tera watt).

1.2 Why is hydrogen so important?

Hydrogen is ~75% of the known universe. On earth, it's not an energy source like oil or coal. Only an energy carrier like electricity or gasoline a form of energy, derived from a source, that can be moved around [5-7]. The most versatile energy carrier, can be made from any source and used for any service, readily stored in large amounts.

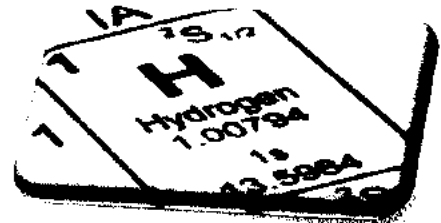


Figure1.1: hydrogen the first element in periodic table

Almost never found by itself; must be liberated,

“Reform” HCs or CHs with heat and catalysts.

“Electrolyze” water (split H₂O with electricity).

Experimental methods: photolysis, plasma, microorganisms.

1 kg of H₂ contains same energy as 1 U.S. gallon

of gasoline, which weighs not 2.2 but 6.2 pounds

1.2.1 How hydrogen can be used as fuel source?

Hydrogen is a promising solution to global oil dependence. Hydrogen's availability is limited in atmosphere that's why it is produce from other elements and compounds. One method to produce hydrogen is reforming natural gas but the most simplest and efficient way to produce hydrogen is called “electrolysis”. Electrolysis involves the splitting of water required an external DC supply [8].

1.2.2 Draw Back Of Electrolysis?

Drawback of electrolysis is that it required external voltage for hydrogen production.

1.3 Hydrogen applications

1.3.1 Internal combustion engines

Internal combustion engine is a type of heat engine which utilizes an air to combust the fuel, expansion of gases at high temperature and high pressure apply force on some components of the engine, these forces allow a gap in components which cause conversion of chemical energy into the mechanical energy.



Figure1.2: Internal combustion engine which uses a hydrogen as a source fuel

1.3.2 Fuel cells

Secondly, it can be used in fuel cells to store energy and produce electricity, fuel and a power source for vehicles. A fuel cell is like a battery in that it generates electricity from an electrochemical reaction. Fuel cells and batteries both convert chemical energy into electrical energy and it's by product into heat.

However, a closed store of energy is holded within a battery and once this store energy is depleted it must be replaced or discard or another option is to recharge it by using a DC supply to reverse the

electrochemical reaction. A fuel cell run indefinitely as long as hydrogen and oxygen supply is available [9] . Hydrogen is refer to as a fuel source and it gives it a name "fuel cell" and there is no combustion involved hydrogen oxidation take place electrochemically, during oxidation oxygen and hydrogen atom combine

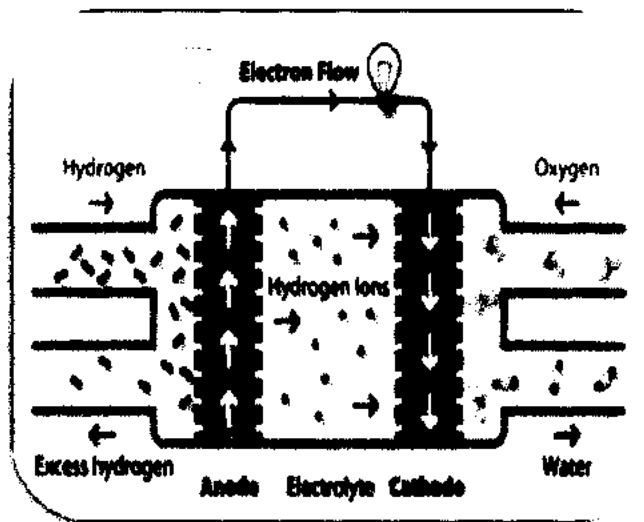


Figure1.3: (PEMF) proton exchange membrane fuel cells mechanism.

to form water, and electrons are released in this process and flow through an external circuit as a carriers for electric current.

Fuel cells can vary from tiny devices producing only a few watts of electricity, right up to large power plants producing megawatts.

"The "forever fuel" that we can never run out of"

Water + energy \longrightarrow hydrogen + oxygen

Hydrogen + oxygen \longrightarrow water + energy

1.4 Hydrogen demand upto 2050

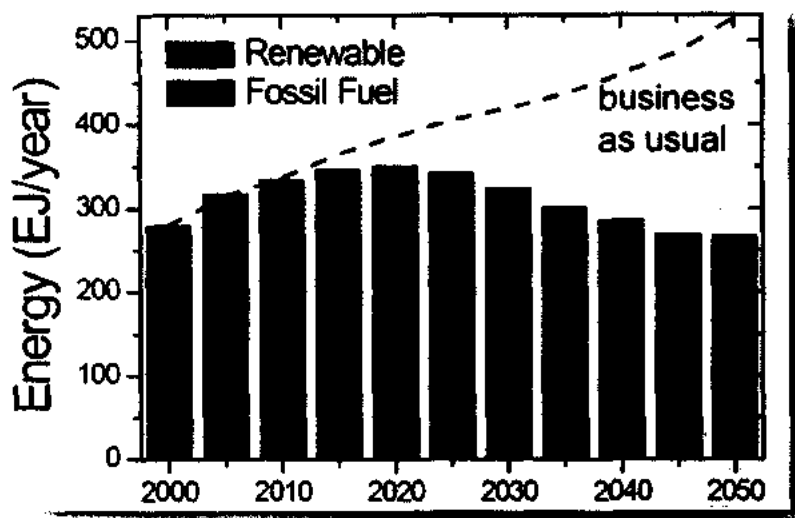


Figure1.4: Global energy demand up to 2050

World's energy demand will increase to double up to 2050, so there is a need of a renewable energy source in cover coming the world's requirement of energy i.e electricity and hydrogen etc. Sun is a best source to full fill this requirement, therefore there is a need of efficient system which full fill the global energy demand up to 2050 , PEC water splitting approach is best solution to all the problems, through which we will be able to get renewable energy i.e hydrogen , and electricity [10].

1.5 Artificial Photosynthesis:

A chemical process called artificial photosynthesis is replica of photosynthesis. It is a process that converts sunlight, water, and carbon dioxide into carbohydrates and oxygen [11-25]. This term is related to any scheme for harvesting and capturing energy from sunlight in the chemical bonds of the fuel. Photocatalytic water splitting is the main research area in artificial photosynthesis [25-29], Photocatalytic water splitting converts water into hydrogen and oxygen.

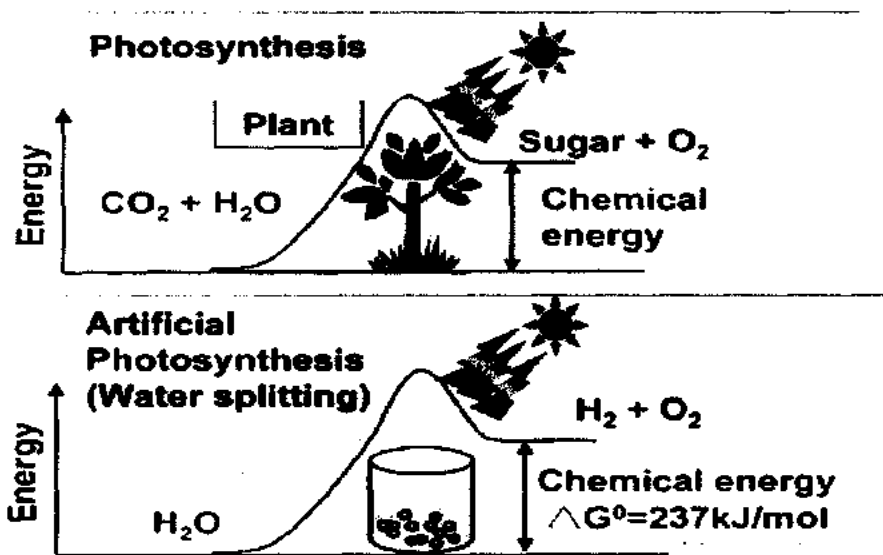


Figure 1.5: photocatalytic water splitting an artificial photosynthesis

There are many technologies such as solar heating, solar photovoltaics, solar thermal electricity for harvesting solar energy [29-38], but artificial photosynthesis is the one that could full fill all energy demands as it produces actual liquid fuel.

1.6 PEC water splitting approach:

The important technical issue facing humanity is the development of the long lasting sustainable energy economy. Although global energy demand is full fill by sufficient coal reserves which provide energy needed for centuries, but this strategy rise with catastrophic societal expense, to achieve environmentally sound and cost effective technologies that will meet the global need of energy consumption that is 15 Tera watt

is just by scientific discoveries and innovations, that global energy demand will increase to 30 Tera watt by the year 2050 [39-51]. The only technology called “solar PhotoElectro-Chemical (PEC) “hydrogen production that has potential to full fill all energy demands of the future and it provide cost effective ,clean and domestically produced energy carrier by advantage of 120,000 TW of sun radiations that strikes the earth surface.

1.6.1 History:

Discussion for PEC water splitting for hydrogen production has been carried out for decades but first demonstration was in 1972. Estimated world record solar to hydrogen efficiency still achieved is 12.4% and was achieved over a decade ago in 1998 [52].

-PEC technology combines the features of electrolysis and light harvesting of solar energy [53, 54]. In this PEC cells semiconductor which acts as a working electrode is immersed in a electrolyte and irradiated with sunlight ,then conversion in energies take place i.e photon energy to electrical energy ,which is used for splitting of the water i.e into hydrogen and oxygen (chemical energy) [55]. Solar energy is inherently converted into a more store able form of energy i.e in the chemical bonds. A general schematic [55-58] of a laboratory photo electrochemical cell is shown in Figure 1.6.

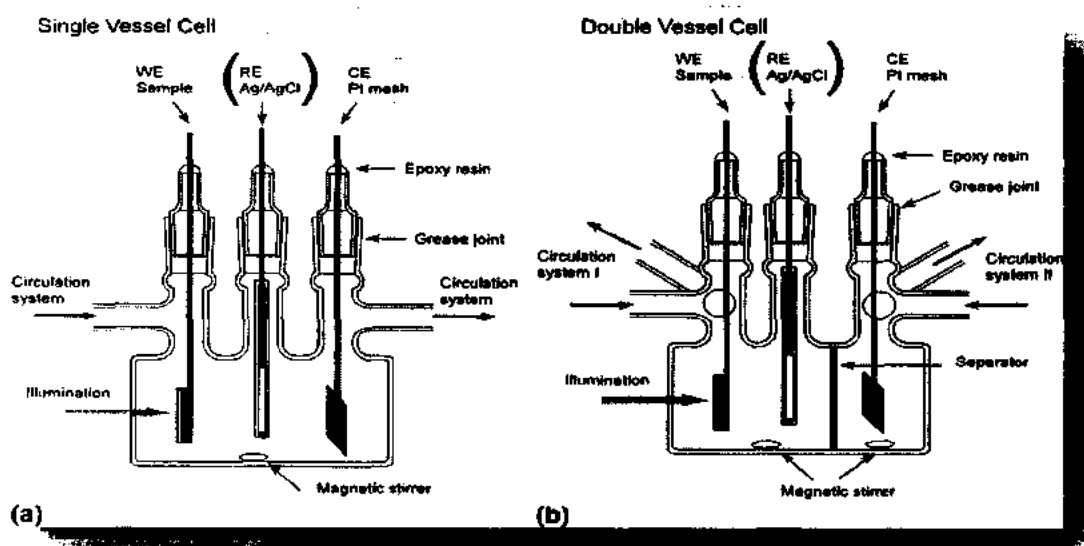
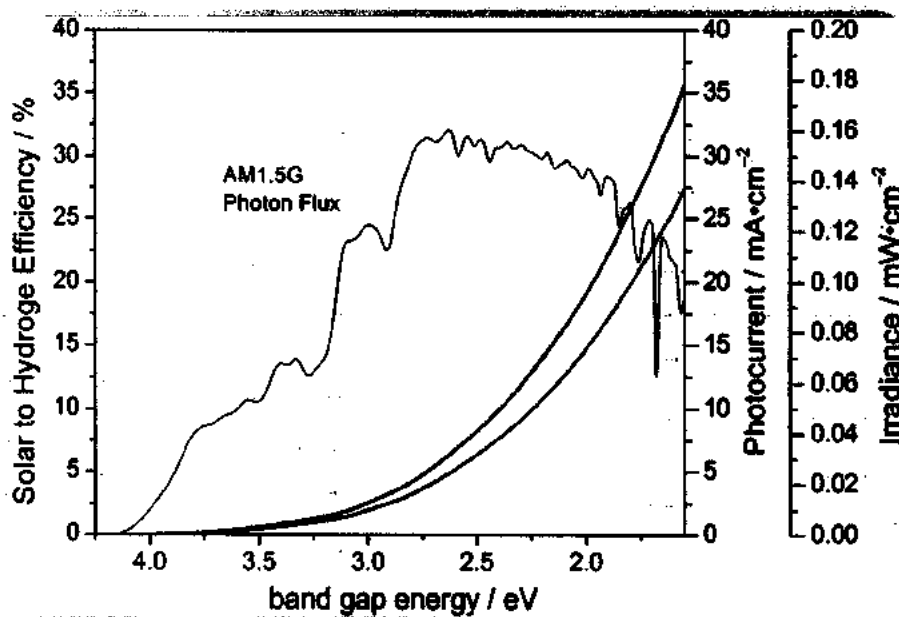


Figure1.6: photo electrochemical cell (PEC) (a) single and (b) double vessel cell.

For PEC water decomposition to occur there are several criteria's which should be full filled.

- Sufficient voltage should be generate by semiconductor system upon irradiation to split water.
- Band gap of bulk should make efficient use of solar spectrum.
- Band edge potentials on the surface must straddle the oxygen and hydrogen redox potentials.
- Semiconductor system should have long term stability in electrolyte.
- Charge transfer mechanism from the surface of the semiconductor to the solution must only for the water splitting mechanism rather than corrosion or for energy losses due to kinetic over potentials.



To date no material still satisfied these requirements fully.

Figure 1.7: STH conversion efficiencies in accordance with band gaps, photo currents and photo irradiance

1.7 Efficiency definitions of PEC

To characterize PEC device the most important measurement is STH (solar to hydrogen) efficiency. Materials are thus define by their high STH efficiency, and it is

the single measurement through which all PEC cells can reliably ranked against one another.

Unfortunately published literature have in valid mathematical relations and calculations to find the solar to hydrogen conversion efficiency and mostly improper experimental methods for calculating efficiency values and wide scale reporting of STH which is not a true efficiency benchmark.

There are several advantages and pitfalls for different type of efficiency measurements

Due to the several different measures of efficiency that's why there exists much pluralism in demonstrating PEC efficiency [59-62].

Four primary measures of efficiency exists and they are split into two main categories as described below,

1. The Benchmark efficiency (suitable for main stream reporting)

- Solar-to-hydrogen conversion efficiency (STH)

2. The Diagnostic efficiencies (to understand material performance)

- Applied bias photon-to-current efficiency (ABPE)
- External quantum efficiency (EQE) = incident photon-to-current efficiency (IPCE)
- Internal quantum efficiency (IQE) = absorbed photon-to-current efficiency (APCE).

1.7.1 Benchmark efficiency

The most important measurement of all the efficiencies for pec water splitting device when exposed to solar air mass 1.5 Global illumination is STH efficiency under zero bias conditions [63-69].

Meaning of zero biasing is that there is no external applied voltage between counter electrode (CE) and working electrode (WE). For 2 electrode system WE and CE should be short circuited, for measuring solar to hydrogen efficiency calculating the solar to hydrogen conversion efficiencies open circuit voltage v/s voltage should never ever be involved.

Same PH electrolyte should be used to calculate the accurate solar to hydrogen conversion efficiencies.

$$\text{STH efficiency} = \frac{\text{Chemical energy produced}}{\text{Solar energy input}}$$

$$\text{STH} = \left[\frac{(\text{mmol H}_2/\text{s}) \times (237 \text{ kJ/mol})}{P_{\text{total}} (\text{mW/cm}^2) \times \text{Area} (\text{cm}^2)} \right]_{\text{AM 1.5G}}$$

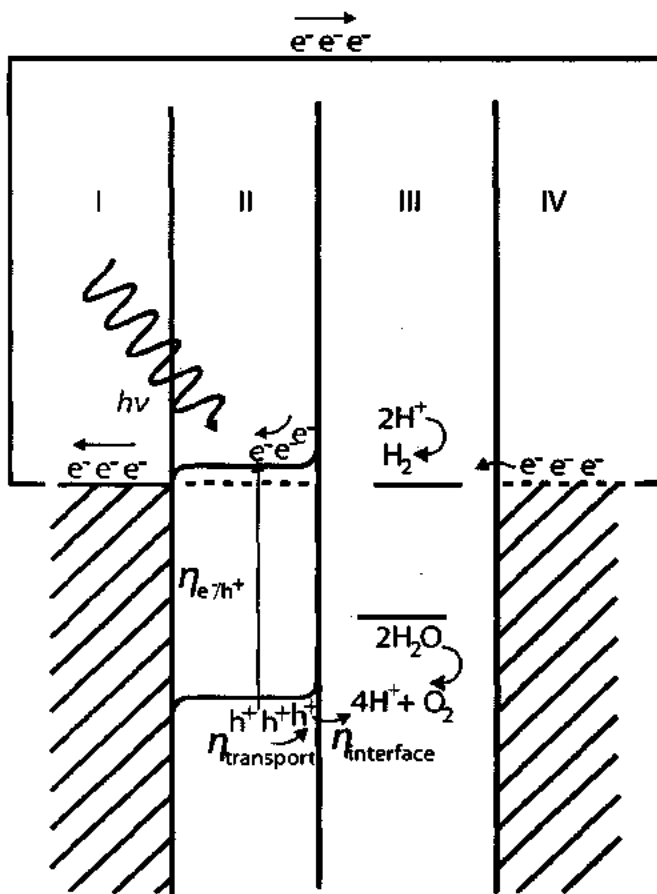


Figure 1.8 various process held in PEC water splitting cell e^-/h^+ excitation, transportation of charge, absorption of photons and reactions at interface. Region I (ohmic contact), region II (n-type semiconductor), region III (electrolyte), region IV (counter electrode)

1.8 Production of H₂ from Water Using Solar Light

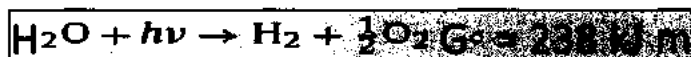
It is a great technological challenge to develop that sort of renewable energy carrier that doesn't utilize fossil fuel. Production of hydrogen as a renewable energy carrier is of great important and it is only attractive option ahead. Industrial production of hydrogen consumes huge amount of fossil fuel and required large amount of budget and resulting by products involves CO₂ emissions.

Hydrogen water splitting is the clean approach towards the hydrogen production and without utilization of huge amount of fossil fuel and budget and by products [70].

In photo electrochemical cell (PEC) water splitting, solar light is converted into chemical energy and increase in Gibbs free energy by water splitting [71-73].



Figure 1.9: H₂ evolution in PEC cell



Photosynthesis in green plants resembles PEC water splitting or we can say that it is artificial photosynthesis. Similarly, semiconductor heterogeneous photo catalysts have lot of advantages over the PEC systems and due to the lower cost and simplification in its synthesis and utilization[74, 75].

Approximately, 100 metal oxide photocatalytic system has been reported so far and they are active for water splitting and production of hydrogen and oxygen [76-78], they required ultraviolet (<400) mostly due to the large band gaps of semiconductors. Solar light which fall on earth covers visible region (400-800 nm) figure 1.10 .Therefore, it is essential to utilize the visible light efficiency for the production of hydrogen on a large scale through pec water splitting[79-85]. Different efficiencies can be counted in different spectrum regions i.e in UV region 2% STH conversion efficiency, in visible region upto 600 nm there is a drastic change in STH conversion efficiency that would increase to 16% and upto 800 nm STH conversion efficiency exceed to 32%.

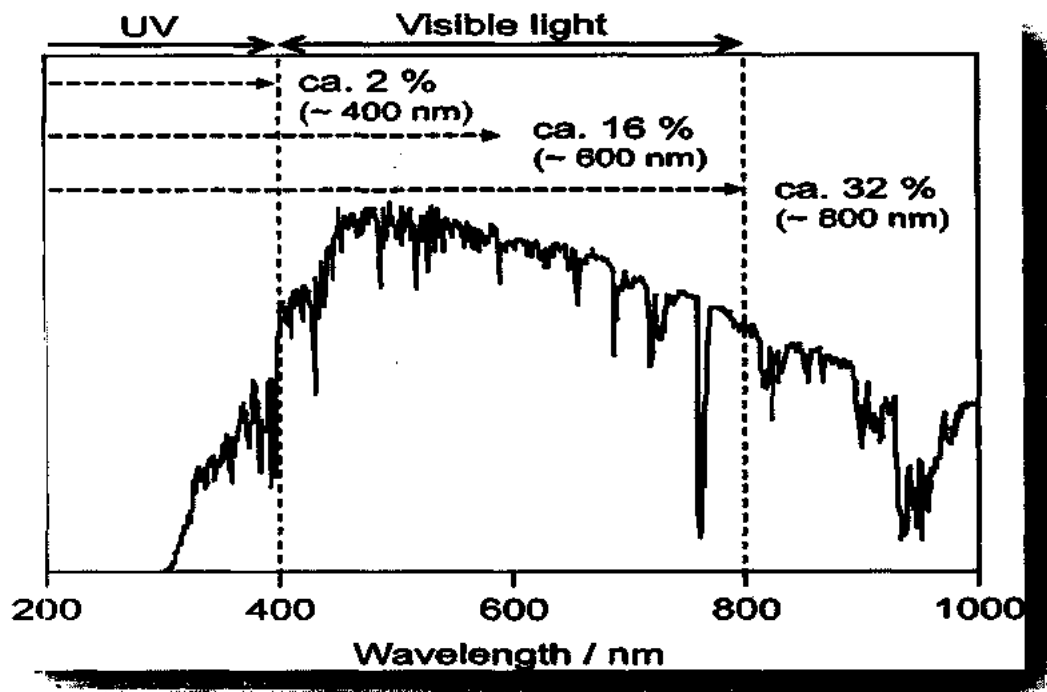


Figure 1.11: solar conversion efficiencies for photoelectron chemical water splitting phenomena.

1.9 Materials for pec water splitting:

Materials suitable for pec water splitting are semiconductors. Semiconductors absorb photons and release (convert to) electron hole pair [86-97]. How semiconductor materials are best for efficient pec water splitting..... ?

1.9.1 Semiconductor's a suitable material for pec water splitting:

Electrons occupied discrete levels according to quantum mechanics, but Pauli's exclusion principle applied this restrictions because according to this principle "no two electrons can occupy same set of 2 quantum numbers" [98-103]. When molecular orbitals combine together they formed anti-bonding and bonding energy levels, when more and more atoms combined together they give rise to energy levels which are called valence band and conduction band. Valence band is always filled with electrons and conduction band is empty at Zero kelvin.

Conduction and valence band are different from each other by a band known as "forbidden gap or band gap". in forbidden gap no energy state exists.

There are three different types of materials who are classified on the basis of their band gap as shown in the figure 1.12

- Conductors
- Semiconductors
- Insulators

Overlapping of band gap occurs in conductors (1 ev) such as metals, whereas insulators (8 ev) have wide band gap which don't allow free electrons to participate in conduction. In between both of conductors and insulators, semiconductors exists. Semiconductors have band gap of 3ev approximately, at zero kelvin semiconductors behave like insulators, but increasing temperature electrons gain sufficient energy to take part in conduction.

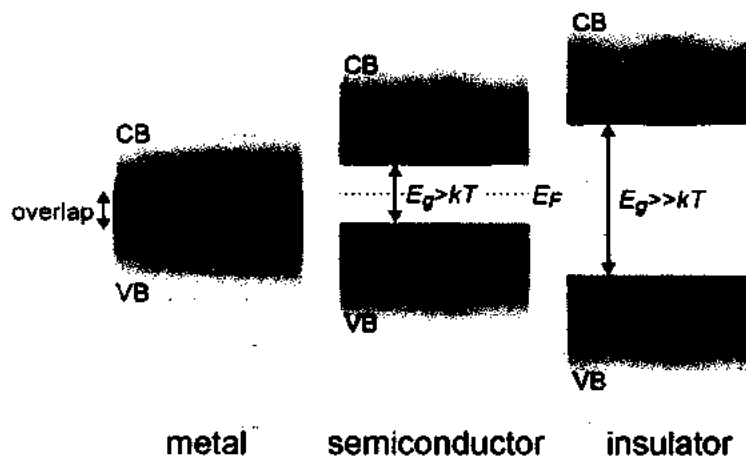


Figure 1.12: band gaps of metal, semiconductor and insulator.

Semiconductors have very unique properties that is the reason they are globally used in different research areas and being utilized as a novel material. Why semiconductors have this unique behaviour?...semiconductors have combine properties of conductors and insulators. Firstly, semiconductors have band gap in range of 1-3ev but this band gap is not sufficient enough for thermal excitation of the electrons to occur at room temperature.

Secondly, semiconductors have energy range which lies in energy range provided by sunlight. This property make semiconductors very unique and reliable for pec water splitting and in solar cells and in many other applications as well. Thermal excitation of electrons occur upon illumination. Creation of two mobile carriers occur due to excitation, first one are photo generated hole in the valence band and second carriers are photo generated electrons n the conduction band. Both the carriers have their own specific role in solar cells and pec water splitting mechanism.

For practical applications intrinsic semiconductors are doped according to the requirement, this doping is mostly done due to the relatively poor conductivity of the semiconductors. Through doping there conductance is rectify. This type of semiconductors are extrinsic semiconductors. There are two types of dopants depending on their valencies, acceptors and donors. When semiconductor is doped with 3rd group elements then holes are majority carriers who have tendency to accept electrons, that's why these semiconductors are called acceptor doped semiconductor's or p-type semiconductors [104-112]. When semiconductor is doped with 5th group elements then electrons are majority carriers who have tendency to donate electrons, that's why these semiconductors are called donor doped semiconductor's or n-type semiconductors[113-117].

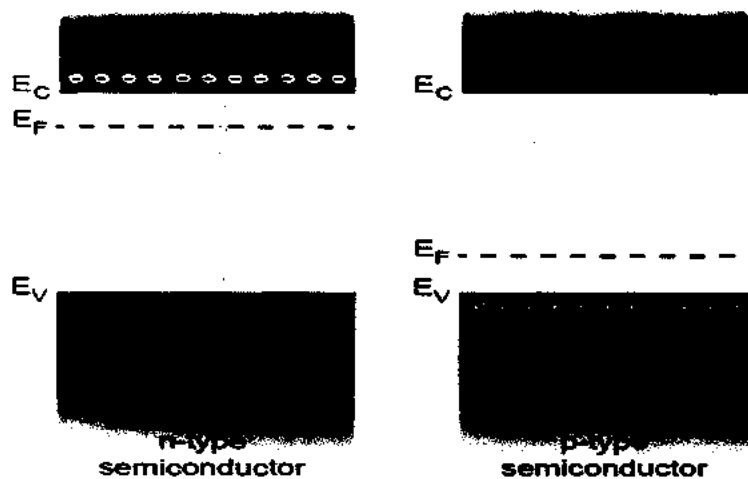


Figure 1.13 Energy band diagram for N-type and P-type semiconductor's.

1.10 Interface of semiconductor and electrolyte

In pec cells arrangement of electrodes are such that semiconductor anode and counter electrode is immersed in electrolyte. Now here is a question that what mechanism occur when semiconductor has a contact with the electrolyte.

When semiconductor contact with the electrolyte, charge transfer mechanism take place .charge transfer mechanism take place unless the electrochemical equilibrium is reached, which don't allow further charge transfer reaction to take place.

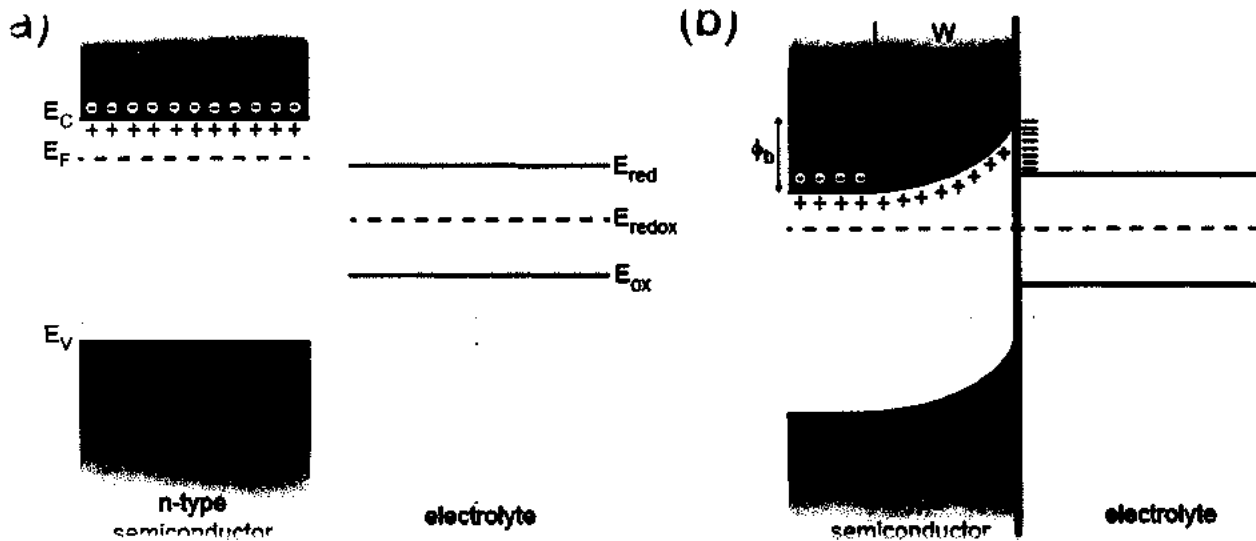


Figure 1.14: energy band diagram when n-type semiconductor are at equilibrium (a) Formation of Space Charge region when potential is applied (b).

In the figure 1.14 whole charge transfer mechanism is shown, in semiconductor species the number of ionized (+) acceptors and ionized (-) donors are at equilibrium.

When n-type semiconductors is in contact with the electrolyte charge transfer mechanism take place such that electrons move towards the electrolyte from the semiconductor ,when redox potential of the electrolyte and Fermi level of semiconductor reached at the same level the no further transfer of electron take place further, at this equilibrium condition ,upward bending of n-type semiconductor takes

place and formation of space charge region/layer where electrons are depleted across the semiconductor/electrolyte interface.

Space charge region has a vital role in pec water splitting because this region established a potential drop , this potential drop established a electric field , this electric field act as a barrier between the photo generated holes and photo generated electrons and don't allow them to recombine ,in other words it hinders recombination. More width of the space charge region, there will be slow recombination which increase the solar to hydrogen conversion efficiency (STH) [118-125].

In n-type semiconductor motion of carriers are such that photo generated electrons semiconductor/FTO interface. Similarly, Photo generated holes move towards the semiconductor/electrolyte interface.

Hence, different types of efficiencies are associated with STH conversion efficiency within this mechanism [125-132].

$$\text{Separation efficiency } (\eta_{\text{STH}}) = \frac{\text{total amount of electrons and holes reaching the interface}}{\text{Total amount of photogenerated } e^-/h^+ \text{ pair}}$$

$$\text{Catalytic efficiency } (\eta_{\text{cat}}) = \frac{\text{Amount of holes that undergo water oxidation}}{\text{To the ones reaching the semiconductor/electrolyte interface}}$$

$$\text{Absorption efficiency } (\eta_{\text{abs}}) = \frac{\text{Amount of electron-hole pair regenerated}}{\text{Amount of the incident photons}}$$

Accession No. TH-14946

$$1.11 \text{ STH}(\eta_{\text{STH}}) = \eta_{\text{sep}} * \eta_{\text{cat}} * \eta_{\text{abs}}$$

Hence, for n-type semiconductors water oxidation take place across the anode due to the transfer of holes from semiconductor/electrolyte interface and reduction at the cathode because electrons from the external circuit reaches the cathode and undergo water reduction reaction[133-142].

Same process occur for PEC splitting for p-type semiconductor except reverse the reactions and oxidation takes place on its surface and reduction on the counter electrode. Half reactions occurs at the surface of the semiconductor in PEC water splitting mechanism. Depending on the type of the semiconductor oxidation and reduction take place i.e

- n-type semiconductor is called "photo anode (oxidation)"
- p-type semiconductor is called "photo cathode (reduction)"

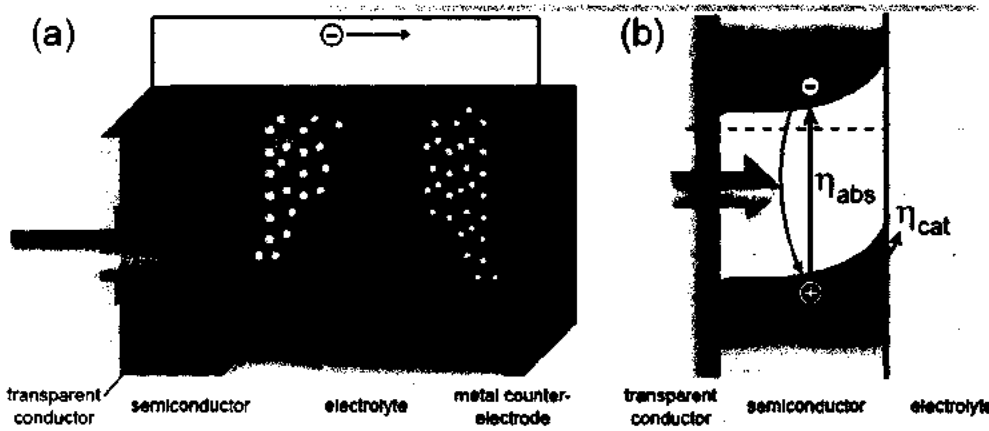


Figure 1.15: upon illumination on n-type semiconductor (a) efficiencies involved due to PEC mechanism.

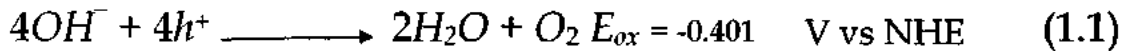
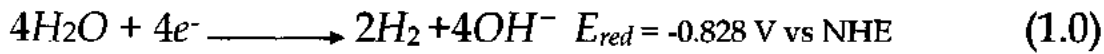
Fermi level of the semiconductor is at higher potential than that of the solution or electrolyte. To achieve equilibrium electrons must move/flow into the electrolyte from the semiconductor, this dampness of the electrons into the electrolyte reduce the E_f and equilibrium is maintained, this disrupting charge neutrality of semiconductors develop the built in voltage (V_{sc}).

$$V_{sc} \text{ (built in voltage)} = \text{Electrostatic potential at the surface} - \text{Electrostatic potential at the bulk}$$

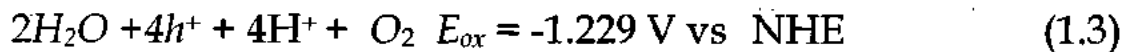
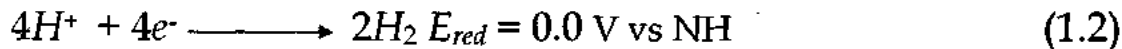
This built in voltage forms "depletion region ". Depletion region is deprived of the electrons- hole pair or we can say that it is field free region, this charge difference creates electric field

1.12 Mechanism followed for PEC water splitting.

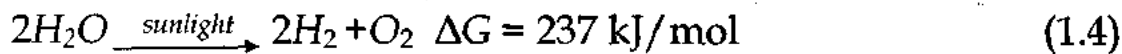
For n type semiconductor band bending is upward .PEC cell schematic illustration of n-type semiconductor [143-145]and counter electrode as a metal is immersed in desired electrolyte is shown in figure [146-158], Reduction and oxidation reactions for alkaline electrolyte are,



Reduction and oxidation reactions involve in acidic electrolyte are,



Overall water splitting mechanism can be written as the follows:



$$\text{Absorption efficiency } (\eta_{abs}) = \frac{\text{Amount of incident photons created}}{\text{Amount of incident photons}}$$

There are two possible transport mechanism through which electrons and holes are separated, (1) Drift (2) Diffusion.

1.13 Graphene as a transporter

Due to graphene's excellent electron mobility and enhanced surface area ($2600\text{m}^2\text{g}^{-1}$), Graphene can be utilize in enhancing the photocatalytic efficiency of semiconductor (photo-catalyst)[159-175]. In photocatalytic areas the graphene-semiconductor composites have pull a attracted demand.

Graphene is a thin 2D sheet of single sp^2 bonded carbon atoms arranged themselves in a periodic hexagonal structure.

Graphene enhanced electrochemical, mechanical and electronic properties, high electrical conductivity (108 S m^{-1}) and high thermal conductivity of ($5000\text{ W m}^{-1}\text{ k}$) had gained a lot of attention, graphene's application in photovoltaics and in energy conversion, materials i.e in batteries and PEC (photo electrochemical cell), energy demand will be double in 2050, hence there is a need of efficient material which full fill all these requirements. According to new researches when Graphene absorb photon then it generates multiple electrons, therefore Graphene is now considering an efficient substrates then ITO and silicon substrates. graphene enhance the STH conversion efficiencies when make composite with metal oxides.

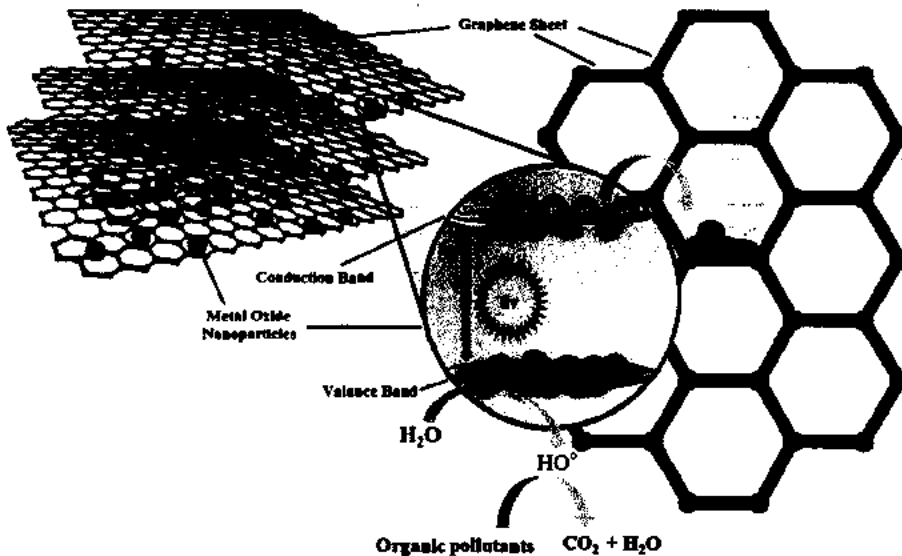


Figure 1.16: Graphene-Metal Oxide nano composite as photocatalysts.

1.14 Scope and aim of the thesis:

In this thesis, semiconductor-Graphene nano composites thin films of different metal oxide e.g α -Fe₂O₃ and WO₃ are explored, which are used as photo anodes in efficient PEC (Photo electrochemical) water splitting.

Research direction and aim is to improve the visible light absorption of α -Fe₂O₃ and WO₃ by utilizing Graphene as a electron acceptor and transporter .Graphene's enhanced surface area (2600 m² g⁻¹), excellent electrical conductivity (10⁸ Sm⁻¹), high thermal conductivity (5000 Wm⁻¹k) and its high tensile strength make it promising material to use in energy conversion devices. Graphene enhance the electrical conductivity and hence its efficiency. In this thesis electrochemical properties of metal oxide nano-composites with graphene are investigated by linear sweep voltammetry (LSV) and observed their synergic effect. Objective of thesis is to enhance the Solar to hydrogen (STH) conversion efficiencies by designing a metal oxide-graphene composite photo anode which should be efficient enough to split the water and improve hydrogen and oxygen evolution rates , hence efficient PEC cell requirement is needed to check un denying need of electricity and renewable energy sources in coming years .

CHAPTER 2
EXPERIMENTAL METHODS AND
MATERIALS

2.1 Synthesis of Graphene from Graphite by modified Hummers method:

Reagents:

1. Commercial graphite
2. Hydro chloric acid
3. Distilled water
4. Ethanol
5. Acetone
6. Potassium permanganate
7. Hydrogen peroxide
8. Fluorine doped tin oxide substrates
9. Sulphuric acid

2.1.1 Purification of commercial graphite:

Modified hummers method is used for purification of commercial graphite.

Take 3g of commercial graphite and mix it in 225 ml of HCL/HFA, then stir the solution for 2 hours to fully disperse the graphite layers.

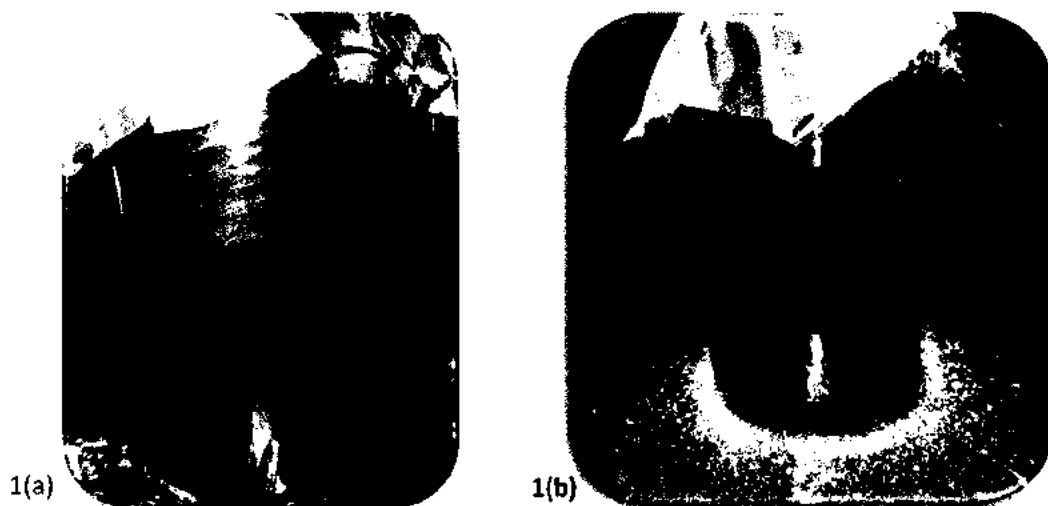


Figure2.1: Dispersed layers of graphite (a) purification of commercial graphite (b)

Neutralise the PH, by several washing steps, washing is done by distilled water. Stir the mixture for 1 hour and then decant, similarly add (40 ml) ethanol and acetone for further washing to normalize the PH .Then filtration through suction pump with 0.2 micron pore size filter paper. After filtration collect the paste in china dish carefully and dry the sample in vaccum oven for 6 hours at 100°C. After drying grind the powder through motor and piston for refinement. Greyish shiny powder is obtained, at the end we get fine pure graphite.

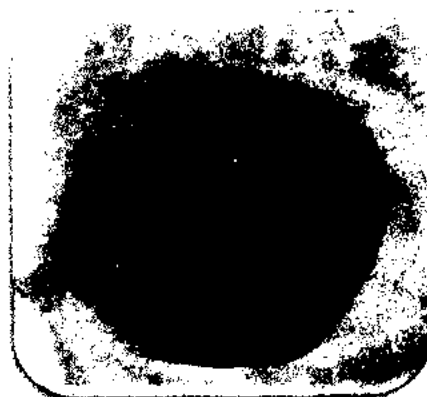


Figure2.2: pure graphite

2.1.2 Oxidation of graphite

Product obtained from the above procedure is 2.4g. Now take 1.25 g of sodium nitrate and 2g of graphite, such that it would be in 1:2 ratio. Then grind it to homogenize the powder.

Take 150 ml/g of sulphuric acid and add 3g (1g sodium nitrate and 2g graphite) and mix them, fumes were observed due to the heat operation of acid.

Ice bath

During regular stirring add 6g of potassium permanganate and 3g of purified graphite. Add potassium permanganate gradually otherwise it will spoil the sample.

After adding potassium permanganate ($KMnO_4$) temperature rises but care should be taken that it should be in range of 5-10°C. Then, stir it for 30 min when temperature settled down then exothermic reaction stop [176-178].

Now, remove the ice bath and simply placed it on the hot plate for 18 hours at 35-40°C. After 18 hours graphite oxide form .Add distilled water for washing and stir it for about 15-min and decant the solution.

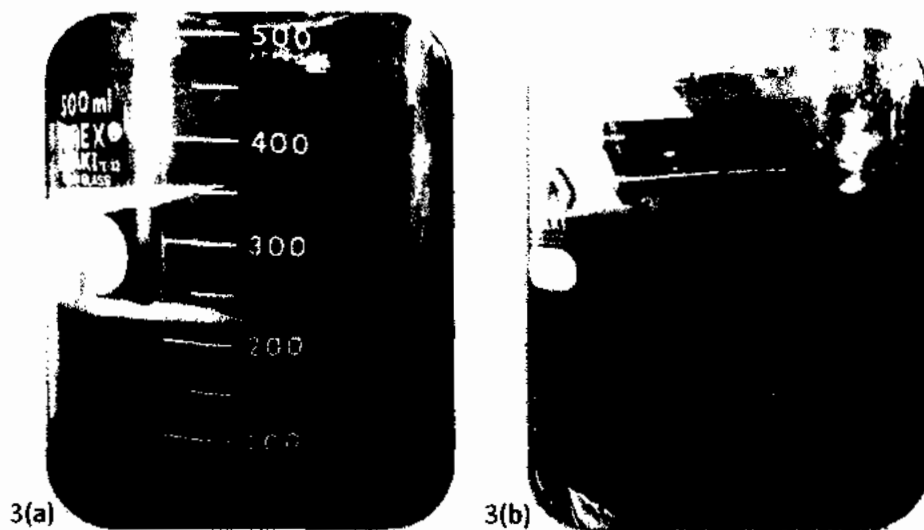


Figure 2.3: brownish paste obtained during oxidation of GO (a) washing of GO (b)

Again add water (50 ml) and also add 5-6 ml of hydrogen peroxide, which is used for oxidation. Add hydrogen peroxide during stirring to normalize the PH.

Add 200 ml of distilled water and again stir it for 10-15 minutes and allow residue to settle down and then decant the solution.

After decantation 30 ml of hydrochloric acid for further washing and 50 ml of distilled water and again decant it. At the end, use ethanol/ acetone (20-30 ml) for washing.

Now stir the solution for 15 min and check the PH, if it is normalized then we get graphene oxide.

Filter the solution it will take 4-5 days through suction pump. After filtration copper like brownish paste is obtained. Collect the paste in china dish and dry it in vacuum oven at 80°C, till it dry. When it will dry we get mat black sheets of graphene, grind to get fine blackish powder of graphene.

2.1.3 Reduction of graphene

Effective way to reduce graphene oxide is through chemical method[179].

Take 1.4 g of graphene oxide in 70 ml of distilled water, add 30% of ammonia and adjust its PH to 10.

Now, add 2 ml of hydrazine and stir it for 10 minutes and transfer it in 100 ml autoclave for 80-200°C for 3 hours.

Its collection by centrifugation. Washing is done with distilled water, then filter the solution and dry it at 80°C for 2 hours. Grind sheets carefully.



Figure2.4: Reduced Graphene Oxide

Shiny black powder of Reduced Graphene Oxide is obtained.

2.2 Hydrothermal Synthesis of Hematite ($\alpha\text{-Fe}_2\text{O}_3$) nano particles with different precursors:

2.2.1 Method 1

Prepare 0.1 molar solution of iron chloride ($\text{FeCl}_3 \cdot 2\text{H}_2\text{O}$) in 50 ml of distilled water. Similarly, also prepare 0.1 molar sodium hydroxide (NaOH) solution in 20 ml of distilled water.

Mix 2 solution in 100 ml beaker, Add 5 ml of tween 80 which is used as a surfactant. Stir the solution for 20 min to homogenize the mixture, After stirring, place that solution in 100 ml autoclave, care should be taken that autoclave is tightly screwed or closed, now place it in vaccum oven for 5 hours at 130°C.



Figure2.5: washing of $\alpha\text{-Fe}_2\text{O}_3$ particles.

After 5 hours and 40 minutes, sample mixture is taken out of the autoclave in 200ml beaker Next step is washing, which is done by distilled water, now decant the solution after 5-6 hours.

Collect the particles by filtration, Colour of particles are rusted sort off.

Now, filter the solution and dry the sample for 3 hours at 80°C.

2.2.2 Method 2

Second method followed the same steps as described in method 1, but we just change the salt and quantities of the precursors.

Prepare 0.1 molar solution of iron nitrate in 50 ml of distilled water .Also, 0.1 molar solution of sodium hydroxide in 25 ml of distilled water. Now mix both solutions and add 4-5 ml of tween 80, Stir the solution for 30 minute to homogenize the mixture.

Place the solution in 100 ml auto clave, and place it in oven for 5 hours at 130°C.

Take the viscous mixture out of auto clave in 200 ml beaker, which is orangish in colour. Next step is washing to neutralize the PH of the solution, done by using distilled water. Filter the solution at the end and dry it at 80°C in vaccum oven for 2 hours. After drying, collect the orangish particles in glass viol.

2.2.3 Method 3

Prepare 0.1 molar solution of iron (III) chloride hexa hydrate ($\text{FeCl}_3 \cdot 6\text{H}_2\text{O}$) in 50 ml of ethylene glycol (EG).



Figure 2.6: viscous suspension of $\alpha\text{-Fe}_2\text{O}_3$ nano particles obtained after hydrothermal treatment (a) washing of $\alpha\text{-Fe}_2\text{O}_3$ nano particles (b) dried powder sample.

Stir the solution for 30 min to homogenize the mixture , now place the solution in auto clave for 15 hours at 130°C in vaccum oven[180, 181]. Reddish mixture is obtained, dilute the solution and filter it, and dry it at 40°C for 5 hours in vaccum oven. Rich red powder is obtained after drying.

2.3 Hydrothermal Synthesis of tungsten trioxide (WO₃) nano particles

2.3.1 Method 1

Add 2 grams of sodium tungstate (Na₂WO₄·2H₂O) in 60 ml of distilled water to prepare solution, stir the solution for 5 minutes and add 0.4 grams of sodium chloride (NaCl) in the solution and stir it for 3 hours.

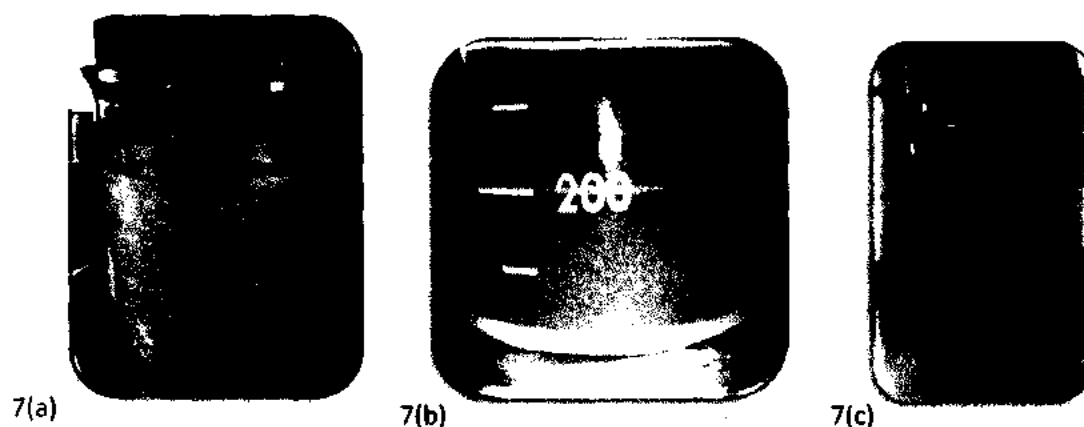


Figure 2.7: solution preparation, washing, dried powder sample (a), (b), (c)

Now add hydrochloric acid (HCL) drop wise to maintain its PH at 2, and stir the solution for 2 hours. Now place the solution in 100 ml auto clave for 6 hours at 180 °C in vaccum oven. Final product is collected by centrifugation by different steps of washing using distilled water. Dry the product in the vaccum oven at 25°C for 30 minutes .Yellowish particles are obtained, collect them in glass viol.

2.3.2 Method 2

Make a solution of 0.4 g of citric acid and 0.52 g of sodium tungstate in 300 ml distilled water. Stir the solution for 30 minutes, and add hydrochloric acid drop wise to maintain its PH to 1 , yellowish turbid solution is formed

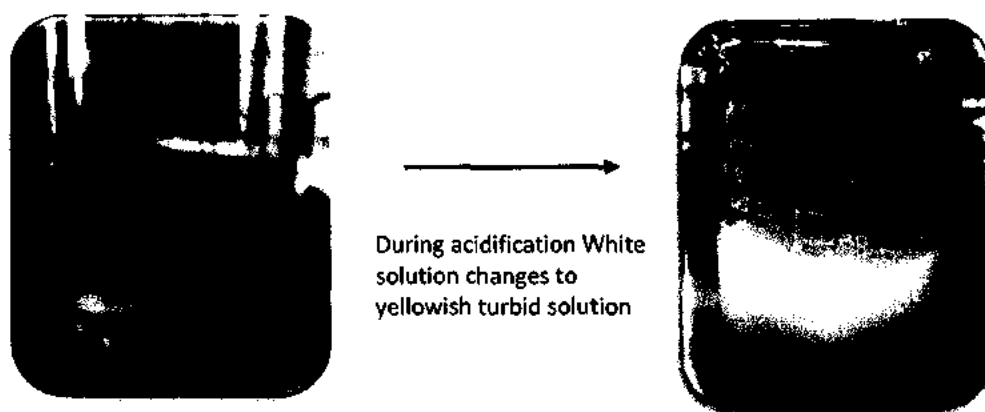


Figure 2.8: acidification during reaction, cause formation of yellowish turbid solution.

Transfer the solution in Teflon lined stain less steel autoclave at 120°C for 12 hours, Allow autoclave to cool down at room temperature[182].

Now, washed the yellow precipitates with ethanol and their collection by centrifugation.

Dry them in vaccum oven at 80°C for 24 hour. Pale yellow nano particles of tungsten trioxide are obtained. Collect them in glass viol.

2.4 Thin film deposition on Fluorine doped tin oxide (FTO) substrates

Thin films are deposited by different methods but here we use 2 methods;

- Hydrothermal deposition method.
- Spray deposition.

2.4.1 Substrates Cleaning:

Kept FTO's in acetone for 3 hours for sonication, then place them in ethanol for 2 hours followed by sonication. At the end sonicate them in distilled water for 1 hours. Dry them under nitrogen environment.

2.4.2 Spray deposition

Precautions

Spray gun should be kept 12 inches above the the substrate .Avoid changing the position and distance it cause non uniform deposition of films.

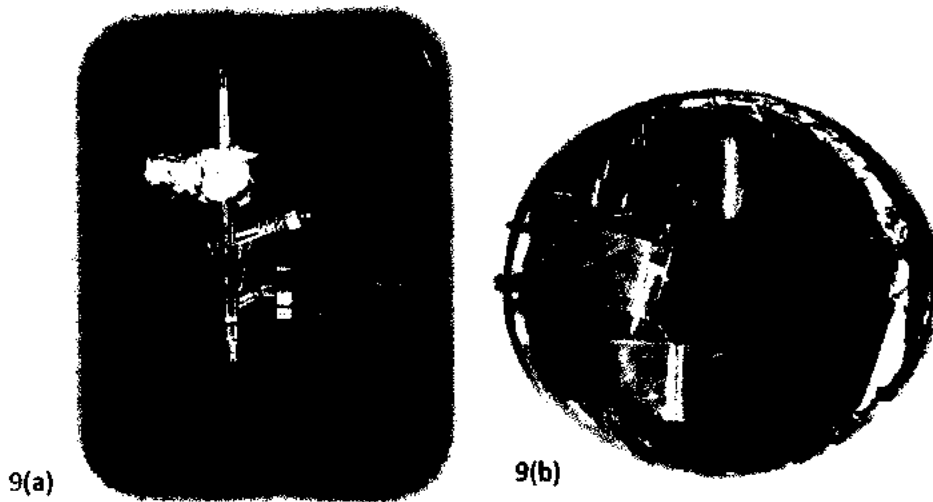


Figure2.9: spray gun (a) films deposited through spray gun (b)

2.4.2.1 Iron oxide (α - Fe_2O_3) nano particles deposition on FTO (prepared from method 1 and method 3)

For a thin film deposition of nano particles, 200mg of iron oxide nano particles were ultra-sonicated in 50 ml of ethanol. Nitrogen is used as a carrier gas in the spray gun to maintain pressure. Nano particles were deposited steadily on the film. The films were then dried properly under nitrogen environment.

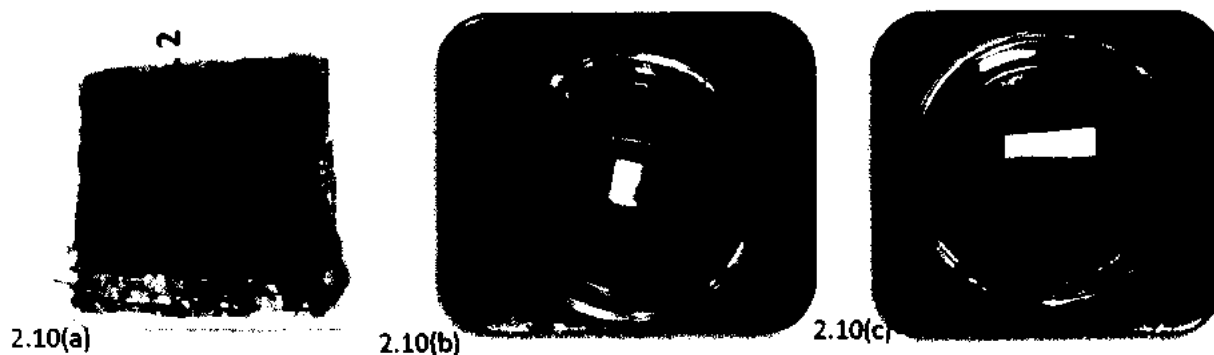


Figure 2.10: Deposition of $\alpha\text{-Fe}_2\text{O}_3$ (M1, M2, and M3) on FTO'S.... (a)(b)(c)

Make connections to the films, contacts wires were attached to the deposited films with silver paste and dried them under the tungsten filament lamp.

2.4.2.2 Tungsten trioxide (WO_3) nano particles deposition on FTO (prepared from method 1 and method 2)

For a thin film deposition of nano particles, 200mg of tungsten trioxide nano particles (M1, M2) were ultra-sonicated in 50 ml of ethanol.

Nitrogen is used as a carrier gas in the spray gun to maintain pressure. The nano particles were deposited steadily on the film. The films were then dried properly under nitrogen environment.

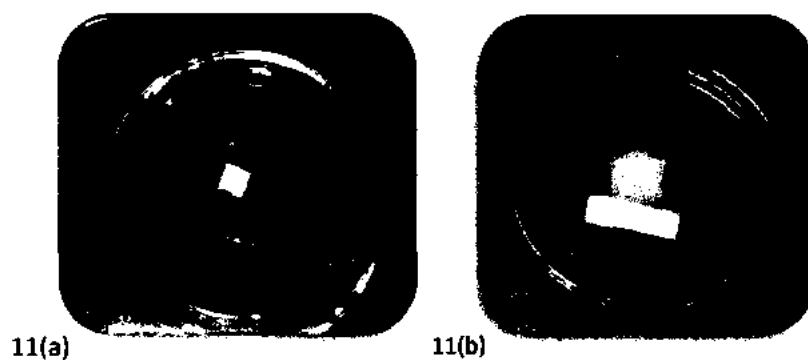


Figure 2.11: deposition of WO_3 nano particles (M1, M2) on FTO... (a)(b)

Make connections to the films, contacts wires were attached to the deposited films with silver paste and dried them under the tungsten filament lamp.

2.4.3 Deposition of nano-composites:



Figure2.12: different nano composites films

2.4.3.1 Iron oxide-tungsten trioxide (α -Fe₂O₃) - (WO₃) nano-composite deposition on FTO

For a thin film deposition, 100 mg of tungsten trioxide nano particles and 100 mg of iron oxide nano particles (method 1) were ultra-sonicated in 50 ml of ethanol, such that both are in 1:1 ratio.

Nitrogen is used as a carrier gas in the spray gun. The (nano particles) were deposited slowly and steadily on the film. The films were then dried properly under nitrogen environment.

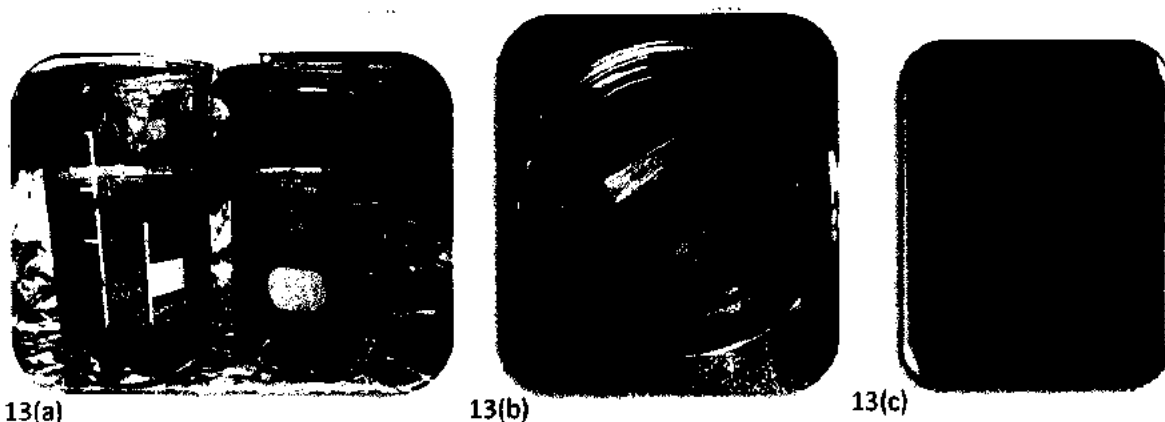


Figure2.13: solvothermal preparation of nano composites (a) α -Fe₂O₃-WO₃ nano composites deposition on FTO (b) (c)

Make connections to the films, contacts wires were attached to the deposited films with silver paste and dried them under the tungsten filament lamp. Similarly, prepare another film with same ratios but iron oxide nano particles used are of (method 2) .

2.4.3.2 Tungsten Trioxide -Graphene (WO₃-RGO) nano- composite deposition on FTO

For a thin film deposition, 100mg of tungsten trioxide nano particles and 100 mg of graphene oxide were ultra-sonicated in 50 ml of ethanol, such that they were in 1:1 ratio. Nitrogen is used as a carrier gas in the spray gun. The (nano particles) were deposited steadily on the film.

The films were then dried properly under nitrogen environment.

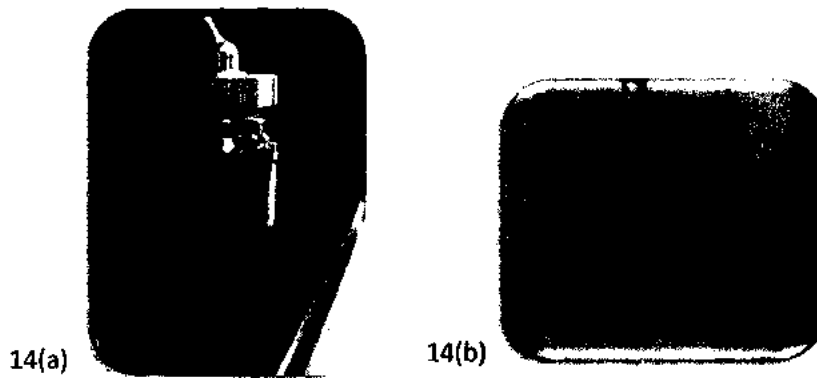


Figure 2.14: ultra-sonicated WO₃-RGO particles in ethanol (a) WO₃-RGO film prepared through spray deposition (b)

Make connection to the film, contacts wires were attached to the deposited film with silver paste and dried them under the tungsten filament lamp.

2.4.3.3 Iron oxide-Graphene (α -Fe₂O₃-RGO) nanocomposite deposition on FTO

For a thin film deposition, 100mg of iron oxide nano particles and 100 mg of graphene oxide were ultra-sonicated in 50 ml of ethanol, such that they were in 1:1 ratio.

Nitrogen is used as a carrier gas in the spray gun. The (nano particles) were deposited steadily on the film. The films were then dried properly under nitrogen environment.

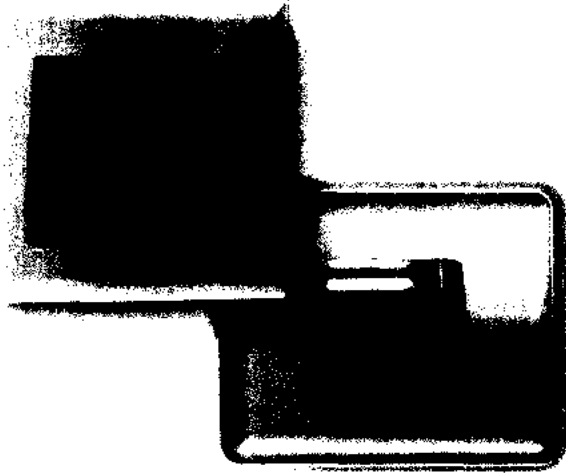


Figure2.15: α -Fe₂O₃-RGO nano composite

Make connection to the film, contacts wires were attached to the deposited film with silver paste and dried them under the tungsten filament lamp.

2.4.3.4 Iron oxide -Tungsten Trioxide-Graphene (α -Fe₂O₃-WO₃-RGO) nano -composite deposition on FTO

For a thin film deposition, 100mg of iron oxide nano particles (method 3) and 100 mg of graphene oxide and 100 mg of tungsten trioxide nano particles (method 1) were ultra-sonicated in 50 ml of ethanol, such that they were in 1:1:1 ratio.

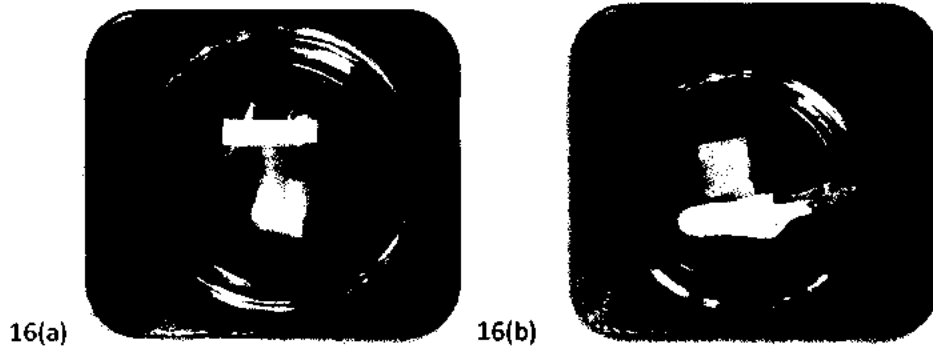


Figure2.16: α -Fe₂O₃-WO₃-RGO nano composite film with (b) and without connection (a)

Nitrogen is used as a carrier gas in the spray gun. The (nano particles) were deposited steadily on the film. The films were then dried properly under nitrogen environment.

Make connection to the film, contacts wires were attached to the deposited film with silver paste and dried them under the tungsten filament lamp overnight.

2.4.3.5 Iron oxide -Tungsten Trioxide-graphene (α -Fe₂O₃-WO₃-RGO) nano -composite deposition on FTO with different concentration

For a thin film 100mg of iron deposition , oxide nano particles(method 3) and 200 mg of graphene oxide and 100 mg of tungsten trioxide nano particles(method 1) and 100 mg WO₃ nano particles from method 2 were ultra-sonicated in 50 ml of ethanol, such that they were in 1:2:2 ratio.

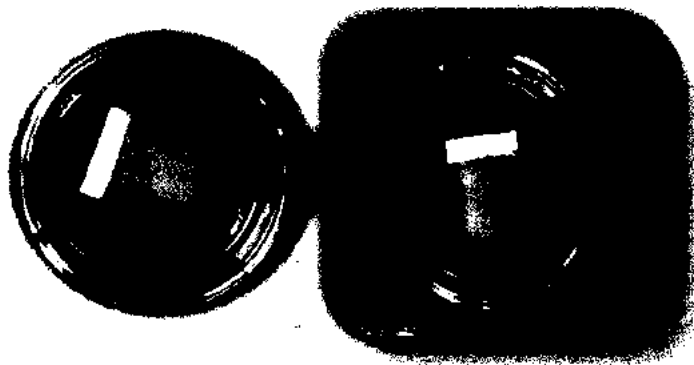


Figure 2.17: α -Fe₂O₃-WO₃-RGO nano composite film.

Nitrogen is used as a carrier gas in the spray gun. The (nano particles) were deposited steadily on the film, the films were then dried properly under nitrogen environment.

Make connection to the film, contacts wires were attached to the deposited film with silver paste and dried them under the tungsten filament lamp overnight.

2.5 Hydrothermal deposition

2.5.1 Hydrothermal deposition of Tungsten Trioxide (WO₃) nano particles on FTO

Make a solution of 0.4 g of citric acid and 0.52 g of sodium tungstate in 300 ml distilled water. Stir the solution for 30 minutes, and add hydrochloric acid drop wise to maintain its PH to 1 , yellowish turbid solution is formed .Transfer the solution in

Teflon lined stain less steel autoclave at 120°C for 12 hours . Place the FTO in autoclave such that its conducting side is in upward face. Allow autoclave to cool down at room temperature. Carefully, remove the FTO from autoclave and rise it with

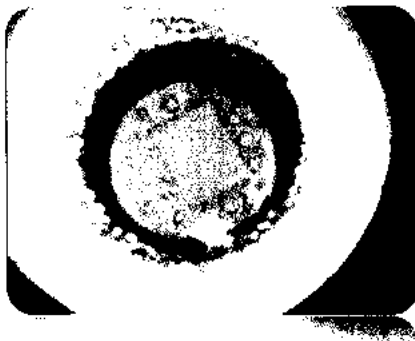


Figure2.18: deposited WO₃ nano particles on FTO placed in autoclave

distilled water to clear its surface from residues. Dry it under nitrogen environment it was pale yellowish in colour.

2.5.2 Hydrothermal Deposition of Tungsten Trioxide-Graphene (WO₃-GO) on FTO

Make a solution of 0.4 g of citric acid and 0.52 g of sodium tungstate in 300 ml distilled water. Stir the solution for 30 minutes, and add hydrochloric acid drop wise to maintain its PH to 1 , yellowish turbid solution is formed .

Add 0.2 g of graphene in the mixture. Transfer the solution in Teflon lined stain less steel autoclave at 120°C for 12 hours.



Figure2.19: hydrothermally deposited WO₃-RGO nano composite film

Place the FTO in autoclave such that its conducting side is in upward face. Allow autoclave to cool down at room temperature. Carefully, remove the FTO from autoclave and rise it with distilled water to clear its surface from residues. Dry it under nitrogen environment, it was greyish in colour.

2.6 Characterization techniques

2.6.1 Scanning electron microscope (SEM)

SEM is an electron microscope that utilizes an electron as a illumination source. Wavelength of electron is many times greater than photons wavelength therefore, it is used in high resolution imaging .SEM provides the information about of surface morphology and composition,[183] high resolution images are taken through SEM, similarly , elemental analysis are also taken from it.

It is comprised of the following parts.

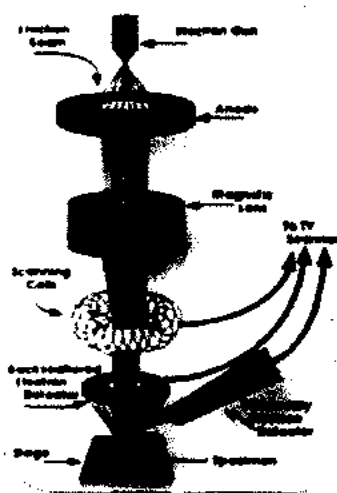


Figure2.20: schematic of SEM

Electron gun, condensed lenses, apertures , scanning system , chamber in which sample is placed and vacuum system as well. Secondary beam is focused on the sample and scanned randomly by EM radiation , pattern is observed when beam strike the sample surface and produce energetic signals , SEM large depth of field and higher resolution make it prior to OM.

I had my focus on the study of the surface and coarseness of GO and its composites with iron oxide and tungsten trioxide.

2.6.2 X- ray diffraction (XRD)

To study the crystalline structures and crystal size and other crystallographic information a techniques known as X-Ray diffraction is extensively used, in this

technique measurements are taken between brags' angle (2 theta) and intensity of the incident beam when it falls on the surface of the specimen. XRD is extensively used for crystallographic measurements [184].

Mechanism involve in XRD is basically a beam of light (x-ray) fall on the surface of the sample by certain incident angle, reflection occurs when it strikes the surface and and is angle of diffraction is known as brags' angle. Detector read these beams and conclude the pattern, these patterns are matched with required JCPDs No's, and to calculate the crystal size sheers formula is used.

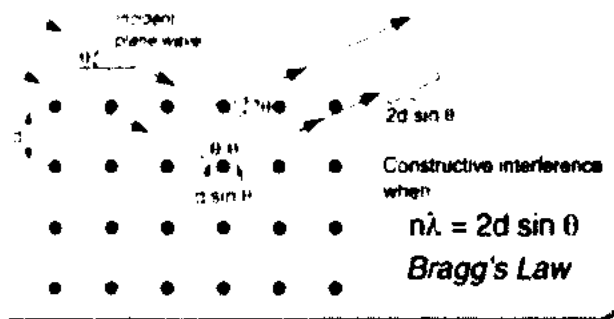


Figure2.21: diffraction phenomena in XRD and brag's law

2.6.3 Ultraviolet visible spectroscopy



Figure2.22: sample preparation for uv-vis analysis.

To measure the sample absorption in UV-visible range a technique known as UV-Visible spectroscopy is used extensively[185], it give information about absorption of sample in certain wavelength i.e in ultra violet or visible range. Absorption in actual deals with the electrons transitions taking place UV-Visible light fall on it , transmission of light is well explained by beer in his BEER- lamberts law, which provides the information of fraction of light before when it was incident on the sample

and after when it pass through the sample and cross section of absorption for transitions of electrons ,BEER law is in simple is just the amount of molecules absorbed in the sample vary the concentrations and absorption , beer lamberts law is not dependent on the intensity .

2.6.4 Photo electro chemical measurements

Current voltage curves are of great importance in calculation of efficiencies in electrochemical analysis, IV curves are taken to check the performance and efficiency of the photo anodes or photo cathodes in photoelectron chemical cells, also analyse the nano composites working.

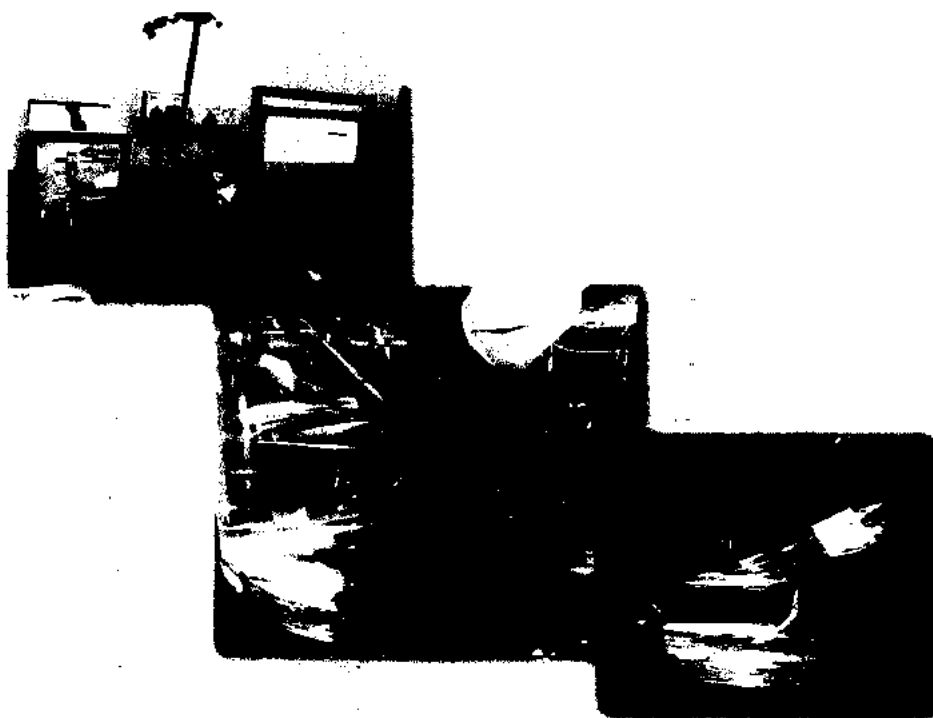


Figure2.22: Gamry Instrument, PEC Cell under Source Illumination

Sodium sulphate is used as a electrolyte solution in PEC measurements , PEC cell is composed of three electrode system in which one is photo anode act as working electrode, other is counter electrode to complete the circuit which is mostly platinum or graphite , other is reference electrode which is Ag/AgCl, for accurate measurements. Connections to cells were made through silver paste and copper wire with less resistance. PEC measurements are taken in dark and white light to check the cell efficiency, measurements in white light are.

CHAPTER 3
Results and discussions

Structural analysis

3.1 X-Ray diffraction analysis

3.1.1 X-RD analysis of oxidized and reduced graphene (GO-RGO)

Figure 3.1(a) shows XRD pattern of GO (graphene oxide).

Graphene oxide shows intense peak at 10.1° degree with d-spacing of 8.57\AA .

Inter layer spacing calculation from xrd is 27.1 nm [186, 187], because chemical oxidation of graphite cause disruption of graphite layers and addition of functional groups of oxygen[188, 189]. These results matched with JCPDs No. (00-012-0212).

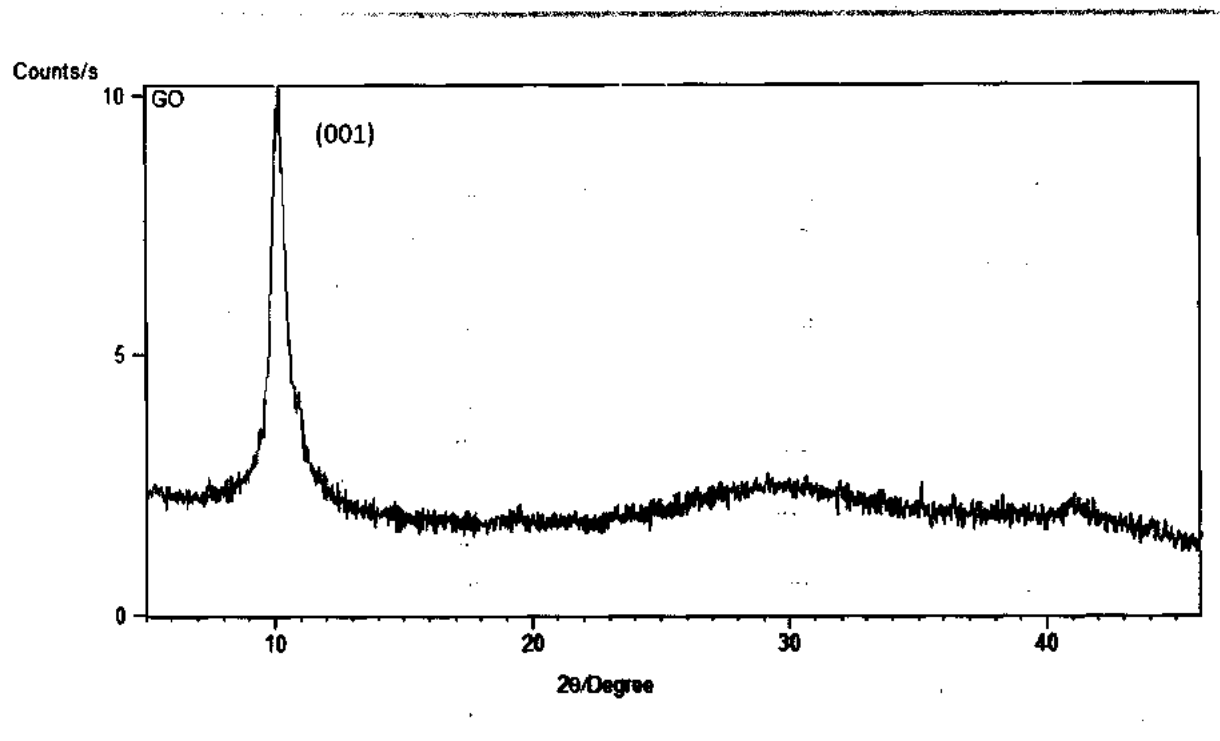


Figure 3.1(a): XRD pattern of Graphene oxide (GO)

Figure 3.1(b) shows the XRD pattern of reduced graphene oxide (RGO) corresponding to (002) plane.

Graphene oxide is reduced chemically, due to strong chemical reduction with hydrazine, a low intensity peak appears at 24.732° at d-spacing of 4.284\AA .

These results matched with JCPDS No. (00.0320.0415), Calculated ~~particle~~ size from XRD is 43nm.

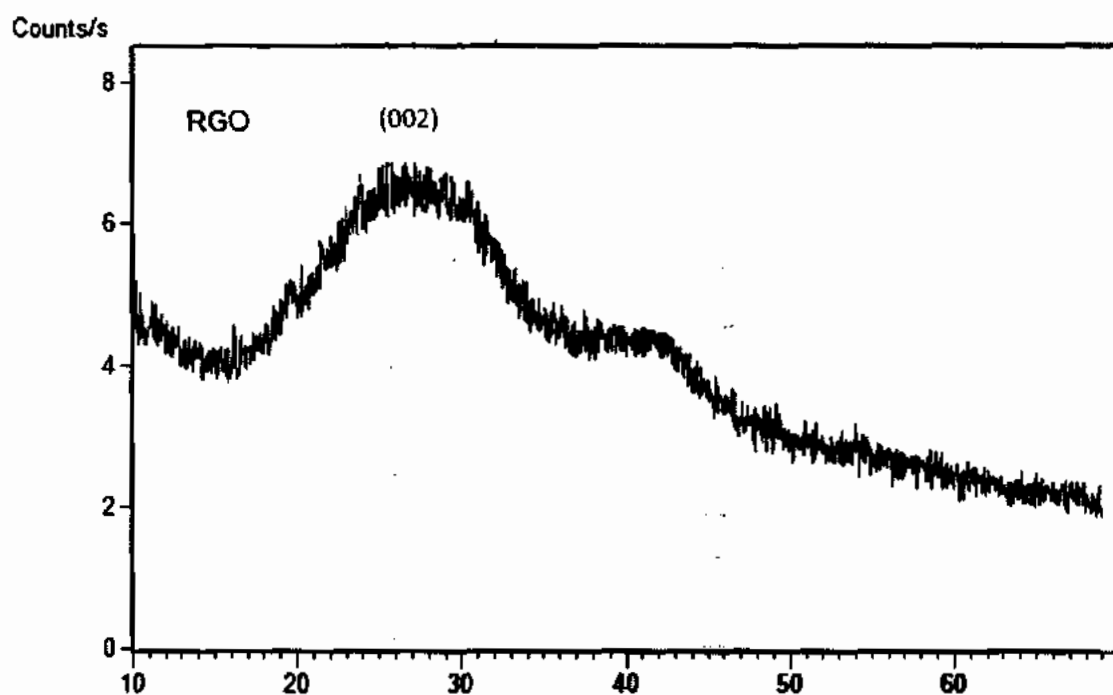


Figure 3.1(b): XRD pattern of Reduced Graphene Oxide (RGO)

3.1.2 XRD- analysis of tungsten trioxide (WO₃)

Figure 3.2 shows the XRD pattern of tungsten trioxide (WO₃) prepared under hydrothermal conditions (120°C) [190-192].

Pattern was matched with JCPDs No. (01-075-2187), ~~particle~~ size calculated from XRD is 47 nm ,Peaks observed at 14.033[°] , 22.853[°] ,24.403[°] ,26.566[°] , 28.242[°], 33.669[°] ,36.594[°] ,37.833[°] ,42.819[°] ,46.627[°] ,49.922[°] ,51.56[°] ,54.630[°] ,55.50[°] ,58.34[°].

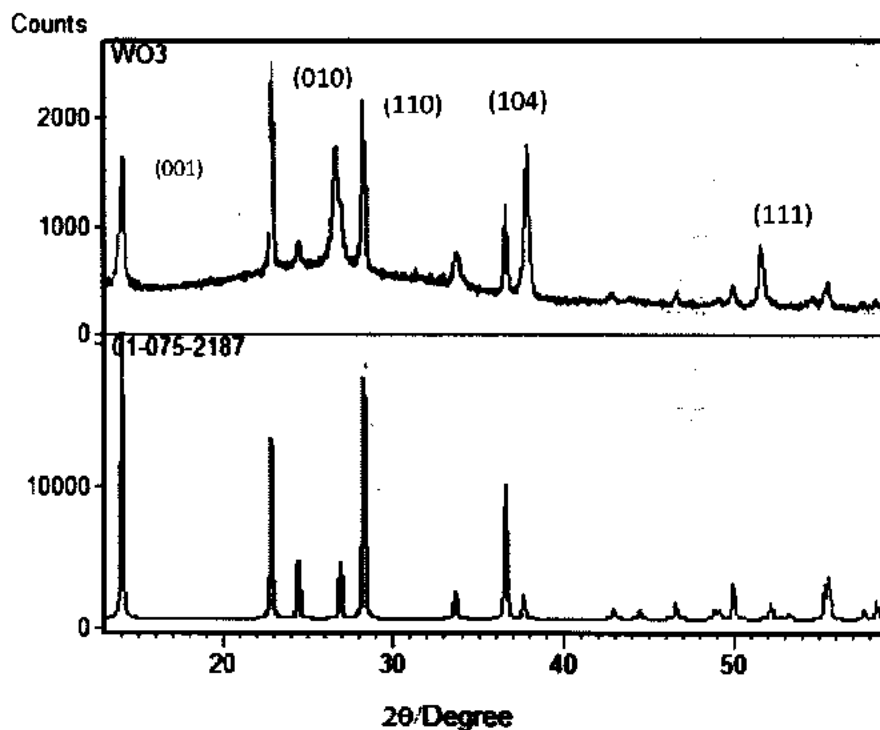


Figure 3.2: XRD pattern of tungsten trioxide (WO₃) matched with JCPDs card no.

3.1.3 XRD-analysis of hematite ($\alpha\text{-Fe}_2\text{O}_3$)

Figure shows 3.3(a) the XRD pattern of hematite prepared under hydrothermal condition (120°C). Pattern was matched with JCPDS No. (00-024-0072), *Particle* size calculated from XRD analysis is 16nm[193, 194].

Figure 3.3 (b) shows peak positions of hematite.

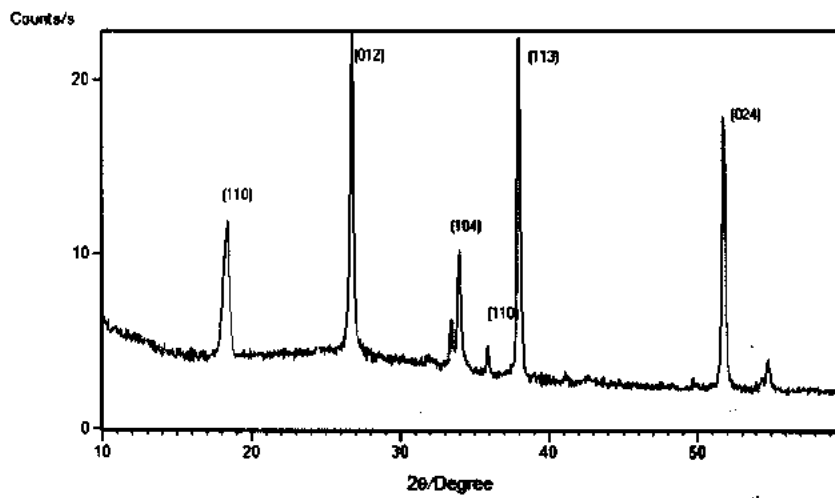


Figure 3.3 (a): XRD pattern of hematite.

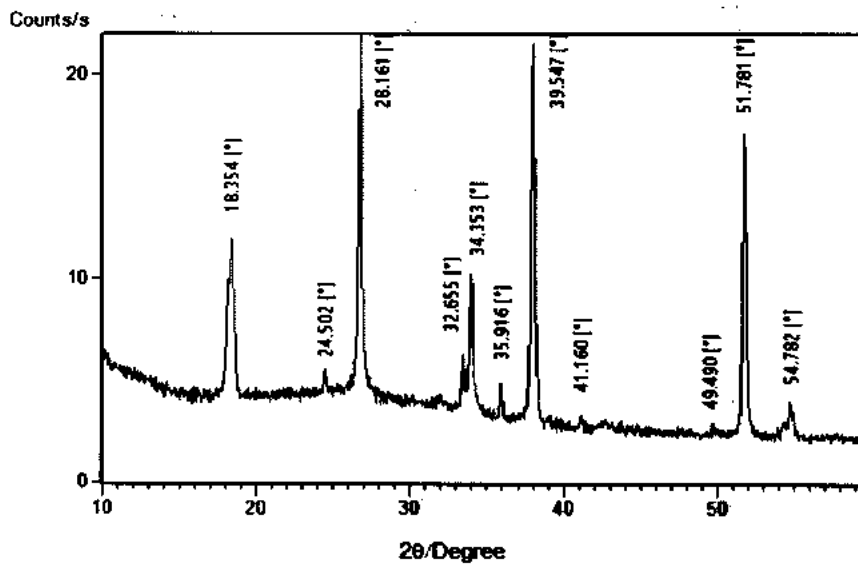


Figure 3.3(b): Peak positions of hematite in XRD- analysis

3.1.4 XRD analysis of Tungsten Trioxide-Graphene nano composite (WO₃-GO)

Figure 3.4(a) shows the XRD pattern of WO₃-GO nano composite prepared under hydrothermal conditions (180°C)[195]. Pattern was matched with JCPDs No. (00-012-0212) and (01-075-2187). Particle size calculated from XRD analysis is 24 nm

Peak positions observed are shown in figure 3.4(b).

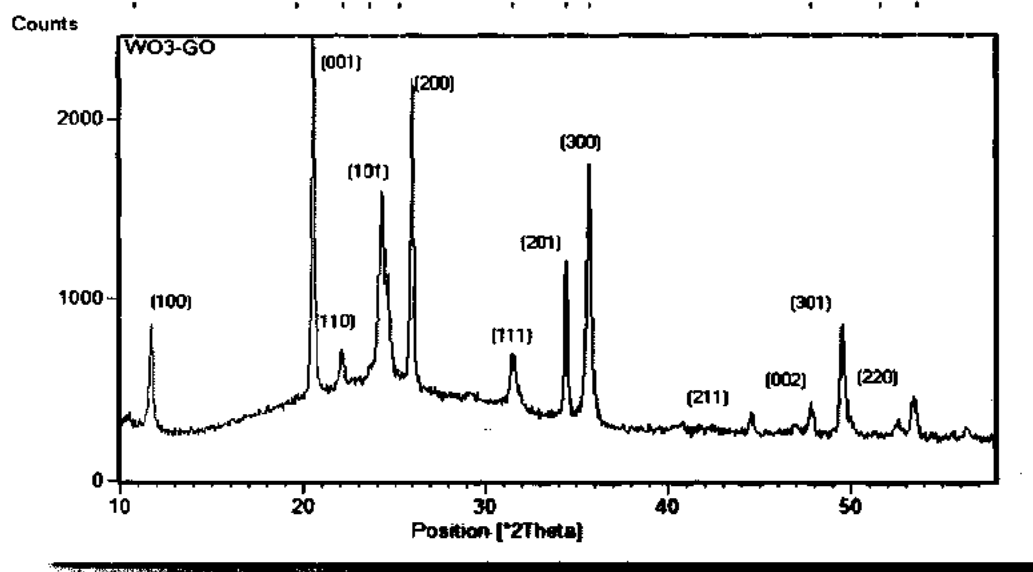


Figure 3.4(a) : XRD pattern of WO₃-GO

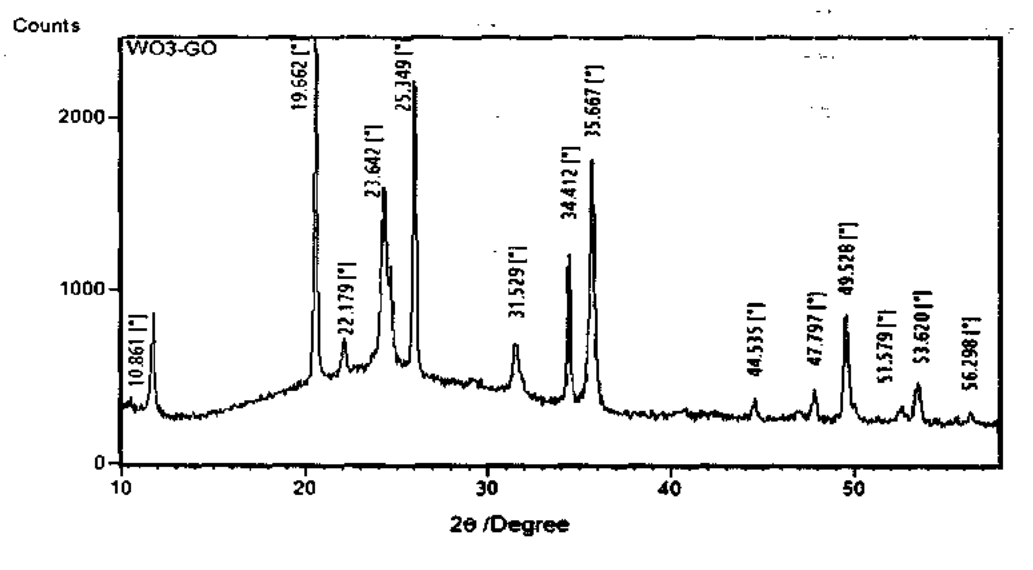


Figure 3.4(b): peak positions of WO₃-GO in XRD analysis

3.1.5 XRD- Analysis of Hematite- Graphene nano composite ($\alpha\text{-Fe}_2\text{O}_3\text{-RGO}$)

Figure 3.5(a) shows the XRD pattern of $\alpha\text{-Fe}_2\text{O}_3\text{-RGO}$ prepared solvothermally with same ratios (1:1). Results matched with JPCDS No. (00-024-0072) and JPCDS No. (00.0320.0415). *Particle* size calculated from XRD analysis is 34 nm. Peak positions observed are shown in figure 3.5(b).

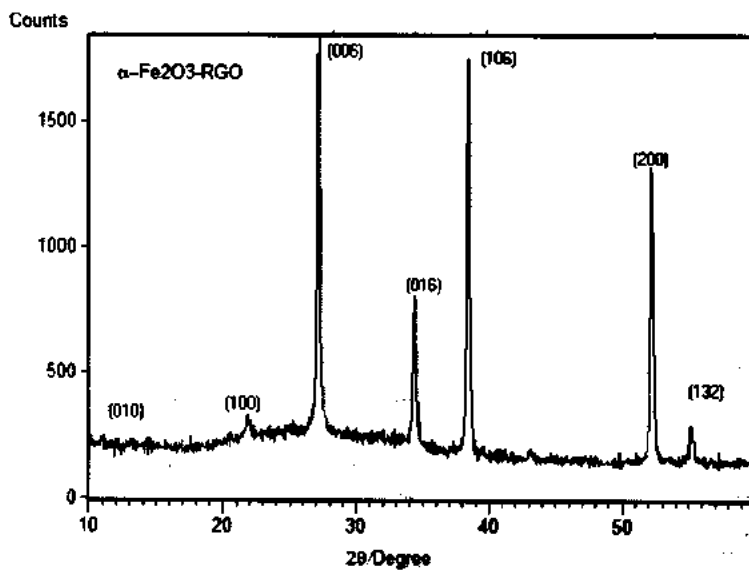


Figure 3.5(a): XRD pattern of $\alpha\text{-Fe}_2\text{O}_3\text{-RGO}$ nano composite.

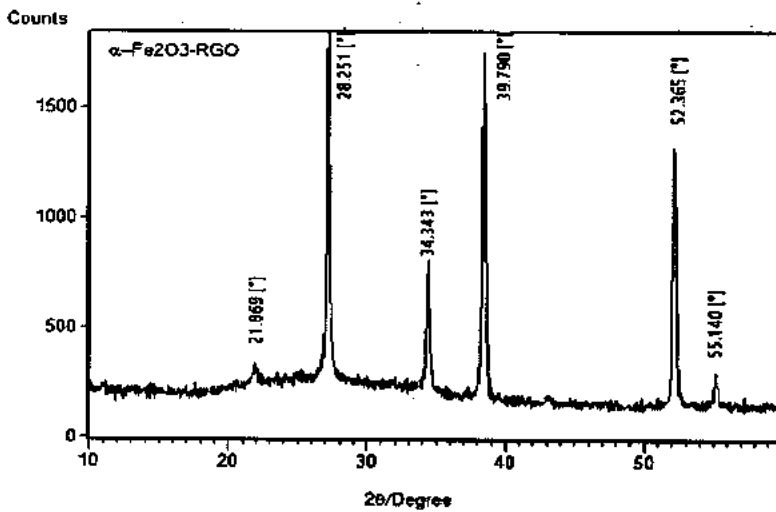


Figure 3.5(b): peak positions of $\alpha\text{-Fe}_2\text{O}_3\text{-RGO}$ nano composite.

3.1.6 XRD- Analysis of $\text{WO}_3\text{-}\alpha\text{-Fe}_2\text{O}_3\text{-RGO}$ nano composite:

Figure 3.6(a) shows the XRD pattern of $\text{WO}_3\text{-}\alpha\text{-Fe}_2\text{O}_3\text{-RGO}$ nano composite, prepared solvothermally with 1:1:1 ratio. Results matched with JPCDs No. (00-024-0072), JPCDs No. (00.0320.0415) and JPCDs No. (01-075-2187). Particle size calculated from XRD analysis is 38 nm. Peak positions observed for nano composites are shown in figure 3.6(b).

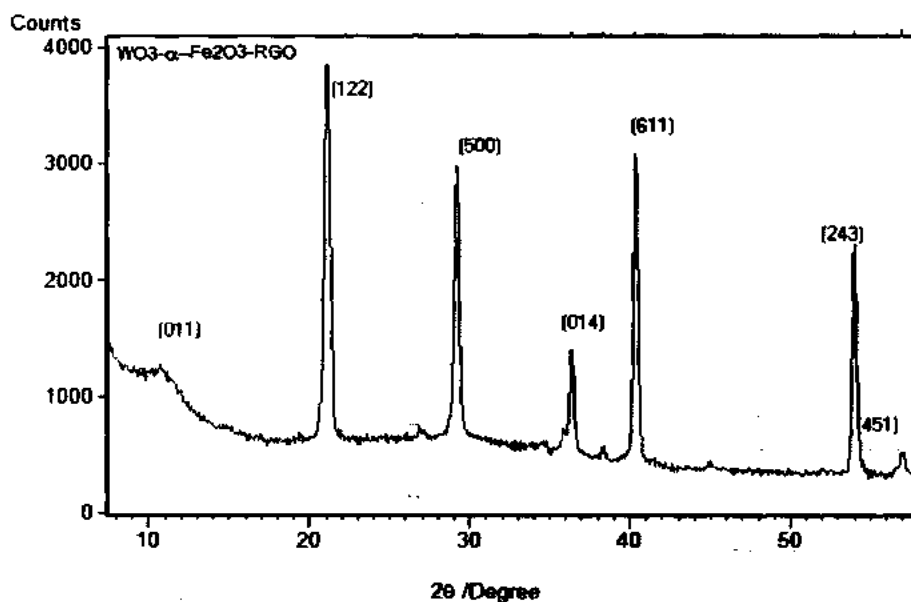


Figure 3.6 (a): XRD pattern of $\text{WO}_3\text{-}\alpha\text{-Fe}_2\text{O}_3\text{-RGO}$ nano composite.

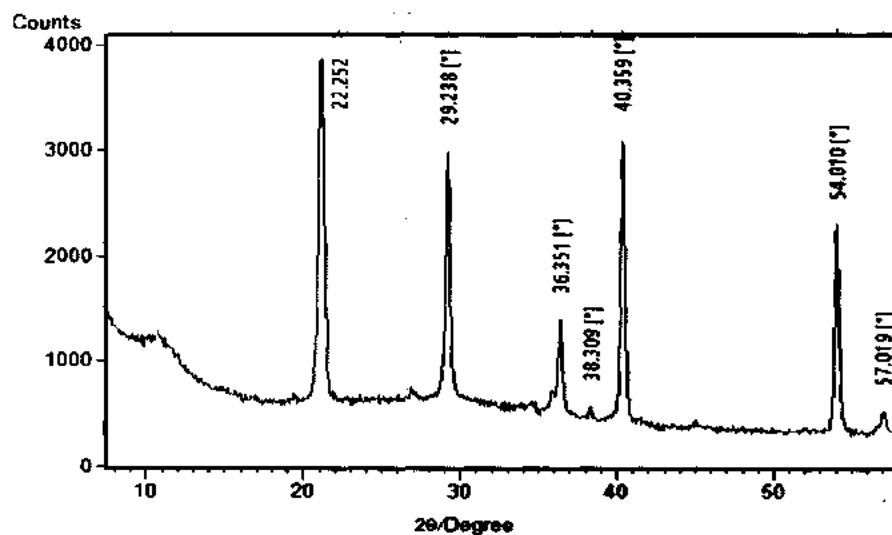


Figure 3.6(b): peak positions of $\text{WO}_3\text{-}\alpha\text{-Fe}_2\text{O}_3\text{-RGO}$ nano composite

3.1.7 XRD- Analysis of $WO_3-\alpha-Fe_2O_3$ -RGO nano composite with different ratios:

Figure 3.7(a) shows the XRD pattern of $WO_3-\alpha-Fe_2O_3$ -RGO nano composite. Results matched with JPCDs No. (00-024-0072), JPCDs No. (00.0320.0415) and JPCDs No. (01-075-2187). P_{04} size calculated from XRD analysis is 42nm. Peak positions observed are shown in figure 3.7 (b).

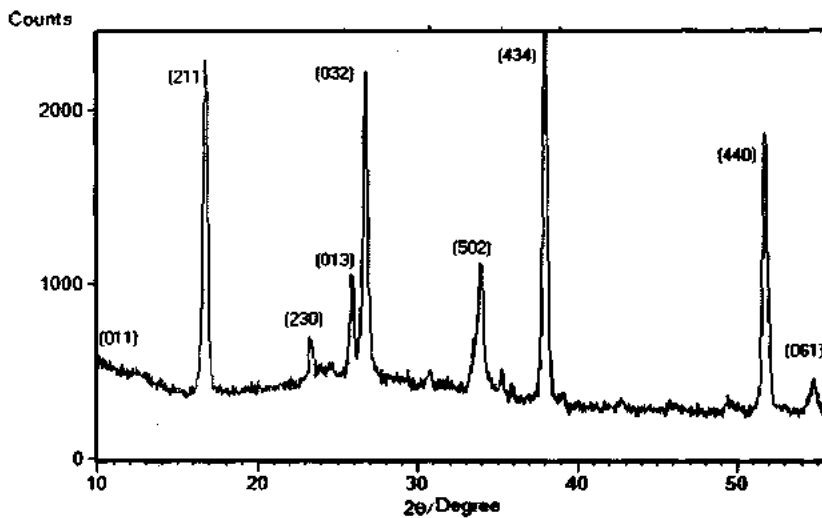


Figure 3.7 (a): XRD pattern of $WO_3-\alpha-Fe_2O_3$ -RGO nano composite

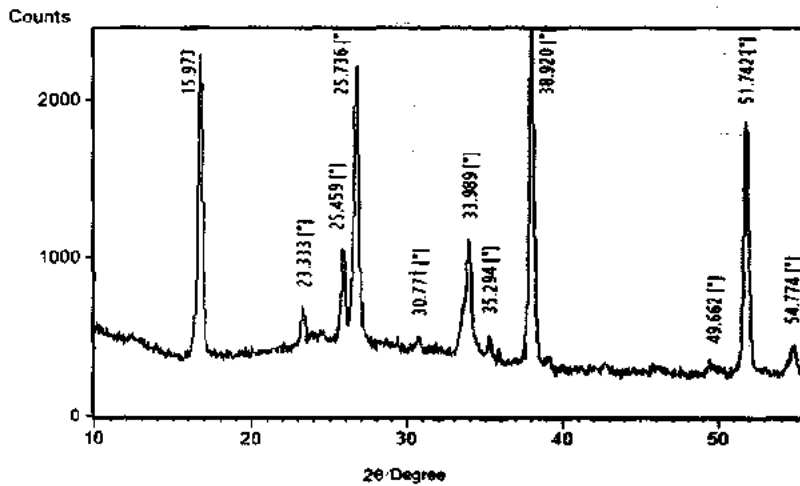


Figure 3.7 (b): Peak positions in XRD analysis of $WO_3-\alpha-Fe_2O_3$ -RGO nano composite

3.1.8 XRD-analysis of $\text{WO}_3\text{-}\alpha\text{-Fe}_2\text{O}_3$ nano composite:

Figure 3.8 (a) shows the XRD pattern of $\text{WO}_3\text{-}\alpha\text{-Fe}_2\text{O}_3$ nano composite, prepared solvothermally with same ratios. Results matched with JCPDs No. (00-024-0072) and JCPDs No. (01-075-2187). Particle size calculated from XRD analysis is 34nm. Peak positions observed from xrd analysis are shown in figure 3.8 (b).

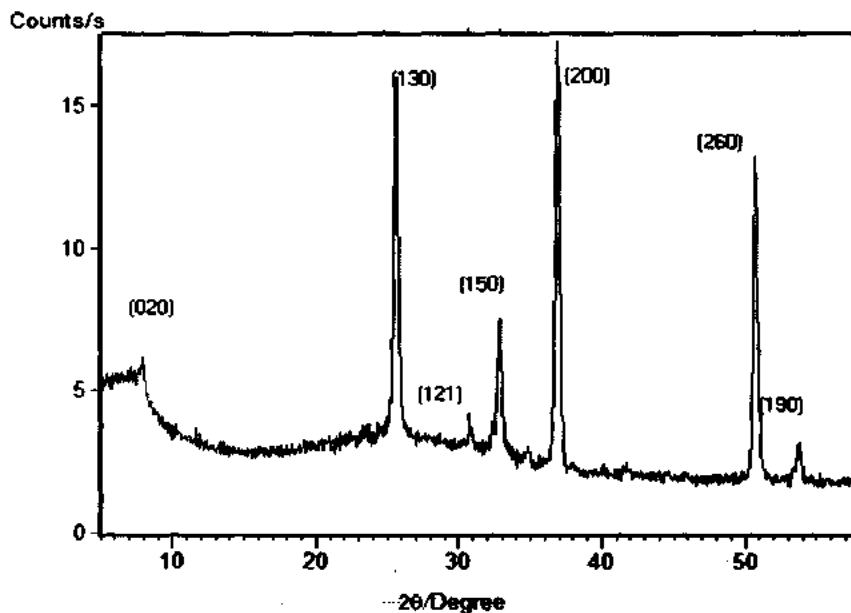


Figure 3.8(a): XRD pattern of $\text{WO}_3\text{-}\alpha\text{-Fe}_2\text{O}_3$ nano composite

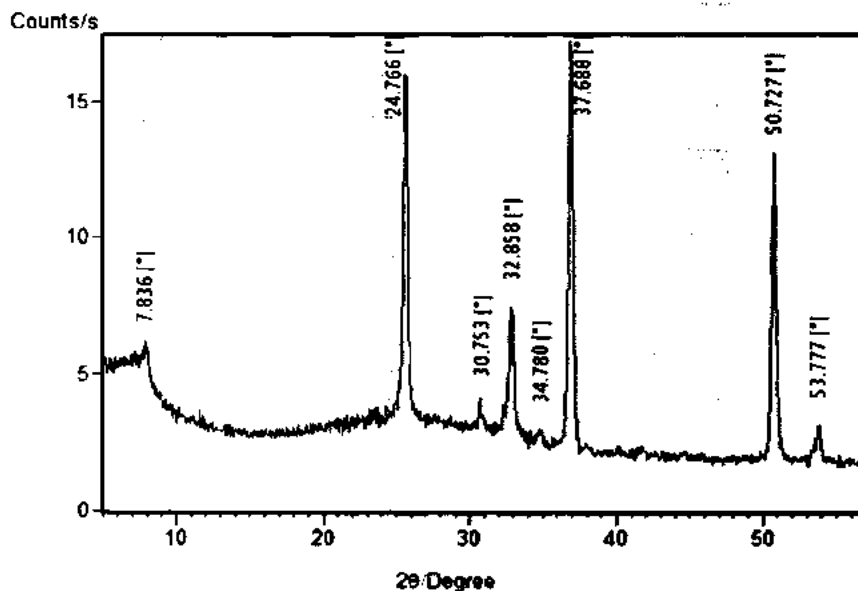


Figure 3.8(b): observed peak positions from XRD analysis for $\text{WO}_3\text{-}\alpha\text{-Fe}_2\text{O}_3$ nano composite

3.1.9 XRD-analysis of $\text{WO}_3\text{-}\alpha\text{-Fe}_2\text{O}_3$ (dark) nano composite:

Figure 3.9(a) shows the XRD pattern of $\text{WO}_3\text{-}\alpha\text{-Fe}_2\text{O}_3$ nano composite, prepared solvothermally with same ratios. Results matched with JCPDs No. (00-024-0072) and JCPDs No. (01-075-2187). Particle size calculated from XRD analysis is 23nm. Peak positions observed from xrd analysis are shown in figure 3.9 (b).

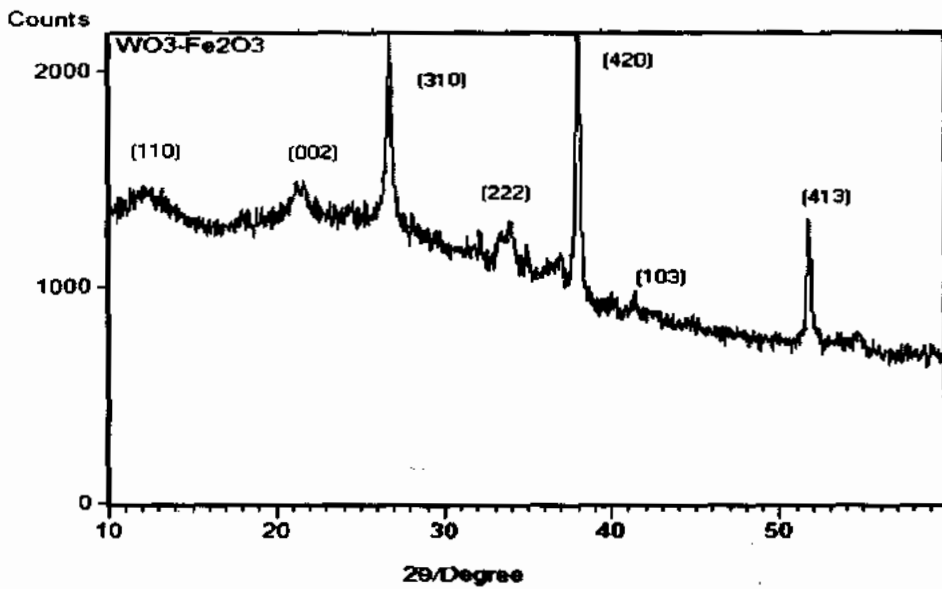


Figure 3.9(a): XRD pattern of $\text{WO}_3\text{-}\alpha\text{-Fe}_2\text{O}_3$ (dark) nano composite

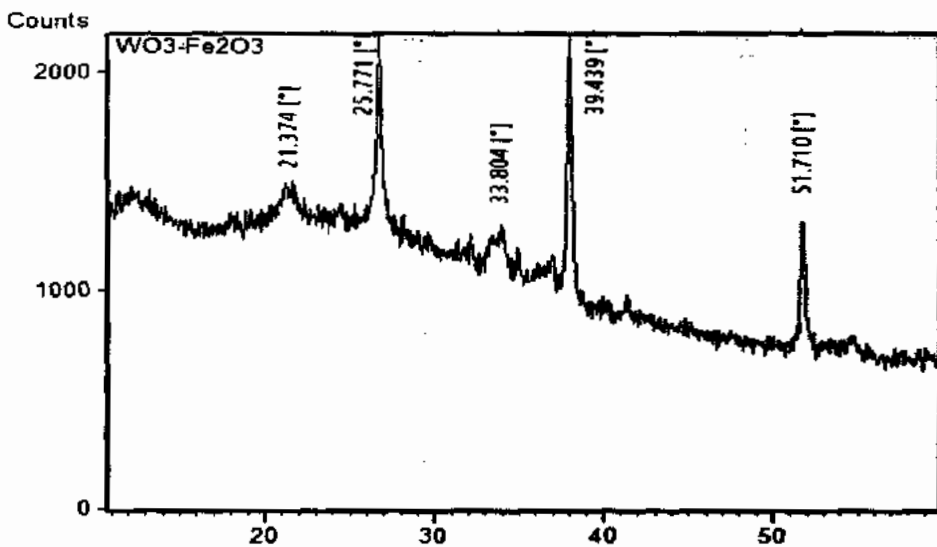


Figure 3.9(b): peak positions of $\text{WO}_3\text{-}\alpha\text{-Fe}_2\text{O}_3$ (dark) nano composite

3.2 Scanning Electron Microscopy (SEM)

3.2.1 SEM analysis of α -Fe₂O₃ nano particles prepared from method 1 and 3

SEM analysis of α -Fe₂O₃ nano particles prepared from 2 different precursors through hydrothermal route , figure (a) present hematite porous square block nano particles with particle size 40 nm, (b) shows the hematite spherical nano particles with ~~size~~ size range 16nm hardly to see through 2 μ m magnification , at different magnifications i.e at 5 μ m and 2 μ m.

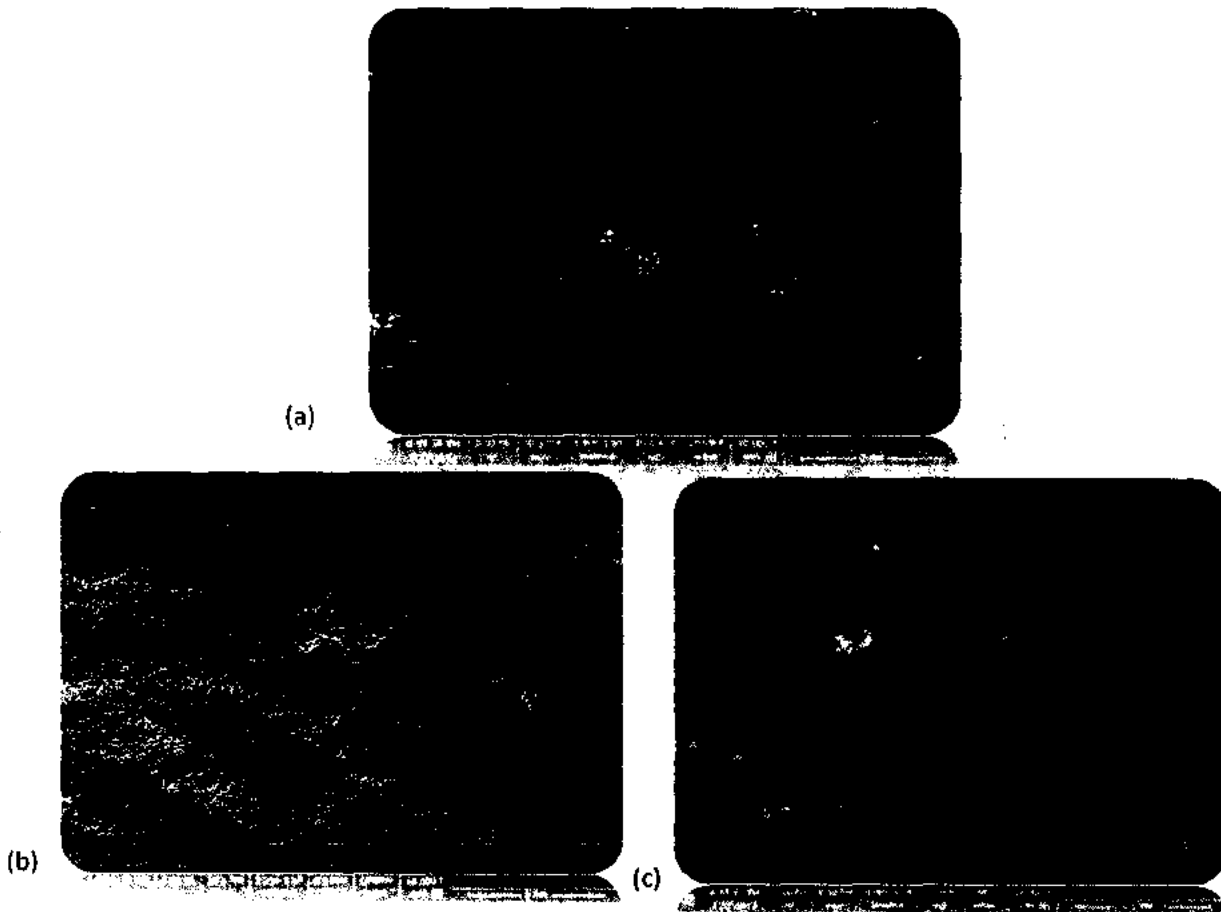


Figure3.10: SEM images of α -Fe₂O₃ nano particles prepared with different precursors, nano particles prepared from method 1 (a) nano particles prepared from method 2 (b)

3.2.2 SEM analysis of WO_3 nano particles prepared from method1

SEM images of WO_3 nano particles prepared from method 1 with nano plate like morphology , at different magnifications i.e at $5\mu\text{m}$, $2\mu\text{m}$ and at 500nm , therefore *Grain* size approximation from SEM analysis is $<150\text{ nm}$.

Images shows the randomly arranged WO_3 nano plates.

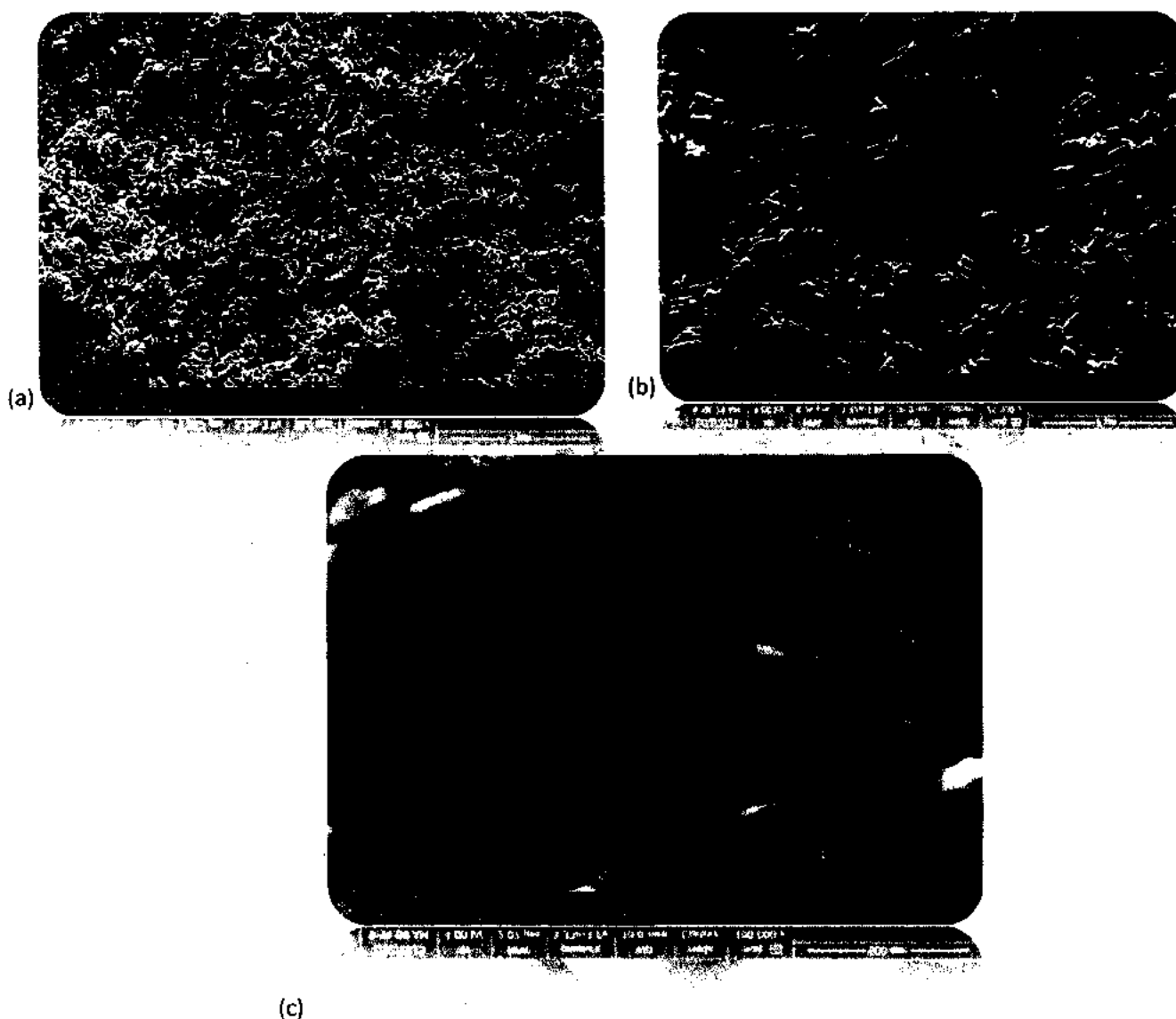


Figure3.11: SEM images of WO_3 nano particle with nano plate like morphology, and at different magnifications i.e at $5\mu\text{m}$, $2\mu\text{m}$ and at 500nm (a)(b)(c).

3.2.3 SEM analysis of GO and RGO:

SEM image of Graphene oxide and reduced Graphene oxide shows layer by layer enwrapped sheets of GO and RGO, at different magnifications i.e at $5\mu\text{m}$, $2\mu\text{m}$ and $1\mu\text{m}$. Figure (a) and (b) shows sheets of GO, similarly figure (c), (d), (e) shows images for RGO, at $1\mu\text{m}$ resolution full covered area sheet is observed.

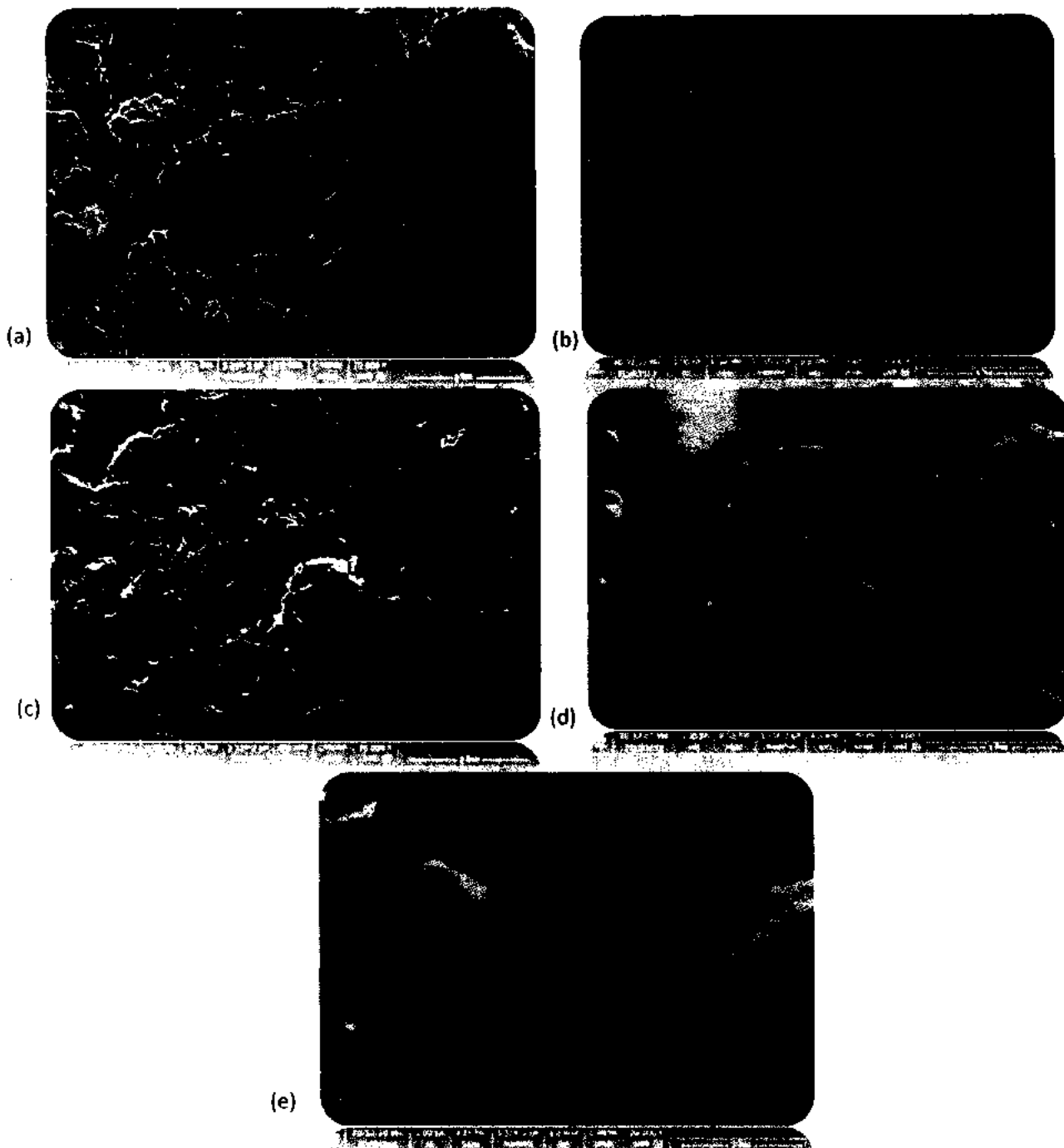


Figure3.12: SEM images of GO and RGO at different magnifications.

3.2.4 SEM analysis of α -Fe₂O₃-RGO nano composite thin film:

SEM analysis of α -Fe₂O₃-RGO nano composite thin films shows an spherical iron oxide nano particles enwrapped between the sheets of graphene .Iron oxide particles are so small in size < 100 nm so they are no clearly visible in SEM images , taken at different resolution of 1 μ m , 2 μ m, 4 μ m.

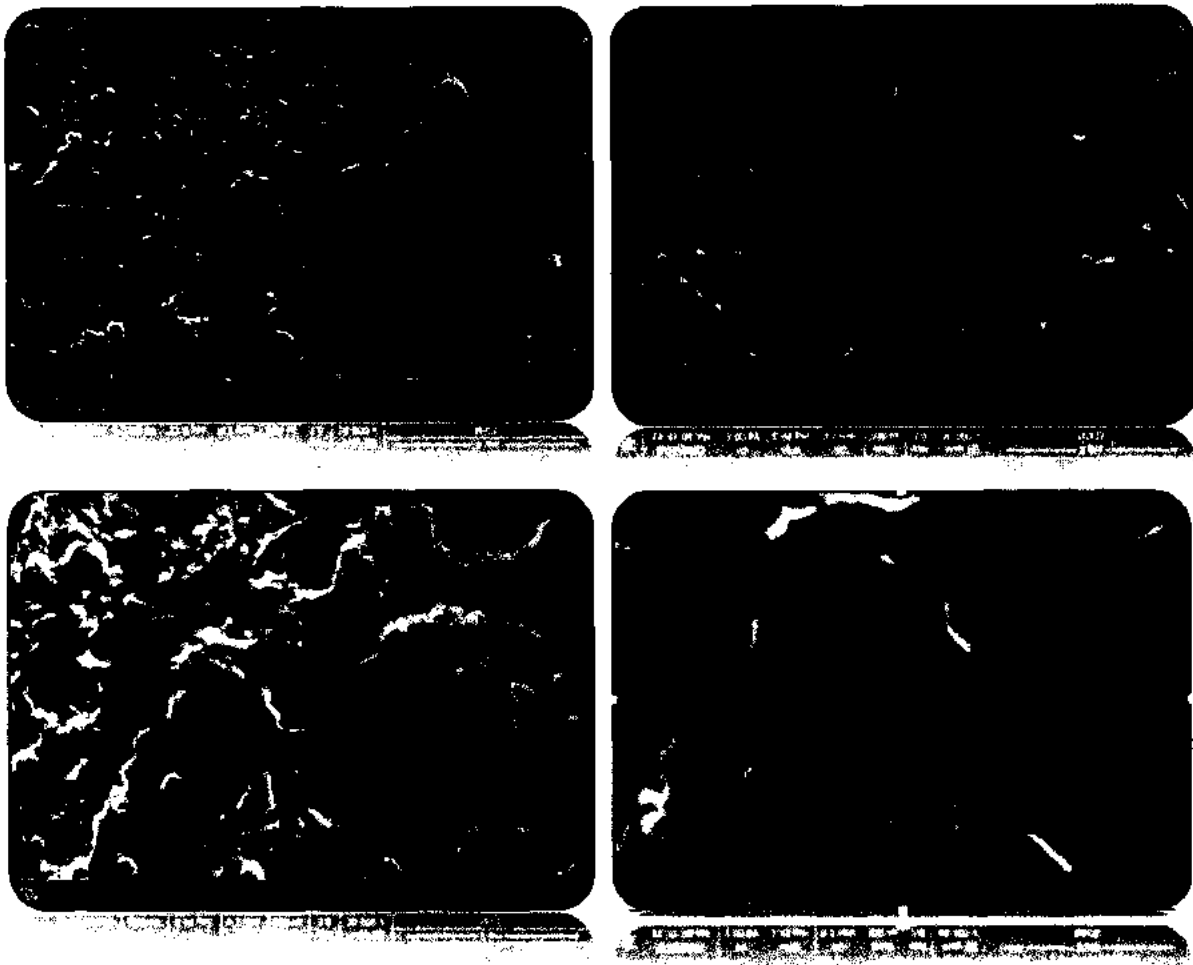


Figure3.13: SEM images of α -Fe₂O₃-RGO nano composite film at different magnification i.e at 4 μ m, 2 μ m, 1 μ m.

3.2.5 SEM analysis of WO_3 - α - Fe_2O_3 nano composite thin film:

SEM images of WO_3 - α - Fe_2O_3 nano composite film shows an porous composition of random square block hematite nano particles (synthesized from method 1) on surface of wo_3 nano plates, both particles are used in (1:1) ration during composition making .SEM images are taken at different magnification i.e at $5\mu m$ and $2\mu m$. Particles in composite vary from 20-200nm in size.

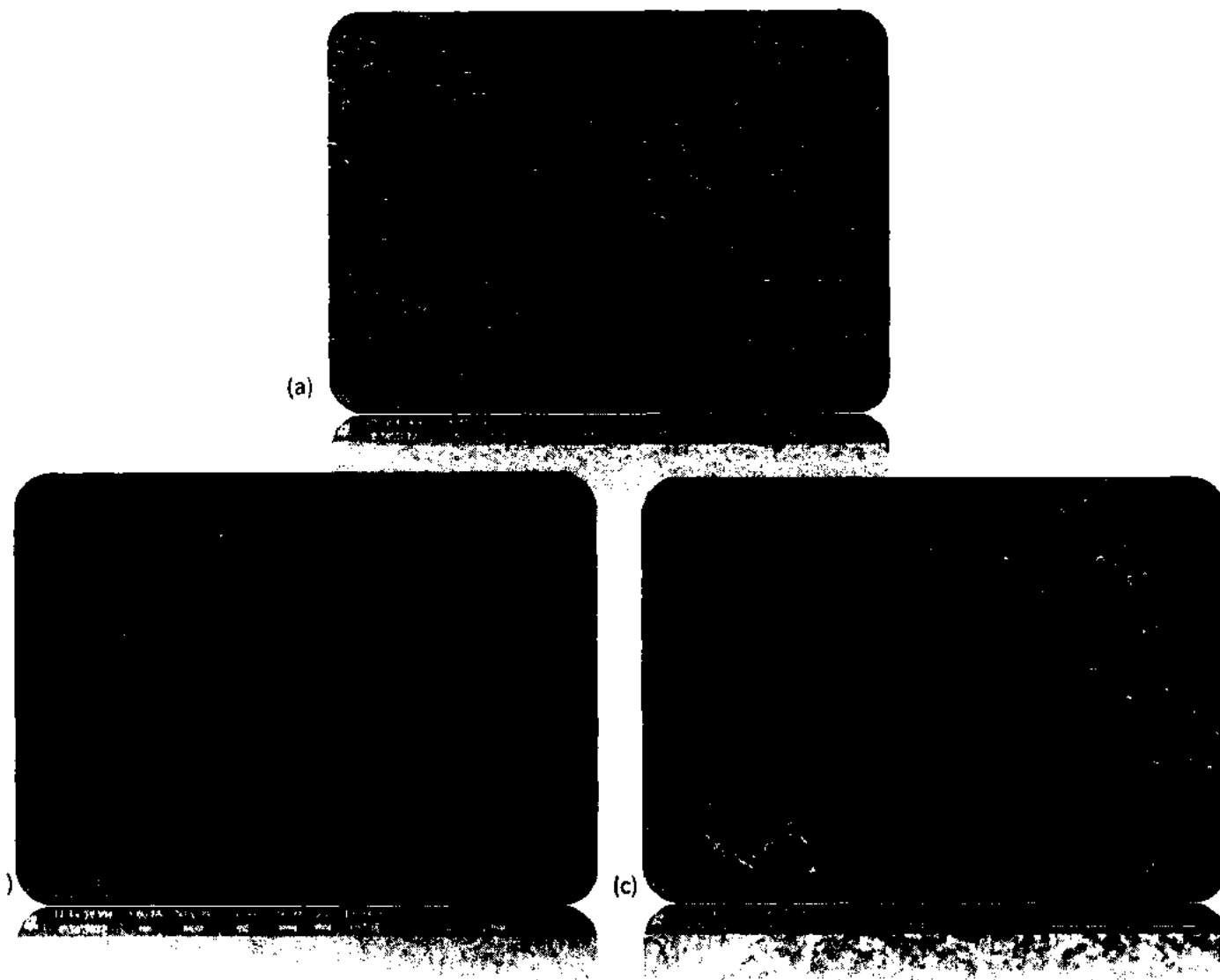


Figure3.14: SEM images of WO_3 - α - Fe_2O_3 nano composite film at different magnification i.e at $5\mu m$ and $2\mu m$ (b),(c) and morphology of faceted WO_3 particles before composition making for comparison.

3.2.6 SEM analysis of WO_3 - α - Fe_2O_3 nano composite thin film :

SEM images of WO_3 - α - Fe_2O_3 nano composite film, shows a random and rough, porous surface of the composite at $2\mu\text{m}$ resolution. Hematite spherical nano particles synthesized from method 3 are not seen clearly in $2\mu\text{m}$ magnification, layer by layer deposition of nano composite formed a flat structure showing a porosity increases by increasing the thickness of the film.



Figure3.15: SEM images of WO_3 - α - Fe_2O_3 nano composite film at $2\mu\text{m}$ magnification.

3.2.7 SEM analysis of WO₃-RGO nano composite thin film

SEM images of WO₃-RGO nano composite prepared hydrothermally at 180°C , shows an random and rough , porous surface of the composite at different magnifications i.e at 2μm and at 5μm. During hydrothermal deposition some sheets of graphene remained un merged with WO₃ particles , but larger area showed the WO₃ nano particles enwrapped separately in porous rough and random structure.

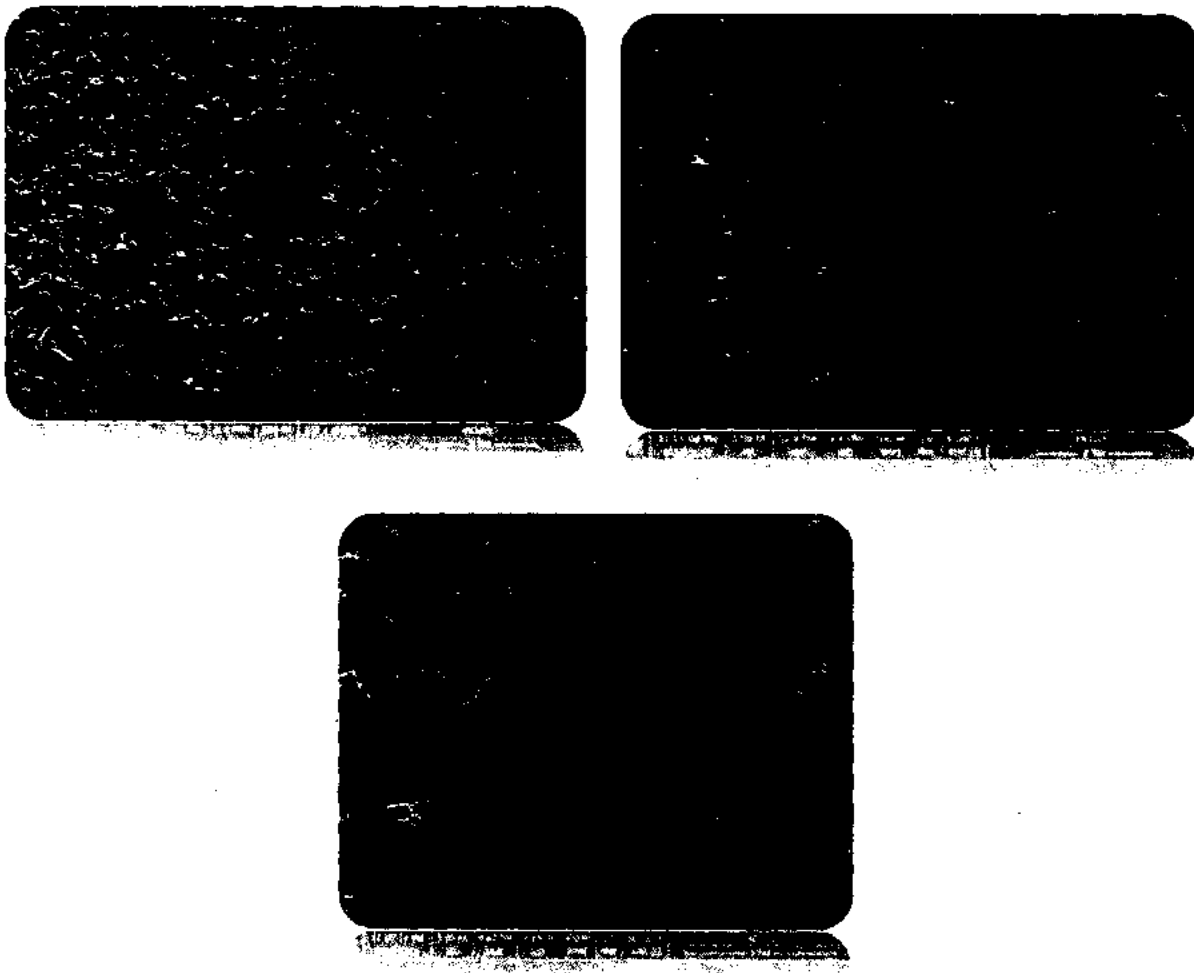


Figure3.16: SEM image of WO₃-RGO nanocomposite at different magnifications i.e at 5μm and at 2μm.

3.2.8 SEM analysis of WO_3 - α - Fe_2O_3 -RGO nano composite thin film prepared with same ratio (1:1:1)

SEM images shows the WO_3 - α - Fe_2O_3 -RGO nano composite, at different magnifications of $4\mu\text{m}$, $2\mu\text{m}$, and $1\mu\text{m}$ respectively. WO_3 nano plates , α - Fe_2O_3 nano spheres are in firm contact with each other and with graphene sheets and it shows the formation of composite , (1:1:1) ratio of each is used in composite making therefore graphene is not fully distributed on the film. At higher magnification $1\mu\text{m}$, WO_3 and α - Fe_2O_3 nano particles are distributed on graphene sheet randomly

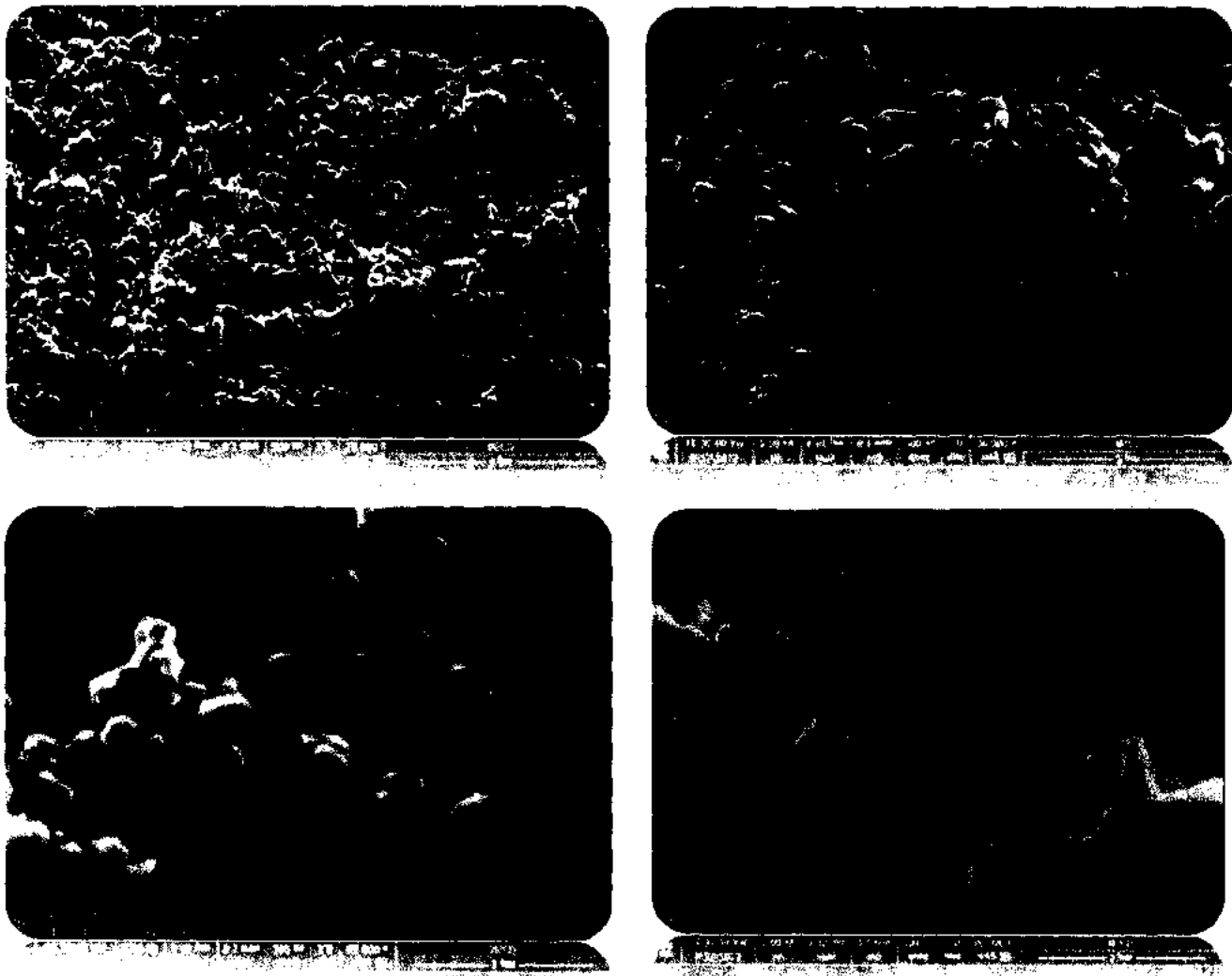


Figure3.17: SEM images of WO_3 - α - Fe_2O_3 -RGO nano composite film at different magnification i.e at $4\mu\text{m}$, $2\mu\text{m}$, $1\mu\text{m}$.

3.2.9 SEM analysis of WO_3 - α - Fe_2O_3 -RGO nano composite thin film prepared with different ratio (2:1:2)

SEM images shows the WO_3 - α - Fe_2O_3 -RGO nano composite, at different magnifications of $4\mu\text{m}$, $2\mu\text{m}$, and $1\mu\text{m}$ respectively. WO_3 nano plates , α - Fe_2O_3 nano spheres are in firm contact with each other and with graphene sheets and it shows the formation of composite , (2:1:2) ratio of each is used in composite making therefore greater quantity of WO_3 and graphene are randomly distributed on the film, larger quantity of WO_3 nanoparticles on graphene sheet allow change in its morphology during composite making and increase in size and enhancement of surface area. At higher magnification $1\mu\text{m}$, WO_3 and α - Fe_2O_3 nano particles are distributed on graphene sheet randomly.

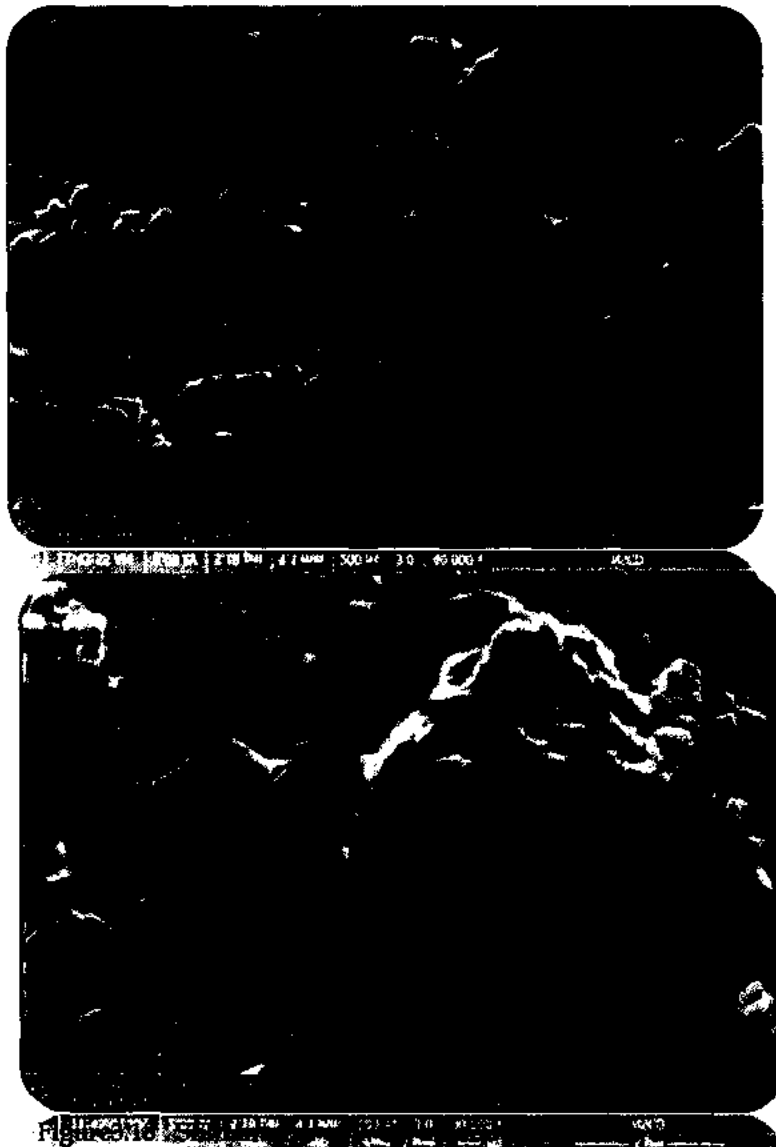
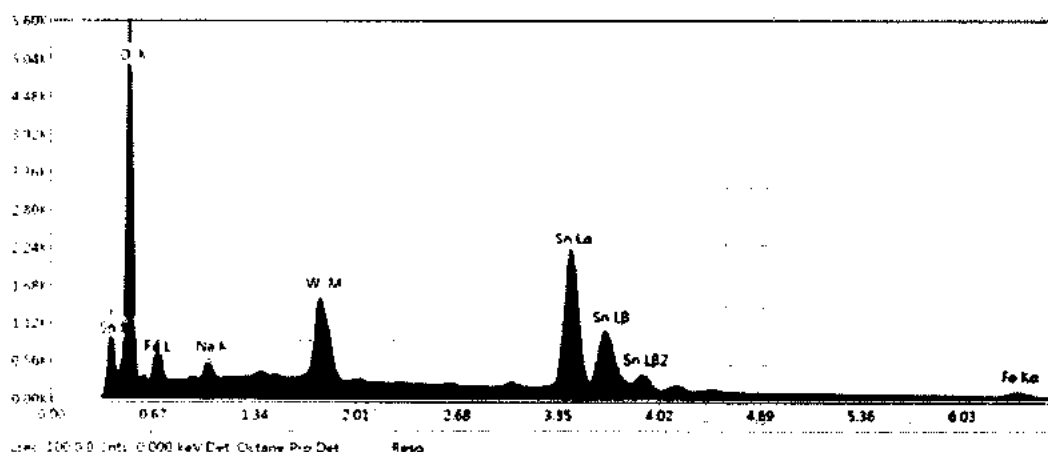


Figure 3.2.9 SEM images of WO_3 - α - Fe_2O_3 -RGO nano composite thin film at different magnifications (a) at $4\mu\text{m}$, (b) at $2\mu\text{m}$, (c) at $1\mu\text{m}$

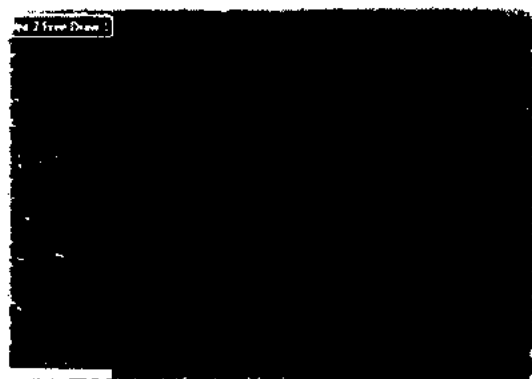
3.3 EDX (Energy Dispersive X-ray Analysis)

3.3.1 EDX Analysis of $WO_3-\alpha-Fe_2O_3$ nanocomposite thin film

EDX analysis is carried out to get the elemental analysis of nano composite $WO_3-\alpha-Fe_2O_3$ thin film. EDX spectra gives different elemental data in nano composite, and observed peaks are of Sn, W, Fe, and O respectively. Sb peak is due to the FTO substrate and it shows that film prepared is very thin and table shows there weight percentage and atomic percentage in nano composite $WO_3-\alpha-Fe_2O_3$ thin film. W, Fe, O supports the elements in nano composite thin film which is used as a photo anode in PEC water splitting.



eZAF Smart Quant Results

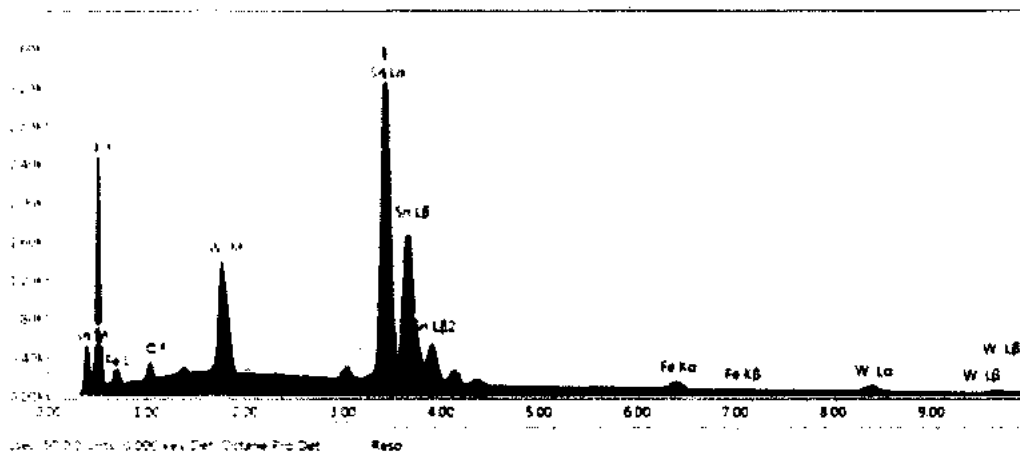


Element	Weight %	Atomic %	Net Int	Error %
O K	17.99	59.2	491.51	7.05
Na K	1.78	4.07	36.62	11.94
Sn L	62.78	27.85	423.47	4.34

Figure 3.19: EDX spectra of nano composite thin film, area selected for EDX analysis and weight % present in nano composite film prepared with (1:1) ratio.

3.3.2 EDX Analysis of $\text{WO}_3\text{-}\alpha\text{-Fe}_2\text{O}_3\text{-RGO}$ nanocomposite thin film prepared with (1:1:1) ratio

EDX analysis is carried out to get the elemental analysis of nano composite $\text{WO}_3\text{-}\alpha\text{-Fe}_2\text{O}_3\text{-RGO}$ thin film. EDX spectra gives different elemental data in nano composite, and observed peaks are of Sn, W, Fe, C and O respectively. Sb peak is due to the FTO substrate and it shows that film prepared is very thin and table shows there weight percentage and atomic percentage in nano composite $\text{WO}_3\text{-}\alpha\text{-Fe}_2\text{O}_3\text{-RGO}$ thin film. W, Fe, O and C supports the elements in nano composite thin film which is used as a photo anode in PEC water splitting.



eZAF Smart Quant Results

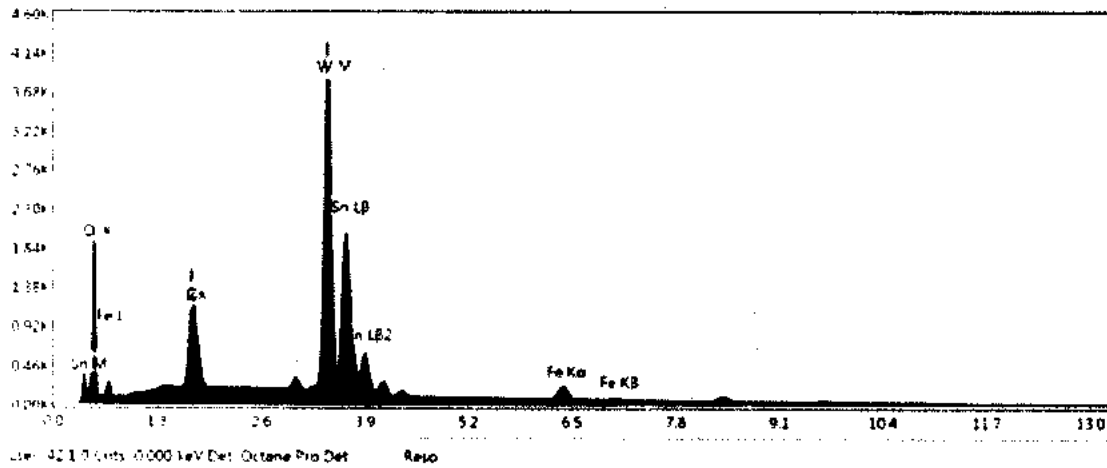


Element	Weight %	Atomic %	Net Int.	Error %
OK	14.36	53.55	447.5	8.35
WM	11.66	3.78	316.11	5.8
FeK	2.78	2.97	40.81	17.04

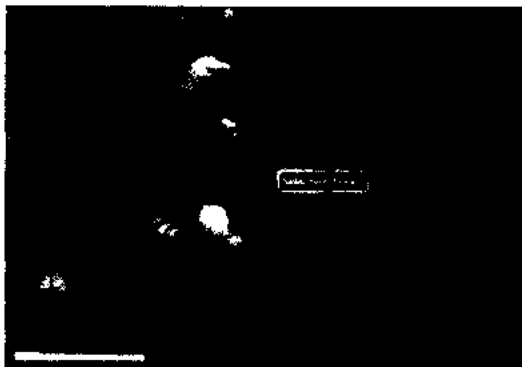
Figure 3.20: EDX spectra of nano composite thin film, area selected for EDX analysis and weight % present in nano composite film prepared with (1:1:1) ratio.

3.3.3 EDX analysis of $\text{WO}_3\text{-}\alpha\text{-Fe}_2\text{O}_3\text{-RGO}$ nanocomposite thin film prepared with (2:1:2) ratio

EDX analysis is carried out to get the elemental analysis of nano composite $\text{WO}_3\text{-}\alpha\text{-Fe}_2\text{O}_3\text{-RGO}$ thin film prepared with (2:1:2) ratio. EDX spectra gives different elemental data in nano composite, and observed peaks are of Sn, W, Fe, C and O respectively. Sb peak is due to the FTO substrate and it shows that film prepared is very thin and table shows there weight percentage and atomic percentage in nano composite $\text{WO}_3\text{-}\alpha\text{-Fe}_2\text{O}_3\text{-RGO}$ thin film. W, Fe, O and C supports the elements in nano composite thin film which is used as a photo anode in PEC water splitting.



eZAF Smart Quant Results

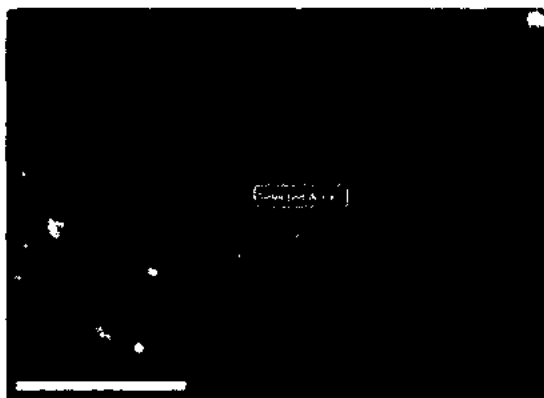
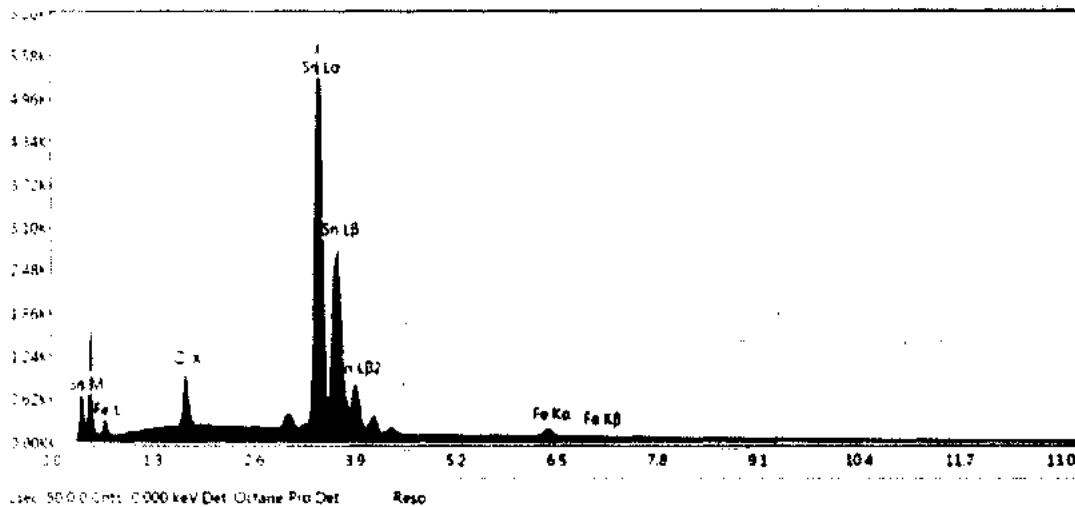


Element	Weight %	Atomic %	Net Int.	Error %
OK	17.82	54.61	418.3	8.72
WM	71.13	29.38	1983.96	2.01

Figure 3.21: EDX spectra of nano composite thin film, area selected for EDX analysis and weight % present in nano composite film prepared with (2:1:2) ratio.

3.3.4 EDX analysis of α -Fe₂O₃-RGO nano composite thin film

EDX analysis is carried out to get the elemental analysis of nano composite α -Fe₂O₃-RGO synthesized hydrothermally. EDX spectra gives different elemental data in nano composite, and observed peaks are of Sn, Fe, C and O respectively. Sb peak is due to the FTO substrate and it shows that film prepared is very thin and table shows there weight percentage and atomic percentage in nano composite WO₃- α -Fe₂O₃-RGO thin film. Fe, O and C supports the elements in nano composite thin film which is used as a photo anode in PEC water splitting



eZAF Smart Quant Results

Element	Weight %	Atomic %	Net Int	Error %
CK	4.02	14.6	206.2	9.64
FeK	2.92	5.34	64.39	14.14

Figure 3.22: EDX spectra of α -Fe₂O₃-RGO nano composite thin film, area selected for EDAX analysis and weight % present in nano composite film.

Optical Analysis

3.3 UV-Vis spectroscopy analysis

3.3.1 UV-Vis analysis of graphene oxide (GO)

Figure shows the UV-Vis spectra of GO, to determine the degree of oxidation of graphene UV-vis analysis is carried out. In the figure shown two peaks are observed, first peak observed around 223 nm is because of $\pi-\pi^*$ transition for bonding of C=C, these peaks matched with literature.

Other peak observed around the 300 nm is because of the carbonyl group $n-\pi^*$ transition. Similarly, ratio of peak intensity is 1.53 (a.u), UV-Vis spectra still reported for GO is less than 2, therefore it satisfy the results reported .

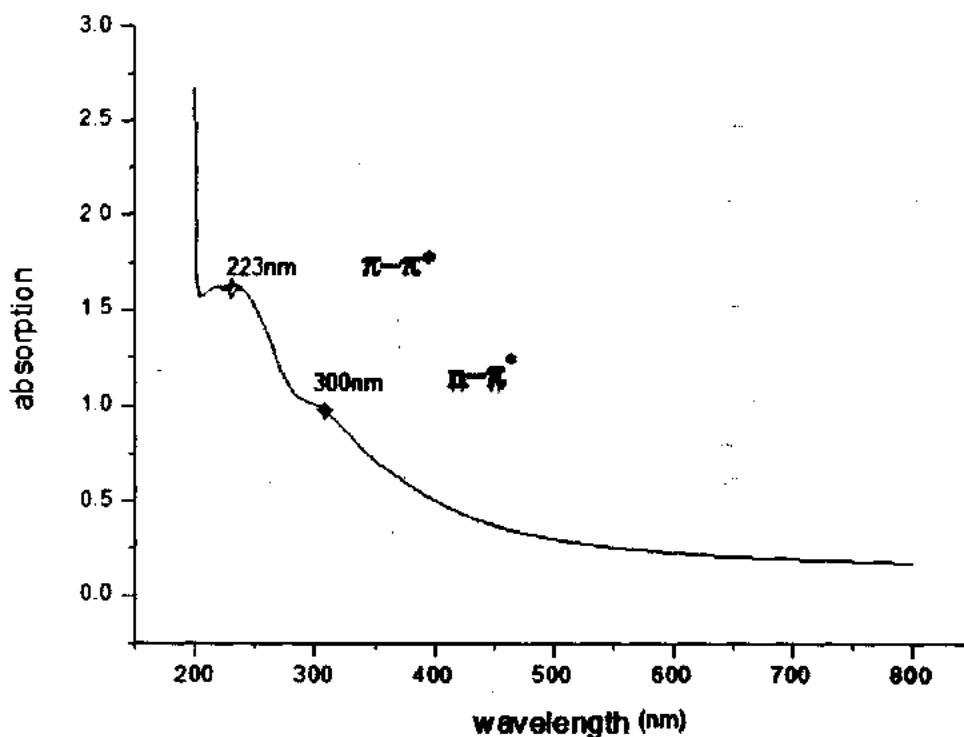


Figure3.23: UV-Visible Spectra of Graphene Oxide (GO)

3.3.2 UV-Vis analysis of reduced graphene oxide (RGO)

Figure shows the UV-Vis spectra of Reduced Graphene Oxide, hydrothermal reduction of graphene oxide with hydrazine cause removal of oxygenated groups that's why only one peak was observed around 263nm [196].

Reduction cause electron transportation between π - π conjugations. Red shifts was observed due to the large absorption of energy in n - π^* conjugation as compared to the π - π conjugations, also due to the restoration of C=C bonds during reduction.

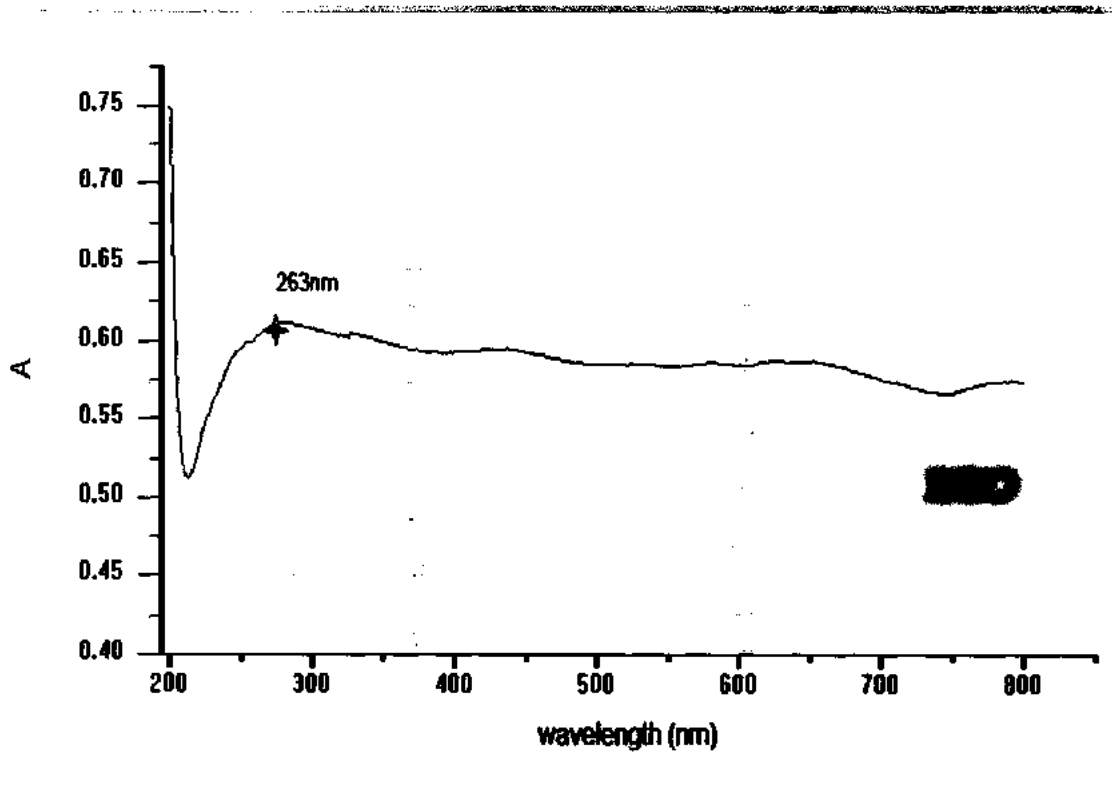


Figure3.24: UV-Visible spectra of reduced graphene oxide (RGO).

3.3.3 UV-Visible analysis of α -Fe₂O₃

Figure shows the UV-Visible spectra of hematite prepared from method 1 hydrothermally. UV-Visible measurements are carried out to determine the size effect, [197] band gap and electronic structure of the hematite nano particles, results shows that 3 peaks are observed. 1 peak between 200-300nm centred around 253 nm, and 2, 3 peaks are observed between 400-600 nm centred around 450 and 560 nm. Frist peak mostly observed due to the transitions which take place from ligand to the metal charge transfer and due to the Fe³⁺- Fe³⁺ excitation. Band gap calculated from linear extrapolation of $(\alpha h\nu)^n$ vs $(h\nu)$ for hematite is 2.1 ev.

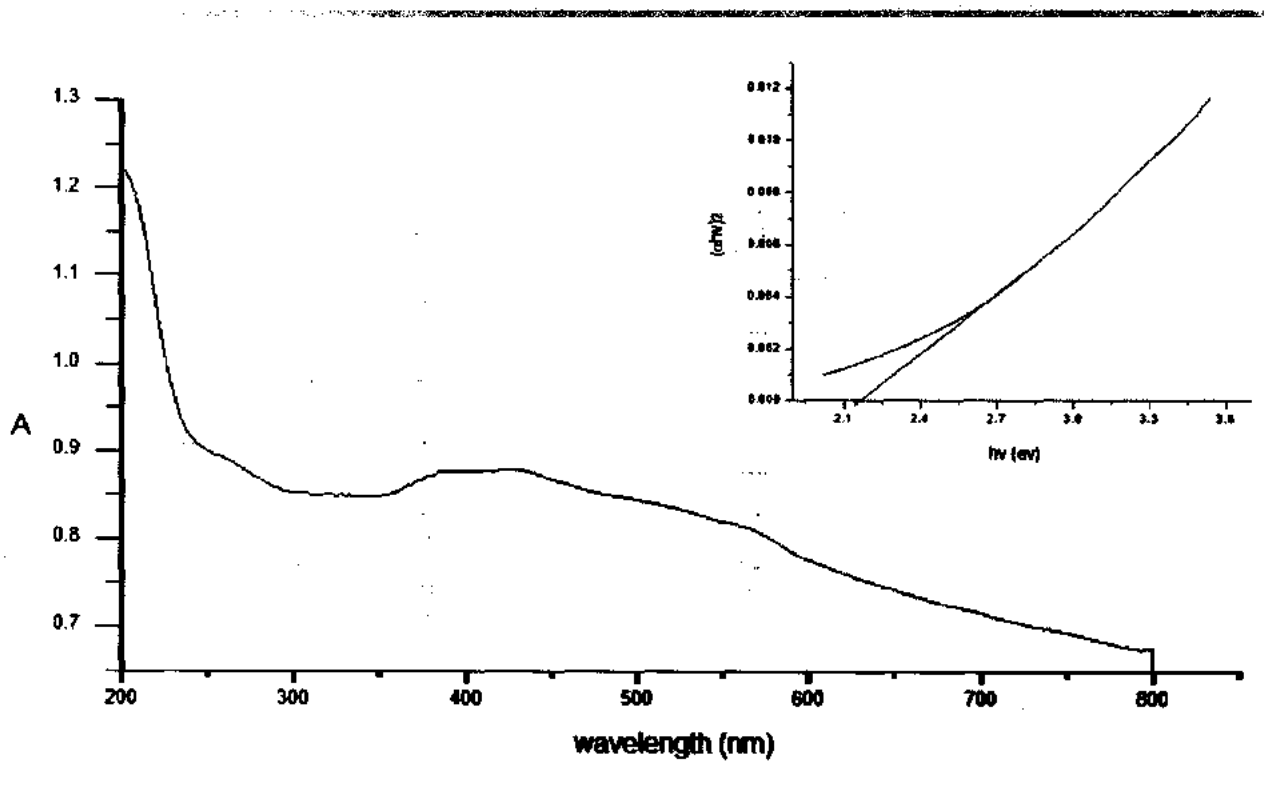


Figure 3.25: UV-Visible spectra of α -Fe₂O₃.

3.3.4 UV-Visible analysis of $\alpha\text{-Fe}_2\text{O}_3$

Figure shows the UV-Visible analysis of hematite prepared from method 3, hydrothermally with changed precursors. Maximum peak is observed at 1.0 (a.u) and at wavelength of 410 nm, band gap calculated from tauc plot is 2.3ev. Good amount of light is absorbed between Wavelength ranges of 250-650 nm

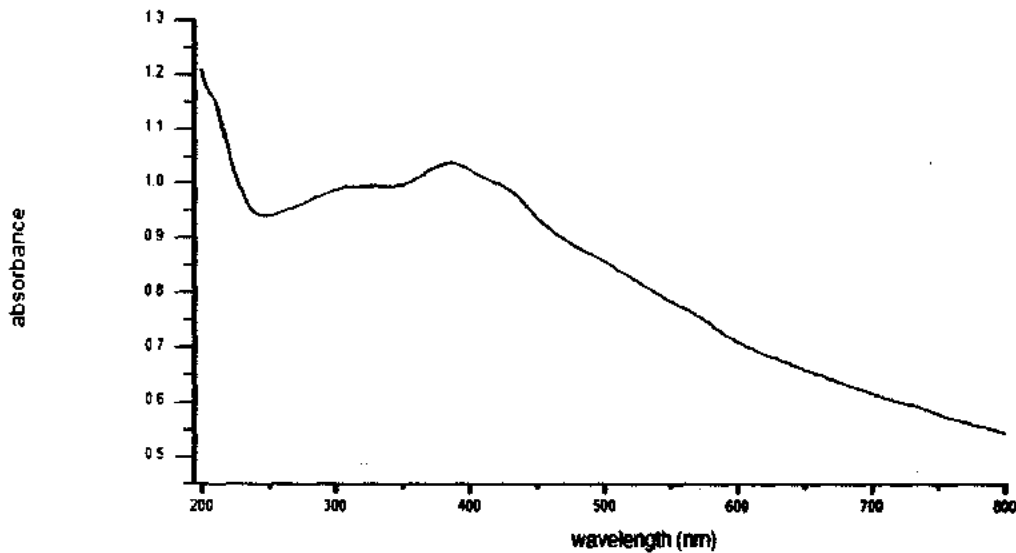


Figure3.25: UV-Visible spectra of $\alpha\text{-Fe}_2\text{O}_3$.

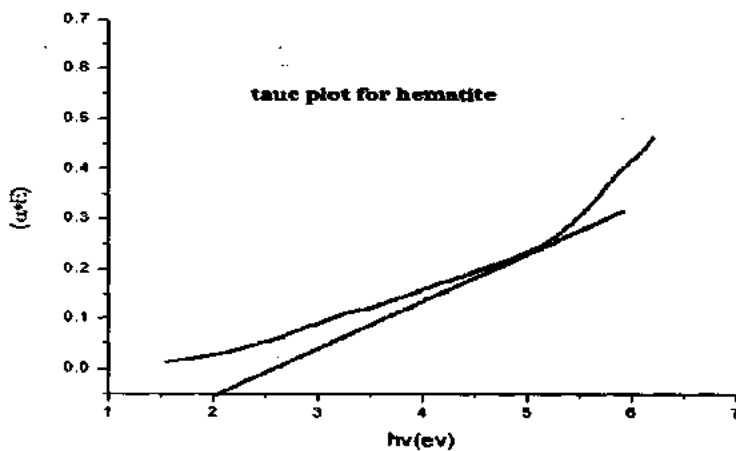


Figure3.26: tauc plot for band gap measurement.

3.3.5 UV-Visible analysis of WO₃

Figure shows the UV-Visible analysis of WO₃ prepared hydrothermally. Maximum peak 3.4(a.u) and at a wavelength of 270 nm, which is in UV range, band gap calculated from tauc plot is 2.4ev for WO₃ [198]. Light is absorbed in wavelength range of 270-550 nm.

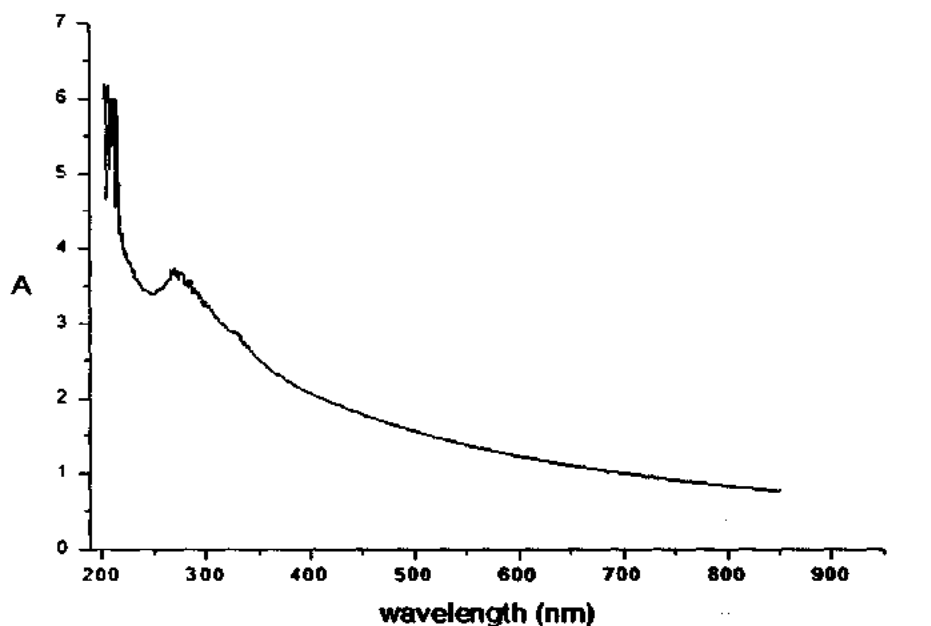


Figure3.27: UV-Visible spectra of WO₃, prepared hydrothermally at 180°C for 6 hour.

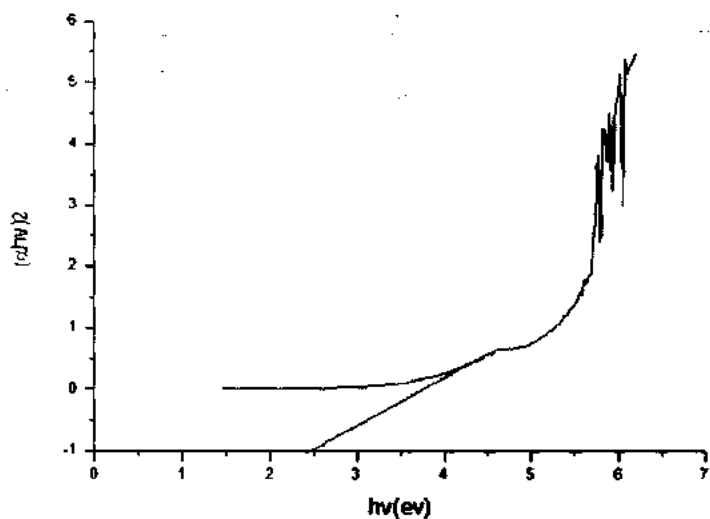


Figure3.28: tauc plot for band gap measurement of wo3

3.3.6 UV-Visible analysis of WO₃ (prepared with different method)

Figure shows the UV-Visible analysis of WO₃ prepared hydrothermally at 120°C for 12 hours. 2 peaks are observed at 1.4 (a.u) and 1.3 (a.u) with wavelength of 250nm and 400nm, band gap calculated from tauc plot is 2.4 ev, which is larger than reported in literature.

Light is absorbed in wavelength range of 200-750 nm, which covers Uv-Vis range.

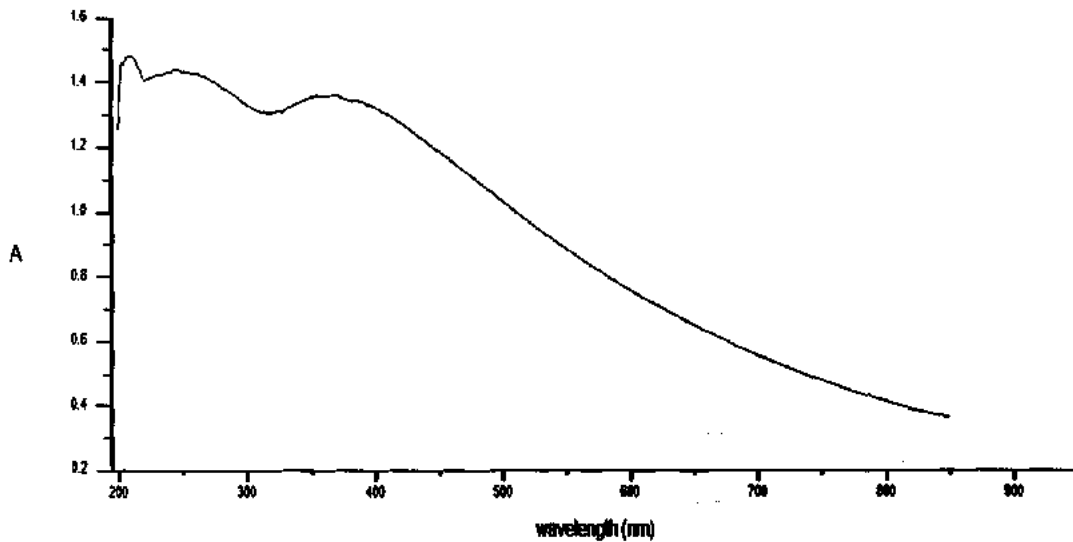


Figure3.29:UV-Visible spectra of WO₃ prepared hydrothermally at 120°C for 12h.

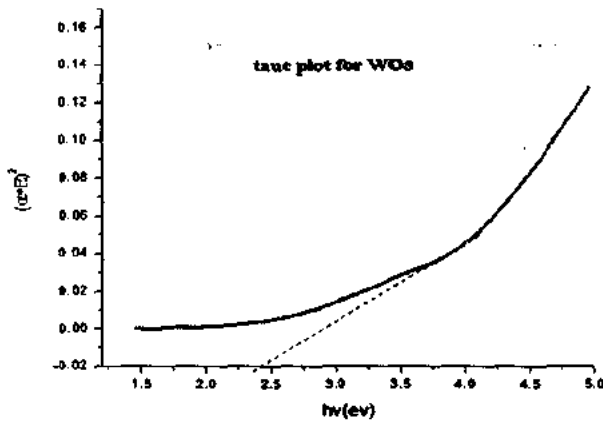


Figure3.30: tauc plot for WO₃ prepared hydrothermally at 120°C for 12h.

3.3.7 UV-Visible Analysis of α -Fe₂O₃ -GO nano composite

Figure shows the UV-Visible spectra of α -Fe₂O₃ -GO nano composite, prepared solvothermally. Maximum light is absorbed between wavelength range 220-910 nm, which means that nanocomposite absorb light in UV-Visible and near IR region. Band gap calculated from linear extrapolation of $(\alpha h\nu)^n$ vs $(h\nu)$ for nano composite is 3.09 eV.

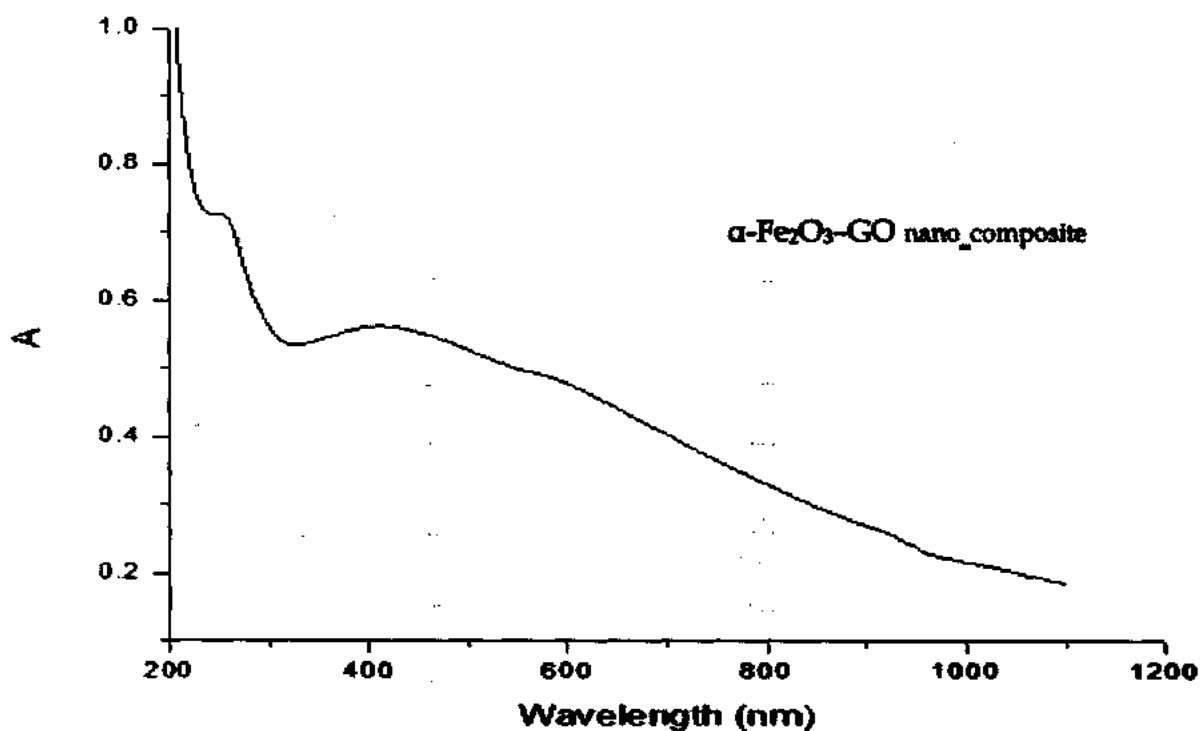


Figure3.31: UV-Visible spectra of α -Fe₂O₃ -GO nano composite

3.3.8 UV-Visible analysis of $\alpha\text{-Fe}_2\text{O}_3(\text{dark})\text{-WO}_3$ nano composite

Figure shows the UV-Visible spectra of $\alpha\text{-Fe}_2\text{O}_3\text{-WO}_3$ nano composite , prepared solvothermally .For UV-Visible analysis of $\alpha\text{-Fe}_2\text{O}_3\text{-WO}_3$ nano composite, make dilution of 0.05 g (nano composite) in 10 ml of iso-propanol followed by the sonication of 30 minutes.

4 absorption peaks are observed on 3.2(a.u), 2.5(a.u) ,2.0 (a.u), 1.3(a.u) at wavelengths of 279nm, 400nm, 610nm, 1030nm. Nano composite of $\alpha\text{-Fe}_2\text{O}_3(\text{dark})\text{-WO}_3$ shows a good absorption in UV-Vis and IR range. Band gap calculated from tauc plot for nano composite is 2.03 eV.

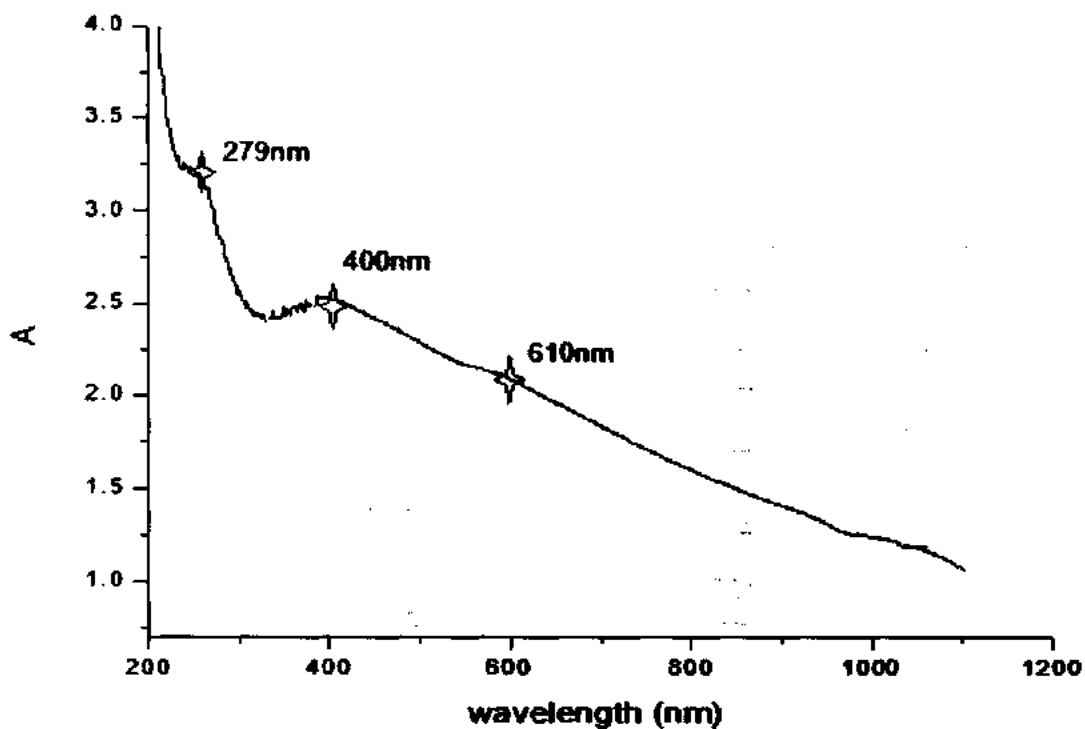


Figure3.33: UV-Visible spectra of $\alpha\text{-Fe}_2\text{O}_3(\text{dark})\text{-WO}_3$ nano composite

3.3.9 UV-Visible analysis of $\alpha\text{-Fe}_2\text{O}_3$ (lite) – WO_3 nano composite

Figure shows the UV-Visible spectra of $\alpha\text{-Fe}_2\text{O}_3$ (lite) – WO_3 nano composite, prepared solvothermally.

For UV-Visible analysis of $\alpha\text{-Fe}_2\text{O}_3$ – WO_3 nano composite , make dilution of 0.09 g (nano composite) in 10 ml of iso-propanol followed by the sonication of 30 minutes. 4 absorption peaks are observed on 1.6 (a.u), 1.3 (a.u) ,1.2 (a.u), 0.7 (a.u) at wavelengths of 230nm, 400nm, 600nm, 920nm. Nano composite of $\alpha\text{-Fe}_2\text{O}_3$ (lite) – WO_3 shows a good absorption in UV-Vis range. Band gap calculated from tauc plot for nano composite is 2.0 eV.

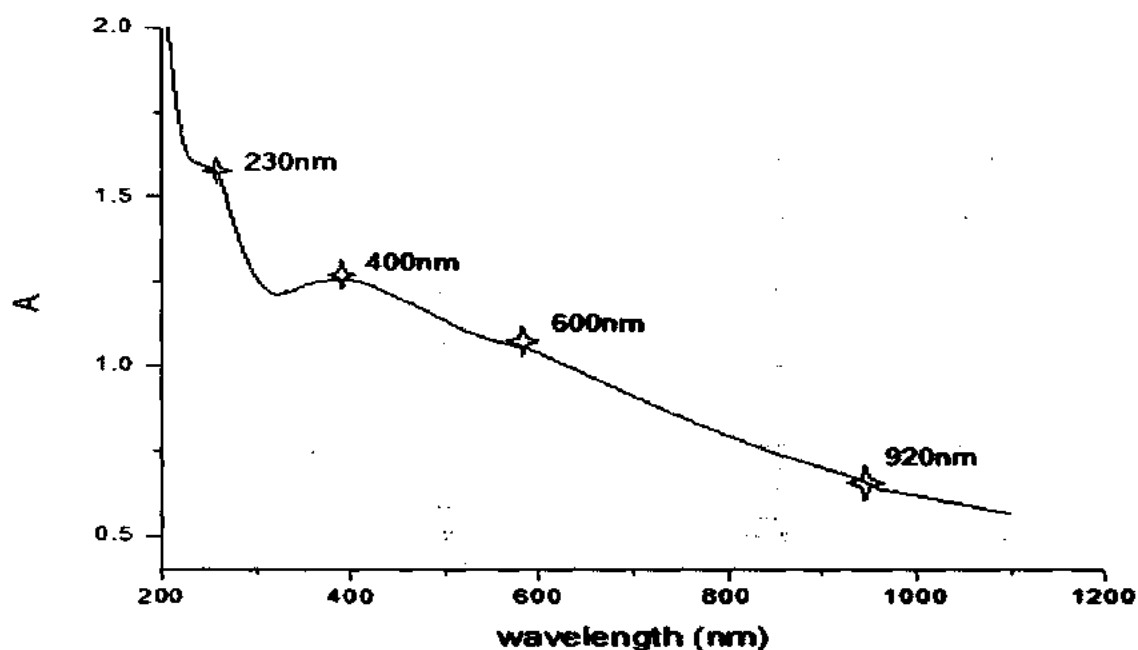


Figure3.34: UV-Visible spectra of $\alpha\text{-Fe}_2\text{O}_3$ (lite) – WO_3 nano composite

3.3.10 UV-Visible analysis of $\alpha\text{-Fe}_2\text{O}_3$ (dark)- WO_3 -RGO nano composite

Figure shows the UV-Visible spectra of $\alpha\text{-Fe}_2\text{O}_3$ (dark)- WO_3 -RGO nano composite, prepared solvothermally with same ratios (1:1:1). For UV-Visible analysis of $\alpha\text{-Fe}_2\text{O}_3$ - WO_3 -RGO nano composite, make dilution of 0.07g (nano composite) in 10 ml of iso-propanol followed by the sonication of 30 minutes. 3 absorption peaks are observed on 1.4 (a.u), 1.3 (a.u), 0.9 (a.u), at wavelengths of 250nm, 400nm, 560nm. Nano composite of $\alpha\text{-Fe}_2\text{O}_3$ (dark)- WO_3 -RGO shows a good absorption in UV-Vis range. Band gap calculated from tauc plot for nano composite is 2.0 eV.

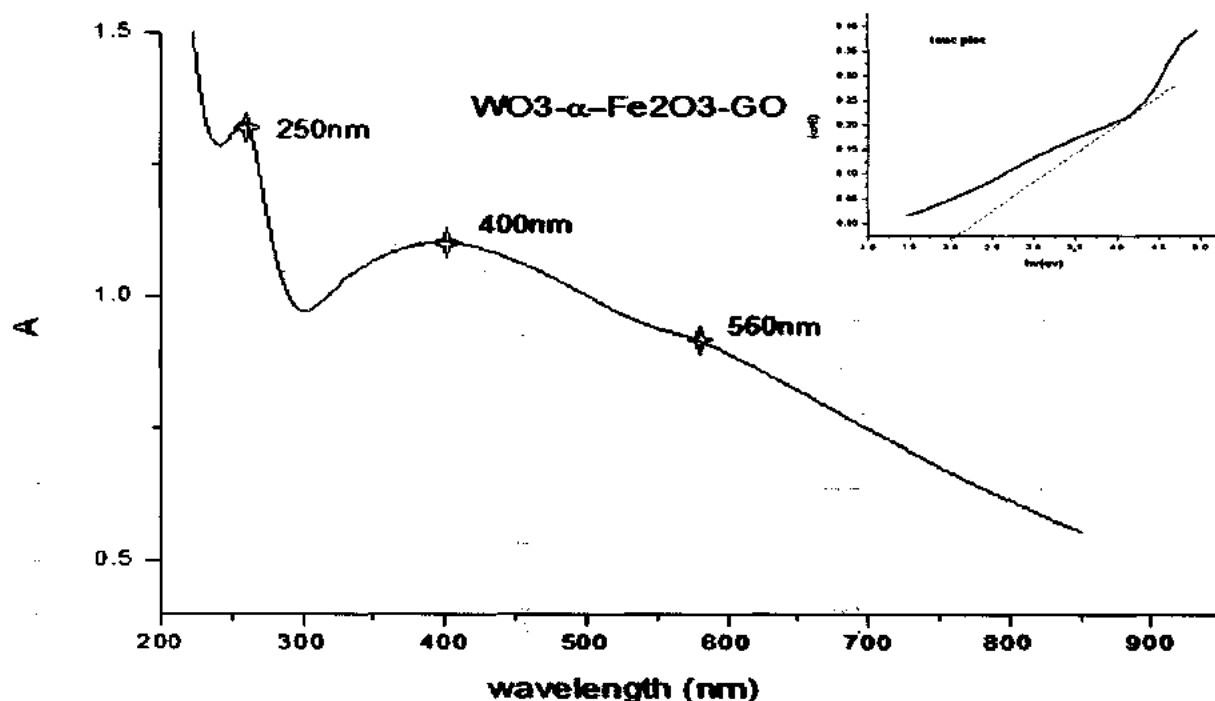


Figure3.35: UV-Visible spectra of $\alpha\text{-Fe}_2\text{O}_3$ (dark)- WO_3 -RGO synthesized with same ratios (1:1:1)

3.3.11 UV-Visible analysis of $\alpha\text{-Fe}_2\text{O}_3$ (dark)- WO_3 -RGO nanocomposite

Figure shows the UV-Visible spectra of $\alpha\text{-Fe}_2\text{O}_3$ (dark)- WO_3 -RGO nano composite, prepared solvothermally with different ratios (1:2:2). For UV-Visible analysis of $\alpha\text{-Fe}_2\text{O}_3$ - WO_3 -RGO nano composite, make dilution of 0.07g (nano composite) in 10 ml of iso-propanol followed by the sonication of 30 minutes.

Absorption peaks are observed on 1.6 (a.u), 1.4(a.u), 1.3 (a.u), at wavelengths of 250nm, 410nm, 600nm. Nano composite of $\alpha\text{-Fe}_2\text{O}_3$ (dark)- WO_3 -RGO shows a good absorption in UV-Vis and IR range. Band gap calculated from tauc plot for nano composite is 2.03 eV.

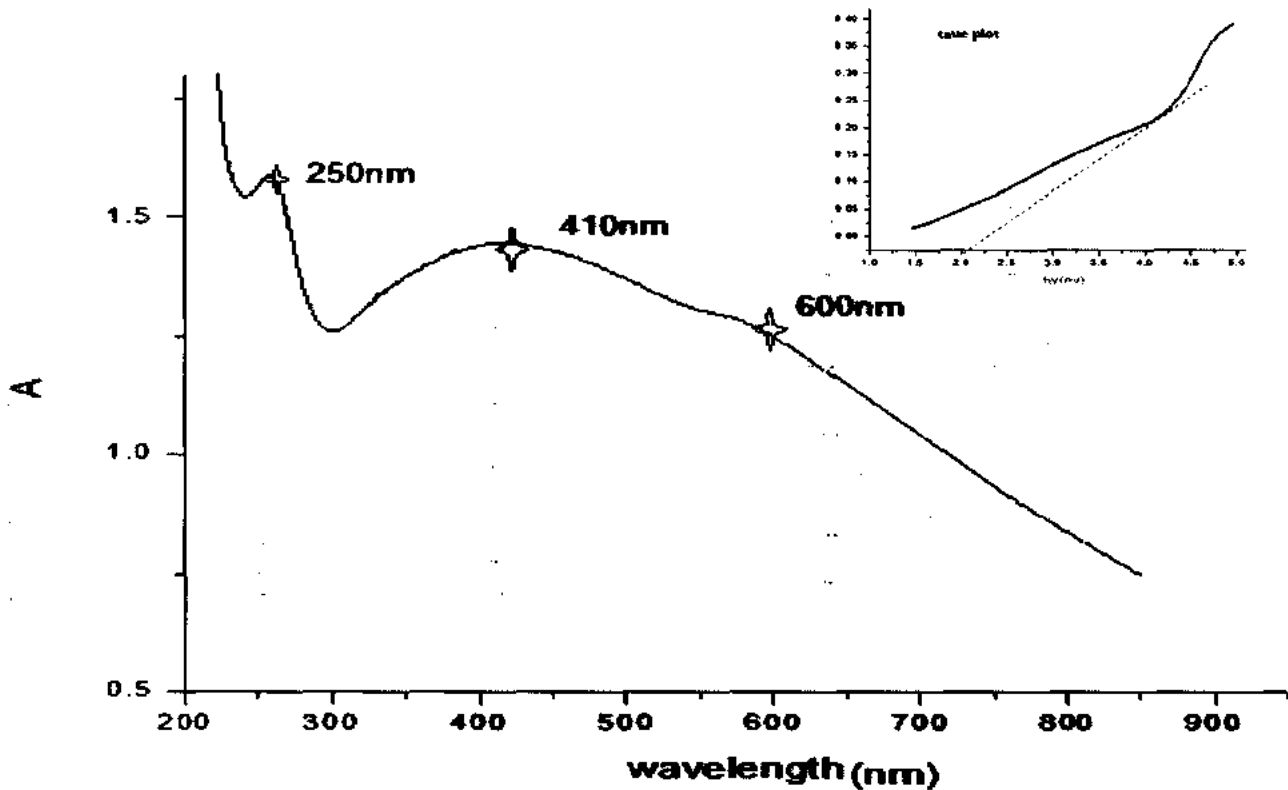


Figure 3.36: UV-Visible spectra of $\alpha\text{-Fe}_2\text{O}_3$ (dark)- WO_3 -RGO nano composite synthesized with different ratios (1:2:2).

3.4 Electrochemical Analysis

Photo electrochemical analysis was conducted in 1 molar sulphuric acid (H_2SO_4) solution for WO_3 and WO_3-GO , and 0.1, 1 molar sodium sulphate solution for all other composites, working electrode potential was analyzed by potentiostat. In three electrode configuration of cell.

- Graphite rod is used as a counter electrode.
- As a reference electrode $Ag/AgCl$ is used (which contains $Ag/AgCl$ solution and saturated KCl).
- For accurate measurements, working sense was attached to the working electrode and counter sense to the counter electrode.
- Measurements are taken in white light and dark, white light measurements are taken under solar simulator having AM 1.5 simulated solar illumination, having input power density of $100mW/cm^2$.

3.4.1 Linear sweep voltammetry of WO_3

Photo anode prepared by depositing WO_3 nano particles on FTO, is used as a working electrode. LSVs are taken for sample, as applied potential of working electrode and potential of molecular species on the surface of WO_3 film, the oxidation starts and molecules try to move away from the surface of n-type WO_3 , to give chance to other molecules to oxidize, therefore current flow starts due to the transportation of electron in and out of the working electrode.

Larger scan rate cause larger current, in dark maximum current is obtained at 1.6 Ma at scan rate of 10mv/s and at voltage (V vs Ag/AgCl) at 0.25 volts. Similarly in one sun light photo anode showed a amazing response towards visible light and current increases to 5.6Ma at potential of 0.1volts and at a scan rate of 10mv/s. By decreasing the scan rate to 5mv/s, photocurrent will decrease to 5.3Ma.

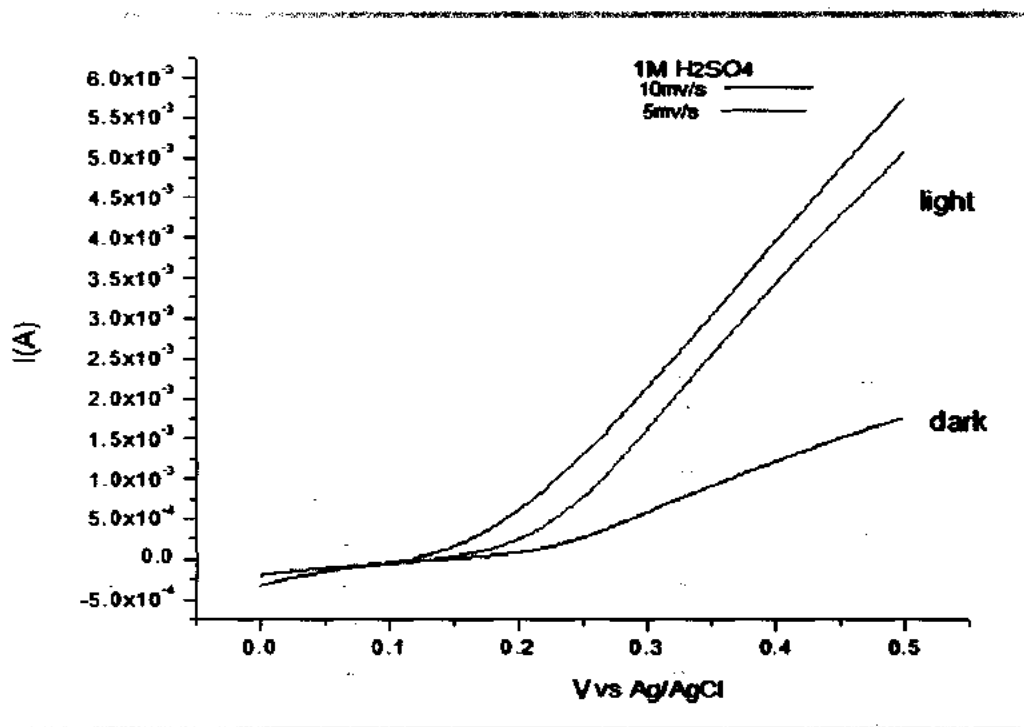


Figure3.37: linear sweep voltammograms of WO₃ on FTO, with different scan rates under light i.e 10mv/s, 5mv/s .

3.4.2 Linear sweep voltammetry of hematite (α -Fe₂O₃)

Photo anode prepared by depositing α -Fe₂O₃ nano particles on FTO, is used as a working electrode. LSVs are taken for sample, as applied potential of working electrode and potential of molecular species on the surface of α -Fe₂O₃ film, the oxidation starts and molecules try to move away from the surface of n-type α -Fe₂O₃, to give chance to other molecules to oxidize, therefore current flow starts due to the transportation of electron in and out of the working electrode.

Larger scan rate cause larger current, in dark maximum current is obtained at 200micro amperes at scan rate of 10mv/s and at voltage (V vs Ag/AgCl) at 0.42 volts. Similarly in one sun light photo anode showed a amazing response towards visible light and current increases to 6.1 milli amps at potential of 0.1volts and at a scan rate of 10mv/s. By decreasing the scan rate to 5 mv/s, photocurrent will decrease to 4.7Ma.

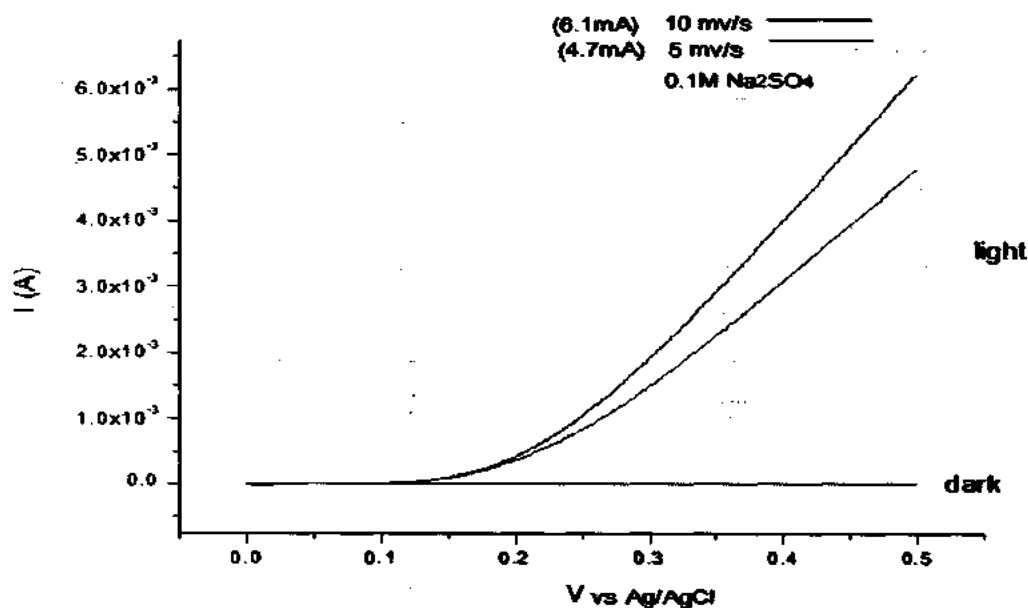


Figure3.38: linear sweep voltammograms of hematite (α -Fe₂O₃) in dark and under AM 1.5 simulated solar light.

3.4.3 Linear sweep voltammetry of WO₃-RGO

Photo anode prepared by depositing WO₃-RGO nano composite on FTO, is used as a working electrode. LSVs are taken for sample, as applied potential of working electrode and potential of molecular species on the surface of WO₃-RGO nano composite film, the oxidation starts and molecules try to move away from the surface of nano composite, to give chance to other molecules to oxidize, therefore current flow starts due to the transportation of electron in and out of the working electrode.

Larger scan rate cause larger current, in dark maximum current is obtained at 20 micro amperes at scan rate of 10mv/s and at voltage (V vs Ag/AgCl) at 0.45 volts. Similarly in one sun light photo anode showed a amazing response towards visible light and current increases to 5.0 milli amps at potential of 0.1volts and at a scan rate of 10mv/s. By decreasing the scan rate to 5 mv/s, photocurrent will decrease to 4.1 and 3.9 mill amps

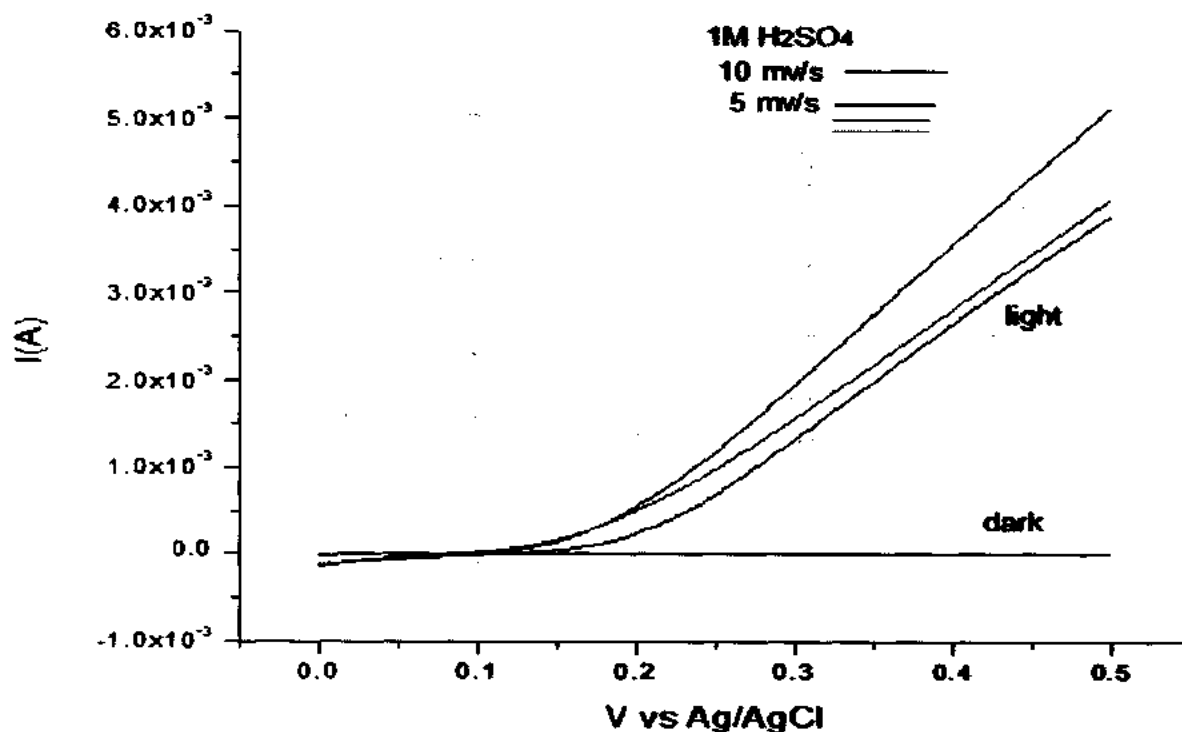


Figure 3.39: linear sweep voltammograms of WO₃-RGO nanocomposite, under dark and under AM 1.5 simulated solar light.

3.4.4 Linear sweep voltammetry of WO₃- α -Fe₂O₃(*lite*) nano composite

Photo anode prepared by depositing WO₃- α -Fe₂O₃ (*lite*) nano composite on FTO, is used as a working electrode. LSVs are taken for sample, as applied potential of working electrode and potential of molecular species on the surface of WO₃- α -Fe₂O₃ (*lite*) nano composite film, the oxidation starts and molecules try to move away from the surface of nano composite, to give chance to other molecules to oxidize, therefore current flow starts due to the transportation of electron in and out of the working electrode.

Larger scan rate cause larger current, in dark maximum current is obtained at 300 micro amperes at scan rate of 5 mv/s and at voltage (V vs Ag/AgCl) at 0.5 volts. Similarly in one sun light photo anode showed a amazing response towards visible light and current increases to 3.3 milli amps at potential of 0.2 volts and at a scan rate of 5 mv/s.

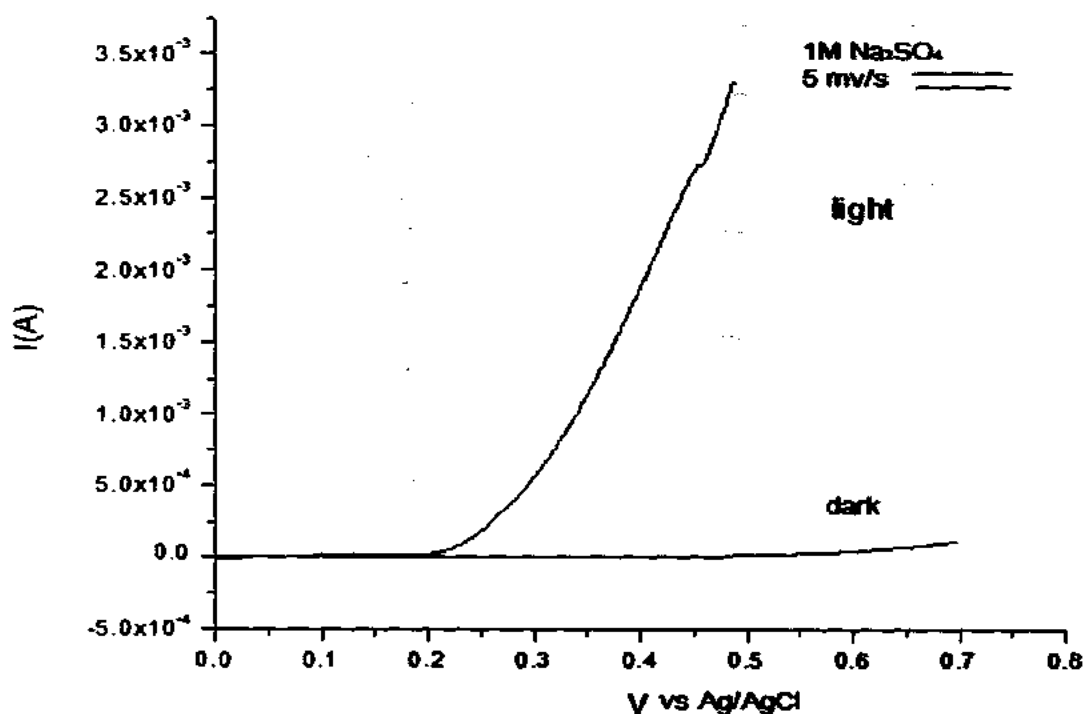


Figure3.40: linear sweep voltammograms of WO₃- α -Fe₂O₃ (*lite*) nanocomposite, under dark and under AM 1.5 simulated solar light.

3.4.5 Linear sweep voltammetry of WO₃- α -Fe₂O₃(dark) nano composite

Photo anode prepared by depositing WO₃- α -Fe₂O₃ (dark) nano composite on FTO, is used as a working electrode. LSVs are taken for sample, as applied potential of working electrode and potential of molecular specie's on the surface of WO₃- α -Fe₂O₃ (dark) nano composite film, the oxidation starts and molecules try to move away from the surface of nano composite, to give chance to other molecules to oxidize, therefore current flow starts due to the transportation of electron in and out of the working electrode[199].

Larger scan rate cause larger current, in dark maximum current is obtained at 900 micro amperes at scan rate of 5 mv/s and at voltage (V vs Ag/AgCl) at 0.35 volts., changing the scan rate in dark will cause increase in photo current upto 1.3 milli amperes. Similarly in one sun light photo anode showed a amazing response towards visible light and current increases to 4.5 milli amps at potential of 0.25 volts and at a scan rate of 10 mv/s.

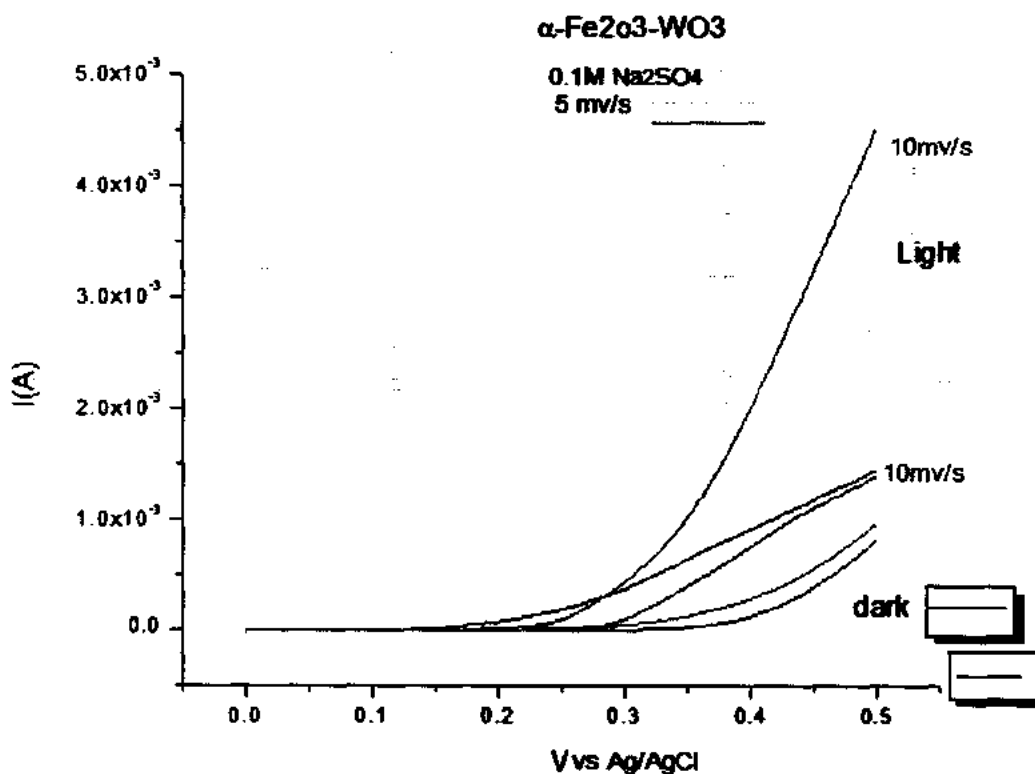


Figure3.41: linear sweep voltammograms of WO₃- α -Fe₂O₃ (dark) nanocomposite, under dark and under AM 1.5 simulated solar light

3.4.6 Linear sweep voltammetry of $\alpha\text{-Fe}_2\text{O}_3$ (dark) -RGO nano composite

Photo anode prepared by depositing $\alpha\text{-Fe}_2\text{O}_3$ (dark)-RGO nano composite on FTO, is used as a working electrode.

LSVs are taken for sample, as applied potential of working electrode and potential of molecular species on the surface of $\alpha\text{-Fe}_2\text{O}_3$ (dark)-RGO nano composite film, the oxidation starts and molecules try to move away from the surface of nano composite, to give chance to other molecules to oxidize, therefore current flow starts due to the transportation of electron in and out of the working electrode[200].

Larger scan rate cause larger current, in dark maximum current is obtained at 200 micro amperes at scan rate of 5 mv/s and at voltage (V vs Ag/AgCl) at 0.8 volts., changing the scan rate (10mv/s) in dark will cause increase in photo current up to 400 and 600 micro amperes. similarly in one sun light photo anode showed a amazing response towards visible light and current increases to 3.1 and 2.9 milli amps at potential of 0.2V, 0.1V and at a scan rate of 10 mv/s.

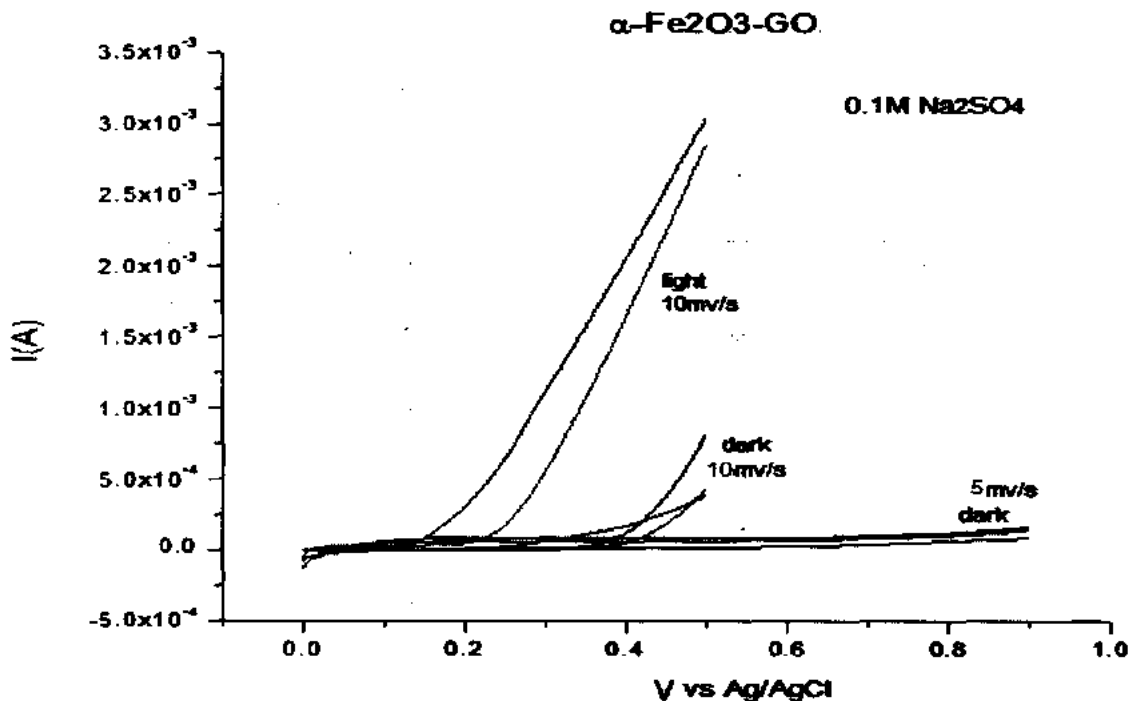


Figure 3.42: linear sweep voltammograms of $\alpha\text{-Fe}_2\text{O}_3$ (dark) -RGO nanocomposite, under dark and under AM 1.5 simulated solar light

3.4.7 Linear sweep voltammetry of WO₃--α-Fe₂O₃ (dark) -RGO nano composite

Photo anode prepared by depositing WO₃--α-Fe₂O₃ (dark) -RGO (nano composite prepared with same ratios (2:1:2)) on FTO , is used as a working electrode. LSVs are taken for sample, as applied potential of working electrode and potential of molecular species on the surface of α-Fe₂O₃ (dark)-RGO nano composite film , the oxidation starts and molecules try to move away from the surface of nano composite , to give chance to other molecules to oxidize ,therefore current flow starts due to the transportation of electron in and out of the working electrode.

Larger scan rate cause larger current,in dark maximum current is obtained at 2.9 milli amperes at scan rate of 5 mv/s and at voltage (V vs Ag/AgCl) at 0.1 volts., similarly in one sun light photo anode showed a amazing response towards visible light and current increases to 5.3 milli amps at potential of 0.15V , and at a scan rate of 5 mv/s.

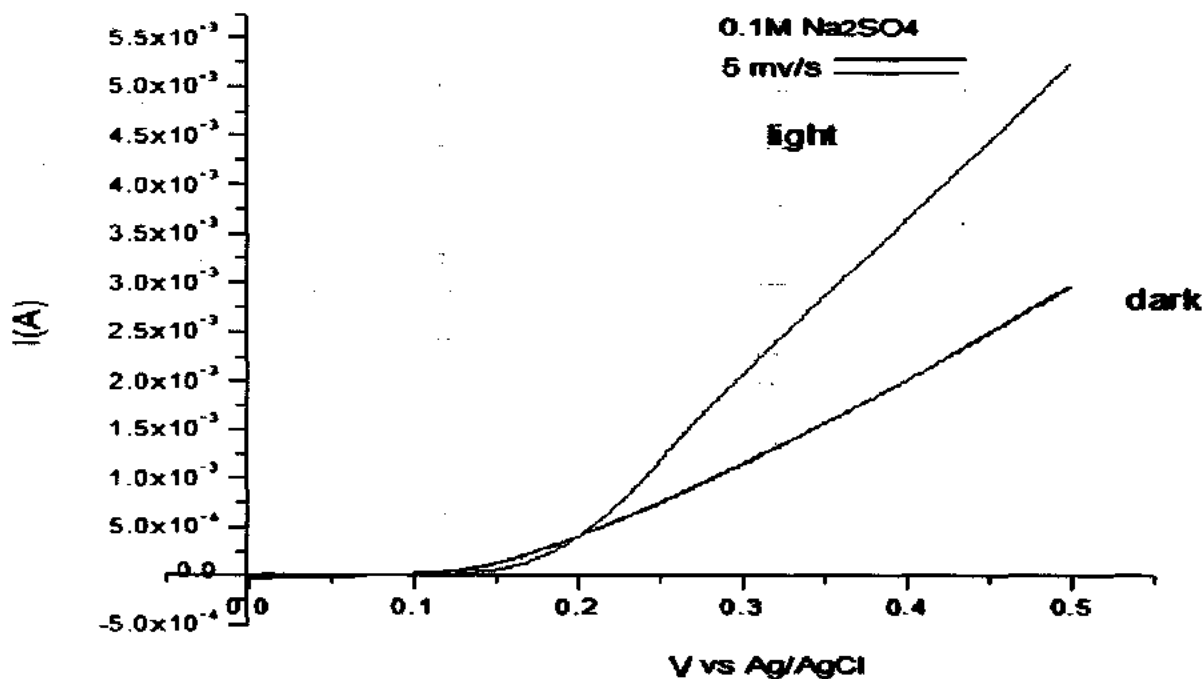


Figure 3.43: linear sweep voltammograms of WO₃--α-Fe₂O₃ (dark) -RGO nanocomposite , under dark and under AM 1.5 simulated solar light

3.4.8 Linear sweep voltammetry of $\text{WO}_3\text{-}\alpha\text{-Fe}_2\text{O}_3\text{(dark)\text{-}RGO}$ nano composite

Photo anode prepared by depositing $\text{WO}_3\text{-}\alpha\text{-Fe}_2\text{O}_3\text{(dark)\text{-}RGO}$ (nano composite prepared with different ratios (1:1:1)) on FTO , is used as a working electrode. LSVs are taken for sample, as applied potential of working electrode and potential of molecular species on the surface of $\text{WO}_3\text{-}\alpha\text{-Fe}_2\text{O}_3\text{(dark)\text{-}RGO}$ nano composite film , the oxidation starts and molecules try to move away from the surface of nano composite , to give chance to other molecules to oxidize ,therefore current flow starts due to the transportation of electron in and out of the working electrode.

Larger scan rate cause larger current,in dark maximum current is obtained at 2.97 milli amperes at scan rate of 10 mv/s and at voltage (V vs Ag/AgCl) at 0.2 volts., similarly in one sun light photo anode showed a amazing response towards visible light and current increases to 3.7 milli amps at potential of 0.15V , and at a scan rate of 10 mv/s.

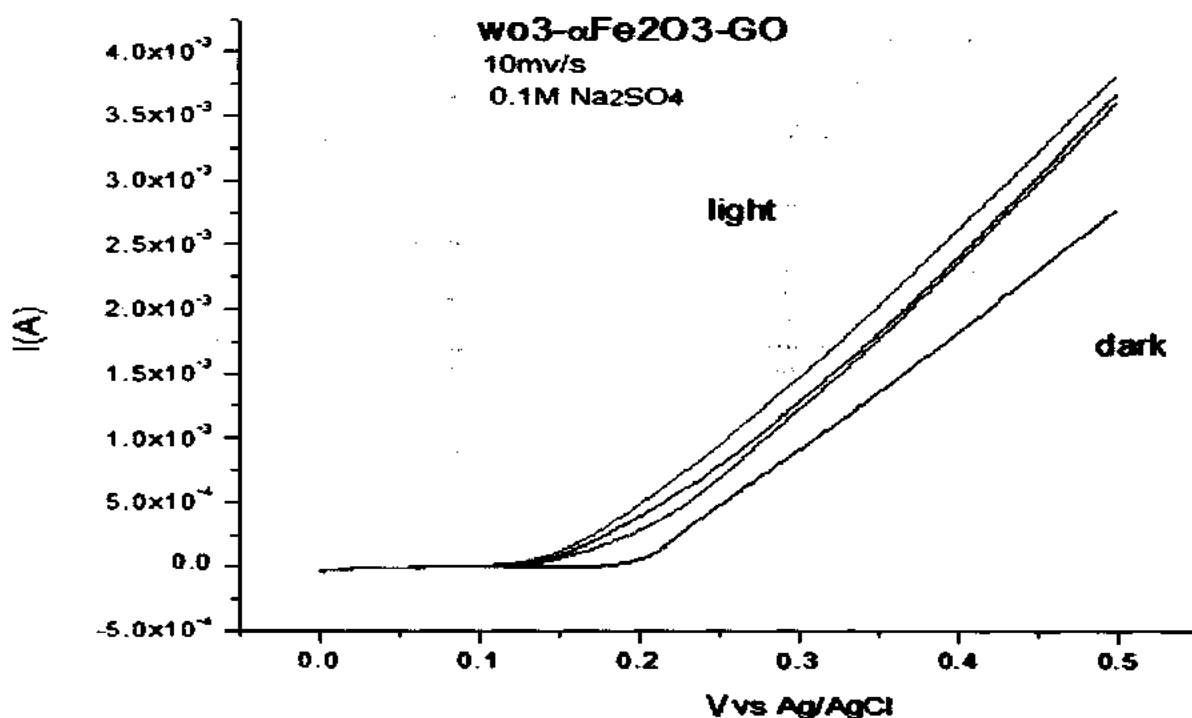


Figure3.44: linear sweep voltammograms of $\text{WO}_3\text{-}\alpha\text{-Fe}_2\text{O}_3\text{(dark)\text{-}RGO}$ nanocomposite , under dark and under AM 1.5 simulated solar light

3.5 Conclusion:

There is a need of cheap production of renewable source i.e hydrogen, photo electrochemical water splitting is a route to get cheap hydrogen and electricity by utilizing solar light for creating a certain potential to split water, optical analysis shows a great absorption by nano composite in ultra-violet and visible range, and our goal was the same to achieve it, similarly morphological analysis shows a roughness and porosity, which means that increase in surface to volume ratio, more reactive sides are available. Elemental analysis prove the composition of nano composites. Metal oxides i.e $\alpha\text{-Fe}_2\text{O}_3$ and WO_3 are known as photocatalyst. WO_3 is an n-type semiconductor but it is known as its photocorrosion against electrolyte, but it absorb visible light due to its large band gap, therefore an other n-type semiconductor photocatalyst is used as a supporter to overcome these short comings, hematite is most suitable and stable semiconductor due to its narrow band gap it shows a good photo response and good stability in electrolyte. When $\text{WO}_3\text{-}\alpha\text{-Fe}_2\text{O}_3$ nano composite come in contact then electron and electrolyte has a direct contact with the FTO substrate, also photo generated holes of $\alpha\text{-Fe}_2\text{O}_3$ are not permitted to pass through WO_3 particle to some extent, therefore photo generated electrons diffusion length increases which enhanced the combination of electron and decrease in photocurrent, therefore to overcome is short coming in nano composite of $\text{WO}_3\text{-}\alpha\text{-Fe}_2\text{O}_3$ and to get good photo response, Graphene is utilized as a transporter, graphene collect the extra electron and move them to external circuit which allow decrease in diffusion length and recombination decreases and enhancement of photo currents. In this thesis graphene is utilized as an efficient transporter which enhance the photocurrents and overcome the short comings of semiconductor metal oxides composites, hence a $\text{WO}_3\text{-}\alpha\text{-Fe}_2\text{O}_3\text{-GO}$ nano composite is our main focus and to observe increase in STH conversion efficiencies. Electrochemical analysis clearly showed an increase in photocurrents i.e for $\text{WO}_3\text{-}\alpha\text{-Fe}_2\text{O}_3$ dark and light photocurrents are 4.5mA and 3.3mA, where as for $\text{WO}_3\text{-}\alpha\text{-Fe}_2\text{O}_3\text{-GO}$ is 5.3mA. Our designed nano composite showed a remarkable change in photocurrents, so utilizing this design of composite commercially will allow large scale production of hydrogen at much cheaper rates.

➤ Solar to hydrogen conversion efficiencies calculated theoretically for PEC cells are:

STH(%)

1) WO ₃	6.3%
2) α-Fe ₂ O ₃	6.8%
3) WO ₃ -RGO	5.6%
4) α-Fe ₂ O ₃ -RGO	3.1%
5) WO ₃ - α-Fe ₂ O ₃ (lite)	3.3%
6) WO ₃ - α-Fe ₂ O ₃ (dark)	4.6%
7) WO ₃ - α-Fe ₂ O ₃ -RGO(1:1:1)	3.9%
8) WO ₃ - α-Fe ₂ O ₃ -RGO(2:1:2)	5.9%

➤ Hydrothermal route leads us to the synthesis of particles :

1. 5.1% still reported for hematite and we obtained 6.89%
2. <5% for WO₃ and we obtained 6.3%.

➤ Efficiencies greater than 1.5 are obtained , which in our opinion are due to the incorporation of graphene , which enhanced the photocurrents and STH efficiencies upto

RGO
incorporation

1. Wo₃-α-Fe₂o₃(lite) → 3.3% → 3.9%
2. Wo₃-α-Fe₂o₃(dark) → 4.6% → 5.9%

➤ Utilization of larger spray guns at commercial level will lead us to a cheap and more suitable deposition route for large scale production of PEC cells.

3.6 References

1. Yang, X., et al., *Enabling practical electrocatalyst-assisted photoelectron-chemical water splitting with earth abundant materials*. *Nano Research*, 2015. **8**(1): p. 56-81.
2. Wang, P., et al., *Stable New Sensitizer with Improved Light Harvesting for Nanocrystalline Dye-Sensitized Solar Cells*. *Advanced Materials*, 2004. **16**(20): p. 1806-1811.
3. Barbir, F., *PEM electrolysis for production of hydrogen from renewable energy sources*. *Solar energy*, 2005. **78**(5): p. 661-669.
4. Panwar, N., S. Kaushik, and S. Kothari, *Role of renewable energy sources in environmental protection: a review*. *Renewable and Sustainable Energy Reviews*, 2011. **15**(3): p. 1513-1524.
5. Dresselhaus, M. and I. Thomas, *Alternative energy technologies*. *Nature*, 2001. **414**(6861): p. 332-337.
6. Winter, C.-J. and J. Nitsch, *Hydrogen as an energy carrier: technologies, systems, economy*. 2012: Springer Science & Business Media.
7. Bak, T., et al., *Photo-electrochemical hydrogen generation from water using solar energy. Materials-related aspects*. *International journal of hydrogen energy*, 2002. **27**(10): p. 991-1022.
8. Edwards, P.P., et al., *Hydrogen and fuel cells: towards a sustainable energy future*. *Energy Policy*, 2008. **36**(12): p. 4356-4362.
9. Momirlan, M. and T.N. Veziroglu, *The properties of hydrogen as fuel tomorrow in sustainable energy system for a cleaner planet*. *International Journal of Hydrogen Energy*, 2005. **30**(7): p. 795-802.
10. Crabtree, G.W., M.S. Dresselhaus, and M.V. Buchanan, *The hydrogen economy*. *Physics Today*, 2004. **57**(12): p. 39-44.
11. Berardi, S., et al., *Molecular artificial photosynthesis*. *Chemical Society Reviews*, 2014. **43**(22): p. 7501-7519.
12. Bora, D.K., A. Braun, and E.C. Constable, *"In rust we trust". Hematite—the prospective inorganic backbone for artificial photosynthesis*. *Energy & Environmental Science*, 2013. **6**(2): p. 407-425.
13. Barber, J. and P.D. Tran, *From natural to artificial photosynthesis*. *Journal of The Royal Society Interface*, 2013. **10**(81): p. 20120984.
14. Gao, Y., et al., *Artificial photosynthesis—functional devices for light driven water splitting with photoactive anodes based on molecular catalysts*. *Physical Chemistry Chemical Physics*, 2014. **16**(24): p. 12008-12013.

15. Ding, X., et al., *Artificial photosynthesis: A two-electrode photoelectrochemical cell for light driven water oxidation with molecular components*. *Electrochimica Acta*, 2014. **149**: p. 337-340.
16. Joya, K.S., et al., *Water-Splitting Catalysis and Solar Fuel Devices: Artificial Leaves on the Move*. *Angewandte Chemie International Edition*, 2013. **52(40)**: p. 10426-10437.
17. Andreiadis, E.S., et al., *Artificial Photosynthesis: From Molecular Catalysts for Light-driven Water Splitting to Photoelectrochemical Cells*. *Photochemistry and photobiology*, 2011. **87(5)**: p. 946-964.
18. BANERJEE, A., *STUDIES ON SOME BIOINSPIRED MATERIALS IN SOLAR ENERGY INDUCED WATER SPLITTING FOR HYDROGEN GENERATION*. 2015.
19. Liu, R., *Nanostructured Semiconductors for High Efficiency Artificial Photosynthesis*. 2013, Boston College.
20. OFFERS, P., *Artificial Photosynthesis and Hydrogen Formation*.
21. Biggins, M., *Preface*. *Slavic & East European Information Resources*, 2001. **1(2-3)**: p. xiii-xvi.
22. Bensaid, S., et al., *Towards artificial leaves for solar hydrogen and fuels from carbon dioxide*. *ChemSusChem*, 2012. **5(3)**: p. 500-521.
23. Bachmeier, A., B. Siritanaratkul, and F.A. Armstrong, *Enzymes as Exploratory Catalysts in Artificial Photosynthesis*, in *From Molecules to Materials*. 2015, Springer. p. 99-123.
24. Magesh, G., et al., *A versatile photoanode-driven photoelectrochemical system for conversion of CO₂ to fuels with high faradaic efficiencies at low bias potentials*. *Journal of Materials Chemistry A*, 2014. **2(7)**: p. 2044-2049.
25. Modestino, M.A., *Self-Assembly and Mass Transport in Membranes for Artificial Photosynthesis*. 2013.
26. Peng, X., et al., *Photovoltaic devices in hydrogen production*. *International Journal of Hydrogen Energy*, 2014. **39(26)**: p. 14166-14171.
27. Gao, Y., et al., *Visible light driven water splitting in a molecular device with unprecedentedly high photocurrent density*. *Journal of the American Chemical Society*, 2013. **135(11)**: p. 4219-4222.
28. Wang, D.Z., F.Z. Zhao, and C.L. Zhu. *Solar hydrogen production research status and prospect*. in *Advanced Materials Research*. 2014. Trans Tech Publ.
29. Ida, S., et al., *Photoelectrochemical hydrogen production from water using p-type and n-type oxide semiconductor electrodes*. *Electrochimica Acta*, 2012. **82**: p. 397-401.
30. Rozhkova, E.A., et al., *Program-Symposium D: From Molecules to Materials—Pathways to Artificial Photosynthesis*.

31. Centi, G. and S. Perathoner, *Artificial Leaves*. Kirk-Othmer Encyclopedia of Chemical Technology.
32. Michl, J., *Photochemical CO₂ reduction: Towards an artificial leaf?* Nature chemistry, 2011. 3(4): p. 268-269.
33. Olaso-González, G., M. Merchán, and L. Serrano-Andrés, *Toward an Understanding of Ultrafast Electron Transfer in Photosynthesis*, in *Photosynthesis. Energy from the Sun*. 2008, Springer. p. 647-651.
34. Allbabaie, L., et al., *Applications of metal oxide materials in dye sensitized photoelectrosynthesis cells for making solar fuels: Let the molecules do the work*. Journal of Materials Chemistry A, 2013. 1(13): p. 4133-4145.
35. Dincer, I., *Green methods for hydrogen production*. international journal of hydrogen energy, 2012. 37(2): p. 1954-1971.
36. Dincer, I. and C. Acar, *Review and evaluation of hydrogen production methods for better sustainability*. International Journal of Hydrogen Energy, 2015.
37. Han, Z. and R. Eisenberg, *Fuel from water: the photochemical generation of hydrogen from water*. Accounts of chemical research, 2014. 47(8): p. 2537-2544.
38. Kärkäs, M.D., et al., *Artificial photosynthesis: from nanosecond electron transfer to catalytic water oxidation*. Accounts of chemical research, 2013. 47(1): p. 100-111.
39. Kolk, A. and A. Mauser, *The evolution of environmental management: from stage models to performance evaluation*. Business strategy and the environment, 2002. 11(1): p. 14.
40. Luther, J., et al., *Solar Technology*. Ullmann's Encyclopedia of Industrial Chemistry, 2000.
41. Centi, G., E.A. Quadrelli, and S. Perathoner, *Catalysis for CO₂ conversion: a key technology for rapid introduction of renewable energy in the value chain of chemical industries*. Energy & Environmental Science, 2013. 6(6): p. 1711-1731.
42. Centi, G., P. Lanzafame, and S. Perathoner, *Introduction and general overview*, in *Catalysis for alternative energy generation*. 2012, Springer. p. 1-28.
43. Moniz, S.J., et al., *Energy & Environmental Science*.
44. Juodkakis, K., et al., *Photoelectrolysis of water: Solar hydrogen—achievements and perspectives*. Optics express, 2010. 18(102): p. A147-A160.
45. Rocheleau, R., E. Miller, and A. Misra. *Photoelectrochemical hydrogen production*. in *Proceedings of the 1996 US DOE Hydrogen Program Review*. 1996.
46. Orbach, R.L., *Energy Production: A Global Perspective*. Alberta Oil Sands: Energy, Industry and the Environment, 2012. 11: p. 1.

47. Lewerenz, H.-J. and L. Peter, *New Perspectives and a Review of Progress. Photoelectrochemical Water Splitting: Materials, Processes and Architectures*, 2013(9): p. 419.
48. Van de Krol, R. and J. Schoonman, *Photo-electrochemical production of hydrogen*, in *Sustainable Energy Technologies*. 2008, Springer. p. 121-142.
49. Reijers, H.T.J., et al. *Hydrogen production through sorption enhanced reforming*. In *Proceedings of the 1st European Hydrogen Energy Conference*. 2003.
50. Moniz, S.J., et al., *Visible-light driven heterojunction photocatalysts for water splitting—a critical review*. *Energy & Environmental Science*, 2015. **8**(3): p. 731-759.
51. Turner, J., *Photoelectrochemical water splitting*. 2004.
52. Maeda, K., *Photocatalytic water splitting using semiconductor particles: history and recent developments*. *Journal of Photochemistry and Photobiology C: Photochemistry Reviews*, 2011. **12**(4): p. 237-268.
53. Zhong, D.K., et al., *Solar water oxidation by composite catalyst/ α -Fe₂O₃ photoanodes*. *Journal of the American Chemical Society*, 2009. **131**(17): p. 6086-6087.
54. Khaselev, O. and J.A. Turner, *A monolithic photovoltaic-photoelectrochemical device for hydrogen production via water splitting*. *Science*, 1998. **280**(5362): p. 425-427.
55. Mayer, M.T., C. Du, and D. Wang, *Hematite/Si nanowire dual-absorber system for photoelectrochemical water splitting at low applied potentials*. *Journal of the American Chemical Society*, 2012. **134**(30): p. 12406-12409.
56. Minggu, L.J., W.R.W. Daud, and M.B. Kassim, *An overview of photocells and photoreactors for photoelectrochemical water splitting*. *International Journal of Hydrogen Energy*, 2010. **35**(11): p. 5233-5244.
57. Li, F., et al., *Towards A Solar Fuel Device: Light-Driven Water Oxidation Catalyzed by a Supramolecular Assembly*. *Angewandte Chemie International Edition*, 2012. **51**(10): p. 2417-2420.
58. Brilliet, J., et al., *Highly efficient water splitting by a dual-absorber tandem cell*. *Nature Photonics*, 2012. **6**(12): p. 824-828.
59. Hisatomi, T., J. Kubota, and K. Domen, *Recent advances in semiconductors for photocatalytic and photoelectrochemical water splitting*. *Chemical Society Reviews*, 2014. **43**(22): p. 7520-7535.
60. Pinaud, B.A., et al., *Technical and economic feasibility of centralized facilities for solar hydrogen production via photocatalysis and photoelectrochemistry*. *Energy & Environmental Science*, 2013. **6**(7): p. 1983-2002.

61. James, B.D., et al., *Technoeconomic analysis of photoelectrochemical (PEC) hydrogen production*. DOE Report, 2009.
62. Brilliet, J., et al., *Examining architectures of photoanode–photovoltaic tandem cells for solar water splitting*. Journal of Materials Research, 2010. **25**(01): p. 17-24.
63. Ampelli, C., et al., *The use of a solar photoelectrochemical reactor for sustainable production of energy*. Theoretical Foundations of Chemical Engineering, 2012. **46**(6): p. 651-657.
64. Pesci, F.M., et al., *Efficient Suppression of Electron–Hole Recombination in Oxygen-Deficient Hydrogen-Treated TiO₂ Nanowires for Photoelectrochemical Water Splitting*. The Journal of Physical Chemistry C, 2013. **117**(48): p. 25837-25844.
65. Zhai, P., et al., *Net primary energy balance of a solar-driven photoelectrochemical water-splitting device*. Energy & Environmental Science, 2013. **6**(8): p. 2380-2389.
66. Yang, J., et al., *Efficient and sustained photoelectrochemical water oxidation by cobalt oxide/silicon photoanodes with nanotextured interfaces*. Journal of the American Chemical Society, 2014. **136**(17): p. 6191-6194.
67. Choudhary, S., et al., *Nanostructured bilayered thin films in photoelectrochemical water splitting—A review*. international journal of hydrogen energy, 2012. **37**(24): p. 18713-18730.
68. Chen, Z., et al., *Accelerating materials development for photoelectrochemical hydrogen production: Standards for methods, definitions, and reporting protocols*. Journal of Materials Research, 2010. **25**(01): p. 3-16.
69. Dotan, H., et al., *On the Solar to Hydrogen Conversion Efficiency of Photoelectrodes for Water Splitting*. The Journal of Physical Chemistry Letters, 2014. **5**(19): p. 3330-3334.
70. Fujishima, A., *Electrochemical photolysis of water at a semiconductor electrode*. nature, 1972. **238**: p. 37-38.
71. Steinfeld, A., *Solar thermochemical production of hydrogen—a review*. Solar energy, 2005. **78**(5): p. 603-615.
72. Yan, H., et al., *Visible-light-driven hydrogen production with extremely high quantum efficiency on Pt–PdS/CdS photocatalyst*. Journal of Catalysis, 2009. **266**(2): p. 165-168.
73. Graetzel, M., *Artificial photosynthesis: water cleavage into hydrogen and oxygen by visible light*. Accounts of Chemical Research, 1981. **14**(12): p. 376-384.
74. Maeda, K., et al., *Photocatalyst releasing hydrogen from water*. Nature, 2006. **440**(7082): p. 295-295.
75. Grätzel, M., *Photoelectrochemical cells*. Nature, 2001. **414**(6861): p. 338-344.
76. Momirlan, M. and T. Veziroğlu, *Recent directions of world hydrogen production*. Renewable and sustainable energy reviews, 1999. **3**(2): p. 219-231.

77. Rocheleau, R.E., E.L. Miller, and A. Misra, *High-efficiency photoelectrochemical hydrogen production using multijunction amorphous silicon photoelectrodes*. *Energy & Fuels*, 1998. **12**(1): p. 3-10.
78. Elam, C.C., et al., *Realizing the hydrogen future: the International Energy Agency's efforts to advance hydrogen energy technologies*. *International Journal of Hydrogen Energy*, 2003. **28**(6): p. 601-607.
79. Mitsui, A., et al., *Progress in Research toward Outdoor Biological Hydrogen Production Using Solar Energy, Sea Water, and Marine Photosynthetic Microorganisms*. *Annals of the New York Academy of Sciences*, 1983. **413**(1): p. 514-530.
80. Turner, J.A., *Sustainable hydrogen production*. *Science*, 2004. **305**(5686): p. 972-974.
81. Kodama, T. and N. Gokon, *Thermochemical cycles for high-temperature solar hydrogen production*. *Chemical Reviews*, 2007. **107**(10): p. 4048-4077.
82. Vellini, M. and J. Tonziello, *Hydrogen Use in an Urban District: Energy and Environmental Comparisons*. *Journal of Energy Resources Technology*, 2010. **132**(4): p. 042601.
83. Shahid, M., N. Bidin, and Y. Mat, *Production and Enhancement of Hydrogen From Water: A Review*. *Journal of Energy Resources Technology*, 2012. **134**(3): p. 034002.
84. Padin, J., T. Veziroglu, and A. Shahin, *Hybrid solar high-temperature hydrogen production system*. *International Journal of Hydrogen Energy*, 2000. **25**(4): p. 295-317.
85. Momirlan, M. and T. Veziroglu, *Current status of hydrogen energy*. *Renewable and Sustainable Energy Reviews*, 2002. **6**(1): p. 141-179.
86. Kim, J.Y., et al., *Graphene-carbon nanotube composite as an effective conducting scaffold to enhance the photoelectrochemical water oxidation activity of a hematite film*. *Rsc Advances*, 2012. **2**(25): p. 9415-9422.
87. Cui, H., et al., *Black TiO₂ nanotube arrays for high-efficiency photoelectrochemical water-splitting*. *J. Mater. Chem. A*, 2014. **2**(23): p. 8612-8616.
88. Huang, Z., et al., *In situ probe of photocarrier dynamics in water-splitting hematite (α -Fe₂O₃) electrodes*. *Energy Environ. Sci.*, 2012. **5**(10): p. 8923-8926.
89. Pendlebury, S.R., et al., *Dynamics of photogenerated holes in nanocrystalline α -Fe₂O₃ electrodes for water oxidation probed by transient absorption spectroscopy*. *Chemical Communications*, 2011. **47**(2): p. 716-718.
90. van de Krol, R., Y. Liang, and J. Schoonman, *Solar hydrogen production with nanostructured metal oxides*. *Journal of Materials Chemistry*, 2008. **18**(20): p. 2311-2320.

91. Lin, Y., et al., *Growth of p-type hematite by atomic layer deposition and its utilization for improved solar water splitting*. Journal of the American Chemical Society, 2012. **134**(12): p. 5508-5511.
92. Kronawitter, C.X., et al., *A perspective on solar-driven water splitting with all-oxide hetero-nanostructures*. Energy & Environmental Science, 2011. **4**(10): p. 3889-3899.
93. Miller, E.L., et al., *Optimization of hybrid photoelectrodes for solar water-splitting*. Electrochemical and Solid-State Letters, 2005. **8**(5): p. A247-A249.
94. Xie, G., et al., *Graphene-Based Materials for Hydrogen Generation from Light-Driven Water Splitting*. Advanced Materials, 2013. **25**(28): p. 3820-3839.
95. Zhang, Z. and P. Wang, *Highly stable copper oxide composite as an effective photocathode for water splitting via a facile electrochemical synthesis strategy*. Journal of Materials Chemistry, 2012. **22**(6): p. 2456-2464.
96. Sivula, K., F. Le Formal, and M. Grätzel, *Solar water splitting: progress using hematite (α -Fe₂O₃) photoelectrodes*. ChemSusChem, 2011. **4**(4): p. 432-449.
97. Navarro Yerga, R.M., et al., *Water Splitting on Semiconductor Catalysts under Visible-Light Irradiation*. ChemSusChem, 2009. **2**(6): p. 471-485.
98. Su, J., et al., *Nanostructured WO₃/BiVO₄ heterojunction films for efficient photoelectrochemical water splitting*. Nano letters, 2011. **11**(5): p. 1928-1933.
99. Liu, C., et al., *A fully integrated nanosystem of semiconductor nanowires for direct solar water splitting*. Nano letters, 2013. **13**(6): p. 2989-2992.
100. Mayer, M.T., et al., *Forming heterojunctions at the nanoscale for improved photoelectrochemical water splitting by semiconductor materials: case studies on hematite*. Accounts of chemical research, 2013. **46**(7): p. 1558-1566.
101. Aryal, K., et al., *Hydrogen generation by solar water splitting using p-InGaN photoelectrochemical cells*. GaN, 2010. **15**(2.01017): p. 2.1.
102. Yin, W.-J., et al., *Band structure engineering of semiconductors for enhanced photoelectrochemical water splitting: The case of TiO₂*. Physical Review B, 2010. **82**(4): p. 045106.
103. Osterloh, F.E., *Inorganic materials as catalysts for photochemical splitting of water*. Chemistry of Materials, 2007. **20**(1): p. 35-54.
104. Yin, Z., et al., *Full Solution-Processed Synthesis of All Metal Oxide-Based Tree-like Heterostructures on Fluorine-Doped Tin Oxide for Water Splitting*. Advanced Materials, 2012. **24**(39): p. 5374-5378.

105. Zhong, D.K., et al., *Photo-assisted electrodeposition of cobalt-phosphate (Co-Pi) catalyst on hematite photoanodes for solar water oxidation*. *Energy & Environmental Science*, 2011. **4**(5): p. 1759-1764.
106. Zhong, D.K. and D.R. Gamelin, *Photoelectrochemical water oxidation by cobalt catalyst ("Co-Pi")/ α -Fe₂O₃ composite photoanodes: Oxygen evolution and resolution of a kinetic bottleneck*. *Journal of the American Chemical Society*, 2010. **132**(12): p. 4202-4207.
107. Hisatomi, T., et al., *Enhancement in the performance of ultrathin hematite photoanode for water splitting by an oxide underlayer*. *Advanced Materials*, 2012. **24**(20): p. 2699-2702.
108. Kim, H.G., et al., *Photocatalytic Nanodiodes for Visible-Light Photocatalysis*. *Angewandte Chemie*, 2005. **117**(29): p. 4661-4665.
109. Aroutiounian, V., V. Arakelyan, and G. Shahnazaryan, *Metal oxide photoelectrodes for hydrogen generation using solar radiation-driven water splitting*. *Solar Energy*, 2005. **78**(5): p. 581-592.
110. Ingram, D.B. and S. Linic, *Water splitting on composite plasmonic-metal/semiconductor photoelectrodes: evidence for selective plasmon-induced formation of charge carriers near the semiconductor surface*. *Journal of the American Chemical Society*, 2011. **133**(14): p. 5202-5205.
111. Paracchino, A., et al., *Highly active oxide photocathode for photoelectrochemical water reduction*. *Nature materials*, 2011. **10**(6): p. 456-461.
112. Ingler, W.B. and S.U. Khan, *A Self-Driven p/n-Fe₂O₃ Tandem Photoelectrochemical Cell for Water Splitting*. *Electrochemical and solid-state letters*, 2006. **9**(4): p. G144-G146.
113. Hisatomi, T., et al., *Cathodic shift in onset potential of solar oxygen evolution on hematite by 13-group oxide overlayers*. *Energy & Environmental Science*, 2011. **4**(7): p. 2512-2515.
114. Chiang, C.-Y., et al., *Copper oxide nanoparticle made by flame spray pyrolysis for photoelectrochemical water splitting—Part II. Photoelectrochemical study*. *international journal of hydrogen energy*, 2011. **36**(24): p. 15519-15526.
115. Cho, I.S., et al., *Branched TiO₂ nanorods for photoelectrochemical hydrogen production*. *Nano letters*, 2011. **11**(11): p. 4978-4984.
116. Chen, Z., et al., *Core-shell MoO₃-MoS₂ nanowires for hydrogen evolution: A functional design for electrocatalytic materials*. *Nano letters*, 2011. **11**(10): p. 4168-4175.
117. Chakrapani, V., J. Thangala, and M.K. Sunkara, *WO₃ and W₂N nanowire arrays for photoelectrochemical hydrogen production*. *international journal of hydrogen energy*, 2009. **34**(22): p. 9050-9059.

118. Klahr, B., et al., *Water oxidation at hematite photoelectrodes: the role of surface states*. Journal of the American Chemical Society, 2012. **134**(9): p. 4294-4302.
119. Radecka, M., et al., *Importance of the band gap energy and flat band potential for application of modified TiO₂ photoanodes in water photolysis*. Journal of power sources, 2008. **181**(1): p. 46-55.
120. Cesar, I., et al., *Influence of feature size, film thickness, and silicon doping on the performance of nanostructured hematite photoanodes for solar water splitting*. The Journal of Physical Chemistry C, 2008. **113**(2): p. 772-782.
121. Yang, X., et al., *Nitrogen-doped ZnO nanowire arrays for photoelectrochemical water splitting*. Nano Letters, 2009. **9**(6): p. 2331-2336.
122. Fujishima, A., T.N. Rao, and D.A. Tryk, *Titanium dioxide photocatalysis*. Journal of Photochemistry and Photobiology C: Photochemistry Reviews, 2000. **1**(1): p. 1-21.
123. Wang, G., et al., *Photoelectrochemical study on charge transfer properties of TiO₂-B nanowires with an application as humidity sensors*. The Journal of Physical Chemistry B, 2006. **110**(43): p. 22029-22034.
124. Hwang, Y.J., A. Boukai, and P. Yang, *High density n-Si/n-TiO₂ core/shell nanowire arrays with enhanced photoactivity*. Nano letters, 2008. **9**(1): p. 410-415.
125. Bard, A.J., *Design of semiconductor photoelectrochemical systems for solar energy conversion*. The Journal of Physical Chemistry, 1982. **86**(2): p. 172-177.
126. Awazu, K., et al., *A plasmonic photocatalyst consisting of silver nanoparticles embedded in titanium dioxide*. Journal of the American Chemical Society, 2008. **130**(5): p. 1676-1680.
127. Wang, H., et al., *Semiconductor heterojunction photocatalysts: design, construction, and photocatalytic performances*. Chemical Society Reviews, 2014. **43**(15): p. 5234-5244.
128. Wang, J., et al., *Cu₂ZnSnS₄ thin films: spin coating synthesis and photoelectrochemistry*. RSC Advances, 2014. **4**(41): p. 21318-21324.
129. Matsumoto, Y., et al., *New photocathode materials for hydrogen evolution: calcium iron oxide (CaFe₂O₄) and strontium iron oxide (Sr₇Fe₁₀O₂₂)*. Journal of Physical Chemistry, 1987. **91**(3): p. 577-581.
130. Torres, G.R., et al., *Photoelectrochemical study of nitrogen-doped titanium dioxide for water oxidation*. The Journal of Physical Chemistry B, 2004. **108**(19): p. 5995-6003.
131. Braun, A., et al., *Direct observation of two electron holes in a hematite photoanode during photoelectrochemical water splitting*. The Journal of Physical Chemistry C, 2012. **116**(32): p. 16870-16875.

132. Zhou, H., et al., *Towards highly efficient photocatalysts using semiconductor nanoarchitectures*. *Energy & Environmental Science*, 2012. **5**(5): p. 6732-6743.
133. Carlson, D. and K. Rajan, *The reversal of light-induced degradation in amorphous silicon solar cells by an electric field*. *Applied physics letters*, 1997. **70**(16): p. 2168-2170.
134. Milczarek, G., et al., *Optimization of a two-compartment photoelectrochemical cell for solar hydrogen production*. *International Journal of Hydrogen Energy*, 2003. **28**(9): p. 919-926.
135. Shiratsuchi, K. and H. Takizawa, *Photoelectric conversion device and solar cell*. 2000, Google Patents.
136. Szyszka, A., *Neunburg vorm wald—Test centre for solar hydrogen technology*. *International journal of hydrogen energy*, 1994. **19**(10): p. 823-841.
137. Agbossou, K., et al., *Electrolytic hydrogen based renewable energy system with oxygen recovery and re-utilization*. *Renewable Energy*, 2004. **29**(8): p. 1305-1318.
138. Preethi, V. and S. Kanmani, *Photocatalytic hydrogen production*. *Materials Science in Semiconductor Processing*, 2013. **16**(3): p. 561-575.
139. Liao, C.-H., C.-W. Huang, and J. Wu, *Hydrogen production from semiconductor-based photocatalysis via water splitting*. *Catalysts*, 2012. **2**(4): p. 490-516.
140. Ang, P. and A. Sommelles, *Hydrogen Evolution at p-InP Photocathodes in Alkaline Electrolyte*. *Journal of The Electrochemical Society*, 1984. **131**(6): p. 1462-1464.
141. Mei, J., et al., *Synthesis of isoindigo-based oligothiophenes for molecular bulk heterojunction solar cells*. *Organic letters*, 2010. **12**(4): p. 660-663.
142. Segal, A. and M. Epstein, *Optimized working temperatures of a solar central receiver*. *Solar Energy*, 2003. **75**(6): p. 503-510.
143. Le Formal, F., et al., *Passivating surface states on water splitting hematite photoanodes with alumina overlayers*. *Chemical Science*, 2011. **2**(4): p. 737-743.
144. Liu, R., et al., *Water Splitting by Tungsten Oxide Prepared by Atomic Layer Deposition and Decorated with an Oxygen-Evolving Catalyst*. *Angewandte Chemie*, 2011. **123**(2): p. 519-522.
145. Hu, Y.-S., et al., *Pt-doped α -Fe₂O₃ thin films active for photoelectrochemical water splitting*. *Chemistry of Materials*, 2008. **20**(12): p. 3803-3805.
146. Jun, H., et al., *Photoelectrochemical water splitting over ordered honeycomb hematite electrodes stabilized by alumina shielding*. *Energy & Environmental Science*, 2012. **5**(4): p. 6375-6382.
147. Weinhardt, L., et al., *Electronic surface level positions of WO₃ thin films for photoelectrochemical hydrogen production*. *The Journal of Physical Chemistry C*, 2008. **112**(8): p. 3078-3082.

148. Tahir, A.A. and K.U. Wijayantha, *Photoelectrochemical water splitting at nanostructured ZnFe₂O₄ electrodes*. Journal of Photochemistry and Photobiology A: Chemistry, 2010. **216**(2): p. 119-125.
149. Tseng, C.-L., C.-J. Tseng, and J.-C. Chen, *Thermodynamic analysis of a photoelectrochemical hydrogen production system*. international Journal of hydrogen energy, 2010. **35**(7): p. 2781-2785.
150. Yang, X., et al., *Balancing photovoltage generation and charge-transfer enhancement for catalyst-decorated photoelectrochemical water splitting: A case study of the hematite/MnOx combination*. Journal of Catalysis, 2013. **304**: p. 86-91.
151. Li, J., J. Lin, and H. Jiang, *Direct hydrogen gas generation by using InGaN epilayers as working electrodes*. Applied Physics Letters, 2008. **93**(16): p. 162107.
152. Lianos, P., *Production of electricity and hydrogen by photocatalytic degradation of organic wastes in a photoelectrochemical cell: the concept of the photofuelcell: a review of a re-emerging research field*. Journal of Hazardous Materials, 2011. **185**(2): p. 575-590.
153. Wang, G., et al., *Double-sided CdS and CdSe quantum dot co-sensitized ZnO nanowire arrays for photoelectrochemical hydrogen generation*. Nano letters, 2010. **10**(3): p. 1088-1092.
154. Cornuz, M., M. Grätzel, and K. Sivula, *Preferential orientation in hematite films for solar hydrogen production via water splitting*. Chemical Vapor Deposition, 2010. **16**(10-12): p. 291-295.
155. Seabold, J.A. and K.-S. Choi, *Effect of a cobalt-based oxygen evolution catalyst on the stability and the selectivity of photo-oxidation reactions of a WO₃ photoanode*. Chemistry of Materials, 2011. **23**(5): p. 1105-1112.
156. Barroso, M., et al., *The role of cobalt phosphate in enhancing the photocatalytic activity of α -Fe₂O₃ toward water oxidation*. Journal of the American Chemical Society, 2011. **133**(38): p. 14868-14871.
157. Maeda, K., R. Abe, and K. Domen, *Role and function of ruthenium species as promoters with TaON-based photocatalysts for oxygen evolution in two-step water splitting under visible light*. The Journal of Physical Chemistry C, 2011. **115**(7): p. 3057-3064.
158. Tang, J., et al., *Mechanism of O₂ production from water splitting: nature of charge carriers in nitrogen doped nanocrystalline TiO₂ films and factors limiting O₂ production*. The Journal of Physical Chemistry C, 2011. **115**(7): p. 3143-3150.
159. Radich, J.G., R. Dwyer, and P.V. Kamat, *Cu₂S Reduced Graphene Oxide Composite for High-Efficiency Quantum Dot Solar Cells. Overcoming the Redox Limitations of S₂/S²⁻ at the Counter Electrode*. The Journal of Physical Chemistry Letters, 2011. **2**(19): p. 2453-2460.

160. Zhang, N., et al., *Assembly of CdS nanoparticles on the two-dimensional graphene scaffold as visible-light-driven photocatalyst for selective organic transformation under ambient conditions*. The Journal of Physical Chemistry C, 2011. **115**(47): p. 23501-23511.
161. Choi, H., et al., *Electrophoretic graphene for transparent counter electrodes in dye-sensitized solar cells*. Electronics letters, 2011. **47**(4): p. 281-283.
162. Perera, S.D., et al., *Hydrothermal synthesis of graphene-TiO₂ nanotube composites with enhanced photocatalytic activity*. ACS Catalysis, 2012. **2**(6): p. 949-956.
163. Zhang, J., et al., *Noble Metal-Free Reduced Graphene Oxide-Zn x Cd_{1-x}S Nanocomposite with Enhanced Solar Photocatalytic H₂-Production Performance*. Nano letters, 2012. **12**(9): p. 4584-4589.
164. Lee, V., et al., *Large-area chemically modified graphene films: electrophoretic deposition and characterization by soft X-ray absorption spectroscopy*. Chemistry of Materials, 2009. **21**(16): p. 3905-3916.
165. Zhang, H., et al., *P25-graphene composite as a high performance photocatalyst*. ACS nano, 2009. **4**(1): p. 380-386.
166. Liao, Y., et al., *Facile synthesis of high-crystallinity graphitic carbon/Fe₃C nanocomposites as counter electrodes for high-efficiency dye-sensitized solar cells*. ACS applied materials & interfaces, 2013. **5**(9): p. 3663-3670.
167. Xie, G., et al., *A photoelectrochemical investigation on the synergetic effect between CdS and reduced graphene oxide for solar-energy conversion*. Chem. Asian J, 2013. **8**: p. 2395-2400.
168. Lee, J.G., et al., *Graphene-Titania Hybrid Photoanodes by Supersonic Kinetic Spraying for Solar Water Splitting*. Journal of the American Ceramic Society, 2014. **97**(11): p. 3660-3668.
169. Lee, D.H., et al., *Three-Dimensional Monolayer Graphene and TiO₂ Hybrid Architectures for High-Efficiency Electrochemical Photovoltaic Cells*. The Journal of Physical Chemistry C, 2015. **119**(12): p. 6880-6885.
170. Zeng, X., et al., *Using graphene-based plasmonic nanocomposites to quench energy from quantum dots for signal-on photoelectrochemical aptasensing*. Analytical chemistry, 2013. **85**(24): p. 11720-11724.
171. Chang, H. and H. Wu, *Graphene-based nanocomposites: preparation, functionalization, and energy and environmental applications*. Energy & Environmental Science, 2013. **6**(12): p. 3483-3507.
172. Zhai, P., et al., *Water-soluble microwave-exfoliated graphene nanosheet/platinum nanoparticle composite and its application in dye-sensitized solar cells*. Electrochimica Acta, 2014. **132**: p. 186-192.

173. Jung, S.W., et al., *Enhanced Photoelectrochemical Response of Graphene-Coated Al₂O₃-TiO₂ Nanocomposite Photoanodes*. *Molecular Crystals and Liquid Crystals*, 2011. **538**(1): p. 272-277.
174. Li, G., X. Chen, and G. Gao, *Bi 2 S 3 microspheres grown on graphene sheets as low-cost counter-electrode materials for dye-sensitized solar cells*. *Nanoscale*, 2014. **6**(6): p. 3283-3288.
175. Meng, F., et al., *Solar hydrogen generation by nanoscale p-n junction of p-type molybdenum disulfide/n-type nitrogen-doped reduced graphene oxide*. *Journal of the American Chemical Society*, 2013. **135**(28): p. 10286-10289.
176. Marcano, D.C., et al., *Improved synthesis of graphene oxide*. *ACS nano*, 2010. **4**(8): p. 4806-4814.
177. Guo, H.-L., et al., *A green approach to the synthesis of graphene nanosheets*. *ACS nano*, 2009. **3**(9): p. 2653-2659.
178. Dreyer, D.R., et al., *The chemistry of graphene oxide*. *Chemical Society Reviews*, 2010. **39**(1): p. 228-240.
179. Long, D., et al., *Preparation of nitrogen-doped graphene sheets by a combined chemical and hydrothermal reduction of graphene oxide*. *Langmuir*, 2010. **26**(20): p. 16096-16102.
180. Basavaraja, S., et al., *Solvothermal synthesis and characterization of acicular α -Fe₂O₃ nanoparticles*. *Bulletin of Materials Science*, 2012. **34**(7): p. 1313.
181. Abdulkadir, I. and A.B. Aliyu, *Some wet routes for synthesis of hematite nanostructures*. *African Journal of Pure and Applied Chemistry*, 2013. **7**(3): p. 114-121.
182. Sungpanich, J., T. Thongtem, and S. Thongtem, *Photocatalysis of WO₃ Nanoplates Synthesized by Conventional-Hydrothermal and Microwave-Hydrothermal Methods and of Commercial WO₃ Nanorods*. *Journal of Nanomaterials*, 2014. **2014**.
183. Scherzer, O., *The theoretical resolution limit of the electron microscope*. *Journal of Applied Physics*, 1949. **20**(1): p. 20-29.
184. Chung, F.H., *Quantitative interpretation of X-ray diffraction patterns of mixtures. I. Matrix-flushing method for quantitative multicomponent analysis*. *Journal of Applied Crystallography*, 1974. **7**(6): p. 519-525.
185. Agrell, H.G., J. Lindgren, and A. Hagfeldt, *Degradation mechanisms in a dye-sensitized solar cell studied by UV-VIS and IR spectroscopy*. *Solar Energy*, 2003. **75**(2): p. 169-180.

185. Agrell, H.G., J. Lindgren, and A. Hagfeldt, *Degradation mechanisms in a dye-sensitized solar cell studied by UV-VIS and IR spectroscopy*. *Solar Energy*, 2003. **75**(2): p. 169-180.
186. Tang, L., et al., *Preparation, structure, and electrochemical properties of reduced graphene sheet films*. *Advanced Functional Materials*, 2009. **19**(17): p. 2782.
187. Stankovich, S., et al., *Synthesis of graphene-based nanosheets via chemical reduction of exfoliated graphite oxide*. *Carbon*, 2007. **45**(7): p. 1558-1565.
188. Park, S., et al., *Hydrazine-reduction of graphite-and graphene oxide*. *Carbon*, 2011. **49**(9): p. 3019-3023.
189. Shao, Y., et al., *Facile and controllable electrochemical reduction of graphene oxide and its applications*. *Journal of Materials Chemistry*, 2010. **20**(4): p. 743-748.
190. Biswas, S.K., et al., *Morphologically different WO₃ nanocrystals in photoelectrochemical water oxidation*. *Journal of Nanoparticle Research*, 2012. **14**(1): p. 1-12.
191. Chen, D. and J. Ye, *Hierarchical WO₃ hollow shells: dendrite, sphere, dumbbell, and their photocatalytic properties*. *Advanced Functional Materials*, 2008. **18**(13): p. 1922-1928.
192. Huang, R., et al., *Effect of hydrothermal temperature on structure and photochromic properties of WO₃ powder*. *Advanced Powder Technology*, 2012. **23**(2): p. 211-214.
193. Chernyshova, I., M. Hochella Jr, and A. Madden, *Size-dependent structural transformations of hematite nanoparticles. 1. Phase transition*. *Physical Chemistry Chemical Physics*, 2007. **9**(14): p. 1736-1750.
194. Jing, Z. and S. Wu, *Synthesis and characterization of monodisperse hematite nanoparticles modified by surfactants via hydrothermal approach*. *Materials Letters*, 2004. **58**(27): p. 3637-3640.
195. Huang, H., et al., *Ultraviolet-assisted preparation of mesoporous WO₃/reduced graphene oxide composites: superior interfacial contacts and enhanced photocatalysis*. *Journal of Materials Chemistry A*, 2013. **1**(47): p. 15110-15116.
196. Zhou, Y., et al., *Hydrothermal dehydration for the "green" reduction of exfoliated graphene oxide to graphene and demonstration of tunable optical limiting properties*. *Chemistry of Materials*, 2009. **21**(13): p. 2950-2956.
197. Diamandescu, L., et al., *Hydrothermal synthesis and characterization of some polycrystalline α -iron oxides*. *Ceramics International*, 1999. **25**(8): p. 689-692.
198. Fu, X., C. Xie, and L. Zhou, *The Influence of the Temperature on the Optical Absorption Properties and Morphologies of WO₃ Nanorods Synthesized by the Hydrothermal Method*. *Journal of Inorganic and Organometallic Polymers and Materials*, 2011. **21**(4): p. 958-961.

199. Sivula, K., F.L. Formal, and M. Grätzel, *WO₃- Fe₂O₃ photoanodes for water splitting: A host scaffold, guest absorber approach*. *Chemistry of Materials*, 2009. **21**(13): p. 2862-2867.
200. Yoon, K.-Y., et al., *Hematite-Based Photoelectrochemical Water Splitting Supported by Inverse Opal Structures of Graphene*. *ACS applied materials & interfaces*, 2014. **6**(24): p. 22634-22639.